

Evaluation of Field-Collected Drifter and In Situ Fluorescence Data Measuring Subsurface Dye Plume Advection/Dispersion and Comparisons to High-Frequency Radar-Observation System Data for Dispersed Oil Transport Modeling

**A Final Report Submitted to
The Coastal Response Research Center**

Submitted by:

**Dr. James R. Payne
Payne Environmental Consultants, Incorporated
1991 Village Park Way, Suite 206B
Encinitas, CA 92024**

Additional Investigators:

**Dr. Deborah French-McCay, Chris Mueller, Kathy Jayko,
Brooke Longval, and Melanie Schroeder
Applied Science Associates, Inc.
Narragansett, Rhode Island**

**Dr. Eric Terrill, Melissa Carter, Mark Otero,
Sung Yong Kim, William Middleton, and Andy Chen
Scripps Institution of Oceanography
La Jolla, California**

**Dr. Walter Nordhausen, Robin Lewis, Mark Lampinen, and Thomas Evans
CA Department of Fish and Game Office of Spill Prevention and Response
San Diego, California**

**Dr. Carter Ohlmann
University of California Santa Barbara
Santa Barbara, California**

Project Period: January 2006 – September 2007

Submission Date: May 11, 2007

Revised:

This project was funded by a grant from NOAA/UNH Coastal Response Research Center.
NOAA Grant Number(s): NA04NOS4190063 (CFDA No. 11-419). Project Number: 06-084



Abstract

Oil-spill transport and fate modeling may be used to evaluate water column hydrocarbon concentrations, potential exposure to organisms, and the impacts of oil spills with and without use of dispersants. Important inputs for such analyses are ocean currents and turbulent dispersion (eddy diffusion) coefficients. Fluorescein dye studies conducted off San Diego, California, were used to evaluate the ability of transport models to hindcast movement and dispersion of dye (and so water movements influencing transport of subsurface oil and dissolved components) using data including surface currents calculated from high-frequency radar (HF Radar), near-surface currents from drifter measurements drogued at several depths (1m, 2m, 4m or 5m), dye concentrations measured by fluorescence, spreading and dye intensity measurements based on aerial photography, and water density profiles from CTD casts.

Typically, the dye penetrated to a depth of 7 to 15 m largely via Langmuir circulation within a half hour after release, but it was not uniform in concentration over that (semi-) mixed layer. For experiments in 5-7 m/s winds where the surface mixed layer was deeper, the drifters drogued at 4-5m tracked the dye most accurately, whereas drifters drogued at 1-2m moved downwind just ahead of the dye plume, as predicted by wind drift theory (Stokes drift). In light winds when the mixed layer was highly stable and wind drift was slow and shallow, drifters drogued at 2 m tracked the dye most accurately, with the 4-m drifters slower than the bulk dye movements. The observations demonstrated that drifters can provide accurate estimates of near-surface currents for near-surface transport modeling.

The observed horizontal trajectories of dye and drifters were sometimes different from those computed with HF Radar derived surface currents, which were integrated, time- (1 hour) and spatially ($\sim 1 \text{ km}^2$) averaged measurements across the top 50 cm of the ocean surface. These differences may be attributable to variable horizontal and vertical surface shear, drifter response to Stokes drift and preferential sorting by Langmuir cells, inherent differences between the averaged velocity measured by the HF radar and Lagrangian drifter measurements, and measurement error of the HF radar (especially at low velocities).

Simulation of dye (or subsurface dissolved and oil-droplet) concentrations also requires estimates of turbulent dispersion (mixing) coefficients, and results are highly sensitive to the assumed values over the likely range. In this study, dispersion rates were estimated based on dye spread as measured by aerial photography and vertical profiles of dye fluorescence over time. This novel approach provided more synoptic measurements of the horizontal distribution than could be obtained from a surface vessel. The results for the conditions studied indicated that the horizontal dispersion coefficient was typically $0.1\text{-}50 \text{ m}^2/\text{sec}$, similar to the range identified in the literature for length scales on the order of a kilometer. Use of such data in an oil fate model can provide estimates of likely dispersed oil and dissolved hydrocarbon concentrations under similar conditions; however, other conditions should be examined before these results are generalized. While the goals of the program were directed towards environmental impact assessment, the data and modeling needs share common elements with operational spill response and have direct applicability to spill response planning/decision making, net environmental benefit analysis, and educating the spill community and public.

Keywords: oil spill modeling, dispersion, eddy diffusion coefficient, fluorescein dye, high-frequency radar, dispersants, natural resource damage assessments

Acknowledgements

Funding for this program was provided by the NOAA/UNH Coastal Response Research Center (Grant No. NA04NOS4190063 – UNH Subcontract No. 06-084 with PECD) and the California Department of Fish and Game Office of Spill Prevention and Response (DFG Agreement Number P0475036 with SIO). The authors would also like to acknowledge the significant in-kind contributions of personnel, equipment/instrumentation, and sampling/observation platforms (boats and aircraft) provided by the United States Coast Guard, the Marine Spill Response Corporation, and CA OSPR. In particular, we also thank the following individuals for their contributions in collecting data and valuable inputs to the study: BM-1 Greg L. Via, BM-1 Hector Ruiz-Santana, MK-1 Mike Maly, MSTC Butch Willoughby, and BM-2 Charles Varela from the United States Coast Guard (USCG) Pacific Strike Team; Paul Lynch and Paul Sanchez from the Marine Spill Response Corporation (MSRC); and Jan Svejksky and Jamie Kum of Ocean Imaging, Solana Beach, CA. We also appreciate the careful review and input provided by anonymous reviewers and Dr. Malcolm Spaulding of the University of Rhode Island, Narragansett, RI. The findings, opinions, and recommendations expressed in this report are those of the authors and do not necessarily reflect those of the sponsoring agencies, subagencies, or the University of New Hampshire.

Table of Contents

1. Introduction.....	1
2. Objectives	5
3. Methods.....	6
3.1 Preparation for and Performance of Field Experiments	6
3.1.1 Permitting.....	6
3.1.2 Dye Deployment	7
3.1.3 Dye Concentrate Preparation and On-Board Mixing.....	8
3.1.4 Photography	10
3.1.5 Geographical Position Data	12
3.1.6 High-Frequency Radar (CODAR)	13
3.1.7 Drifters	13
3.1.8 Meteorological Measurements.....	14
3.1.9 <i>In situ</i> Measurements of Water-Column Stability and Plume Behavior – Point Loma Experiments	15
3.1.10 Instrument Calibration and Intercalibration.....	17
3.1.11 Communications	18
3.1.12 Personnel Safety During Marine and Aerial Operations	18
3.2 Modeling.....	19
3.2.1 Photographic Images.....	19
3.2.2 Mixed Layer Properties.....	20
3.2.3 Current Estimates Based on Drifters and HF Radar	21
3.2.4 Dye Concentration Measurements.....	21
4. Results – Field Data.....	22
4.1 Fluorometer Calibrations and Comparison of Along-Plume Data Profiles – Point Loma Experiments off San Diego.....	22
4.2 Horizontal Movements and Expansion of the Dye – Point Loma Experiments off San Diego.....	24
4.2.1 November 8, 2005 Experiment.....	26
4.2.2 March 21, 2006 Experiment	29
4.2.3 March 22, 2006 Experiment	31
4.2.4 June 21, 2006 Experiment.....	33
4.2.5 June 22, 2006 Experiment.....	34
4.2.6 November 1, 2006 Experiment.....	36
4.2.7 November 2, 2006 Experiment.....	38
4.3 Vertical Penetration of the Dye – Point Loma Experiments off San Diego	40
4.4 Safe Sea Exercise off San Francisco on August 9, 2006	41
4.4.1 Horizontal Movements and Expansion of the Dye – August 9, 2006 Safe Seas Experiment.....	42
4.4.2 Vertical Penetration of the Dye – August 9, 2006 Safe Seas Experiment.....	44
4.5 Drifter & HF Radar Direct Comparisons.....	45
4.6 Analysis of Continuous Sampling Fluorometer Data	46

4.6.1 June 22, 2006 Experiment.....	46
4.6.2 November 2, 2006 Experiment.....	50
5. Results – Modeling.....	53
5.1 Approach.....	53
5.2 Model Algorithms.....	56
5.2.1 Lagrangian transport model.....	56
5.2.2 Wind drift.....	57
5.3 Model Results.....	61
5.3.1 Wind Conditions and Mixed Layer Characteristics.....	61
5.3.2 Advection.....	63
5.3.3 Langmuir Circulation.....	70
5.3.4 Horizontal (D_x) and Vertical (D_z) Diffusion Coefficients.....	72
5.4 SIMAP Model Application to Dye Experiments.....	75
5.5 Discussion of Modeling Results.....	76
6. Discussion and Importance to Oil Spill Response/Restoration.....	79
6.1 Summary of Project Results.....	79
6.2 Implications for Oil Spill Model Development and Application.....	81
6.3 Planned Implementation of Sampling Protocols Developed and Evaluated Through this Study into the CA Dispersed Oil Monitoring Plan (DOMP).....	83
6.3.1 Objective of the CA OSPR DOMP.....	83
6.3.2 Sampling Vessel and Observation Platform Requirements.....	83
6.3.3 General Considerations and Approach.....	84
6.4 Conclusions.....	89
7. Technology Transfer.....	90
References.....	91

List of Appendices

Appendix A. Geoposition Data

Appendix B. Photographic Data

Appendix C. High-Frequency Radar Data

Appendix D. Drifter Data

Appendix E. Wind Data

Appendix F. Oceanographic Data

Appendix G. Fluorescence Data for June and November 2006

Appendix H. SIMAP Model Applications to Dye Experiments

List of Figures

Figure 1-1. Dye release site offshore San Diego, California.	3
Figure 1-2. Dye release site offshore San Francisco, California.	4
Figure 3-2. Fluorescein dye release from the spray booms on the starboard side of the MSRC <i>Response 2</i> (left) and the appearance of the dye mixing into the water surface six minutes after release on 22 June 2006 (right).	8
Figure 3-3. Aerial photograph processing steps.	12
Figure 3-4. Drogue (kite) tied with a 1-, 2-, 4-, or 5-m tether to the drifter floats/transponders (left) and release of a drogued drifter/transponder into the dye plume from the MSRC <i>Response 2</i> on 8 November 2005 (right).	14
Figure 3-5. The Wet Labs ECO FL-UR fluorometer (with fin for proper orientation in the water when under way) and programmable downrigger to raise and lower the unit to preset depths over time.	17
Figure 4-1. Post Cruise Calibration Plots Obtained on the SIO Wet Labs Model ECO FL-UR in situ Fluorometers (FLURRT18 and 19) and the USCG SMART Protocol Turner A-10 Fluorometers (Smart 1 and 2) after the 22 March 2006 Dye Studies.	23
Figure 4-2. Along-plume transect data obtained at a constant depth with the Turner A-10 (green) and Wet Labs (blue) Fluorometers.	24
Figure 4-3. Locations of the dye over time in the 8 November 2005 experiment, as interpreted from the aerial photographs. Waypoints of drifter movements (drogued at 1m) are indicated as diamonds (red and purple shades). Black circles and times indicate locations of the dye during CTD casts.	27
Figure 4-4. Dye plume dimensions and movements over time, and drifter tracks represented by diamonds (all 1-m deployment depth) for the 8 November 2005 experiment. Four images of dye plume are shown with corresponding times (black font). Corresponding times for drifter tracks (diamonds) are in red font.	28
Figure 4-5. Trajectory of a neutrally-buoyant constituent using the HF-Radar vectors up to 16:15 PM (yellow and green line, alternating color by 0.5 hour intervals, with times in green font) compared to drifter movement (red diamonds with times in red font) for the 8 November 2005 experiment.	28
Figure 4-6. Locations of the dye over time in the 21 March 2006 experiment, as interpreted from the aerial photographs. Waypoints of drifter movements (all drogued at 1m) are indicated as diamonds, with times in red font. The trajectory of a neutrally-buoyant constituent using the HF-Radar vectors up to 13:49 (yellow and green line, alternating color by 0.5 hour intervals, with times in green font) may be compared to drifter and dye movements.	30
Figure 4-7. Locations of the dye over time in the 22 March 2006 experiment, as interpreted from the aerial photographs. Waypoints of drifter movements are indicated by the diamonds (at 1 m: red diamonds with times in red font; at 5 m: blue diamonds with times in blue font). The trajectory of a neutrally-buoyant constituent using the HF-Radar vectors up to 14:46 PST (yellow and green line, alternating color by 0.5 hour intervals, with times in green font) is shown.	32
Figure 4-8. Locations of the dye over time in the 21 June 2006 experiment, as interpreted from the aerial photographs. Waypoints of drifter movements are indicated by the diamonds (at 2 m: red diamonds with times in red font; at 4 m: blue diamonds with times	

in blue font). The trajectory of a neutrally-buoyant constituent using the HF-Radar vectors up to 16:00 PDT (yellow and green line, alternating color by 0.5 hour intervals, with times in green font) is shown.....	34
Figure 4-9. Locations of the dye over time in the 22 June 2006 experiment, as interpreted from the aerial photographs. Waypoints of drifter movements are indicated by the diamonds (at 2 m: red diamonds with times in red font; at 4 m: blue diamonds with times in blue font). The trajectory of a neutrally-buoyant constituent using the HF-Radar vectors up to 17:51 PDT (yellow and green line, alternating color by 0.5 hour intervals, with times in green font) is shown.....	35
Figure 4-10. Locations of the dye over time in the 1 November 2006 experiment, as interpreted from the aerial photographs. Waypoints of drifter movements are indicated by the diamonds (at 2 m: red diamonds with times in red font; at 4 m: blue diamonds with times in blue font). The trajectory of a neutrally-buoyant constituent using the HF-Radar vectors up to 15:31 PST (yellow and green line, alternating color by 0.5 hour intervals, with times in green font) is shown.....	37
Figure 4-11. Locations of the dye over time in the 2 November 2006 experiment, as interpreted from the aerial photographs. Waypoints of drifter movements are indicated by the diamonds (at 2 m: red diamonds with times in red font; at 4 m: blue diamonds with times in blue font). The trajectory of a neutrally-buoyant constituent using the HF-Radar vectors up to 15:00 PST (yellow and green line, alternating color by 0.5 hour intervals, with times in green font) is shown.....	39
Figure 4-12. Locations of the dye over time in the 9 August 2006 experiment, as interpreted from the aerial photographs.....	43
Figure 4-13. Trajectory of a neutrally-buoyant constituent using the HF-Radar vectors up to 13:30 PDT (grey line with times in black font) for the 9 August 2006 experiment overlaid on dye locations based on shape files derived from selected images. The arrow indicates the HF-Radar speed at the end time of the trajectory simulation.....	44
Figure 4-14. All along-plume transects (black) shown with along-plume axis (parallel to transects) and the cross-plume axis (orthogonal to along-plume axis). The cross-plume axis is oriented such that it serves as a starting reference for all of the along-plume transects.....	47
Figure 4-15. Along-plume sampling transects projected onto the along plume axis with absolute distances. Dye concentrations are vertically and horizontally binned (by medial filtering to remove spikes and reduce noise) in increments of 10 m horizontally and 0.5 m vertically. Maximum dye concentration profiles (in black) indicate the core of the dye plume.....	48
Figure 4-16. The mean velocity profile in the along plume direction is shown with bars indicating envelope of one standard deviation. The vertical shear based on a least square's fit to the profile is 0.031 s^{-1} . Mean HF-Radar (computed at the mean along-plume position) and drifter velocities projected onto the along-plume axis are shown for comparison.....	49
Figure 4-17. All along-plume transects (black) shown with along-plume axis (parallel to transects) and the cross-plume axis (orthogonal to along-plume axis). The cross-plume axis is oriented such that it serves as a starting reference for all of the along-plume transects.....	51

Figure 4-18. The mean velocity profile in the along plume direction is shown with bars indicating envelope of one standard deviation. The vertical shear based on a least square's fit to the profile is 0.006 s^{-1} . Mean HF-Radar (computed at the mean along-plume position) and drifter velocities projected onto the along-plume axis are shown for comparison.....	52
Figure 5-1. Drift speed (left panel) and angle (relative to downwind, right panel) as a function of depth and wind speed.	60
Figure 5-2. Drift speed (left panel) and angle (relative to downwind, right panel) as a function of wind speed, averaged over the water column from 0 m to depth.....	61
Figure 5-3. Vector plot of wind drift, HF-Radar (as measured and less wind drift) and drifter (as measured and less wind drift) velocities during the 8 November 2005 experiment.....	65
Figure 5-4. Vector plot of wind drift, HF-Radar (as measured and less wind drift) and drifter (as measured and less wind drift) velocities during the 21 March 2006 experiment.	65
Figure 5-5. Vector plot of wind drift, HF-Radar (as measured and less wind drift) and drifter (as measured and less wind drift) velocities during the 22 March 2006 experiment.	66
Figure 5-6. Vector plot of wind drift, HF-Radar (as measured and less wind drift) and drifter (as measured and less wind drift) velocities during the 21 June 2006 experiment.....	66
Figure 5-7. Vector plot of wind drift, HF-Radar (as measured and less wind drift) and drifter (as measured and less wind drift) velocities during the 22 June 2006 experiment.....	67
Figure 5-8. Vector plot of wind drift, HF-Radar (as measured and less wind drift) and drifter (as measured and less wind drift) velocities during the 1 November 2006 experiment.....	67
Figure 5-9. Vector plot of wind drift, HF-Radar (as measured and less wind drift) and drifter (as measured and less wind drift) velocities during the 2 November 2006 experiment.....	68

List of Tables

Table 3-1. Dye deployment cruises off Point Loma, San Diego.	7
Table 3-2. Weight of fluorescein dye and freshwater/seawater volumes used for each experiment.....	9
Table 4-1. Dye Deployment Cruises off Point Loma (San Diego).....	25
Table 4.3-1. Dye penetration and the depth of the surface mixed layer.	40
Table 4.4-1. Dye Deployment off San Francisco during the Safe Seas Exercise.....	42
Table 4.5-1. Mean wind, HF-Radar and drifter bearings and magnitudes, and calculated differences over each experiment.	45
Table 4.6-1. Comparison of along-plume velocity profiles and shear estimates from drifters and dye analysis.....	50
Table 5-1. Wind and wave conditions, mixed layer depth, water density, and stability characteristics.....	62
Table 5-2. Observed movements of drifters and HF-Radar-measured current (interpolated to each of the shallowest drifter locations for each fix in time).....	63
Table 5-3. Speed and bearing measured by drifters and HF-Radar with modeled wind drift subtracted (using winds at LJPC1).....	64
Table 5-4. Mean dimensions of Langmuir circulation cells.	71
Table 5-5. Orientations of Langmuir circulation cells to the wind direction at the times of the images examined.	71
Table 5-6. Estimates of horizontal dispersion coefficients (D_x) derived from dimensions of the dye in images over time (based on linear regression; negative values are not significantly different from zero). [W = 0 is with no wind-drift correction; W = 1 is with wind-drift (wind station LJPC1) subtracted]	73
Table 5-7. Estimates of vertical (D_z) dispersion coefficients based on vertical profiles of dye concentration. [Note the units here are cm^2/s , while the values of D_x in Table 5-6 are in m^2/s .].....	74
Table 5-8. Decline of vertical (D_z) dispersion coefficients over time (fit to equation 13, and predicted D_z using equation 14) in the 1 and 2 November experiments.....	75

1. Introduction

New federal regulations regarding response plan oil removal capacity (Caps) requirements for tank vessels and marine transportation-related facilities being developed by the US Coast Guard (USCG, 1999) are expected to result in an increased use of chemical dispersants to treat oil spills in the United States. Other government authorities (US and internationally) are also considering more dispersant use. Extensive U.S. coastal areas > 3 nautical miles from the shorelines off California, Hawaii, the Gulf of Mexico, and much of the East Coast have been designated as “Pre-Approval Zones” for dispersant applications in the event of oil spills (NRC 2005). Pre-approval agreements also exist for parts of Cook Inlet and Prince William Sound in Alaska. The application of dispersants may reduce impacts to wildlife (e.g., seabirds, sea otters) and shoreline habitats, but with the tradeoff that the dispersed oil may cause impacts to water column organisms (e.g., French McCay and Payne, 2001; French McCay *et al.*, 2004). Computer simulations (French McCay *et al.*, 2006) of large dispersed oil slicks (~ 1.5 square miles) indicate that the resulting plumes may persist for several days with hydrocarbon concentrations at levels toxic to aquatic organisms. However, little or no field data are available to validate the model results.

To address this need, oil-spill fate and transport modeling is currently being used by the State of California Department of Fish and Game Office of Spill Prevention and Response (OSPR) to develop the time and spatial scales, and equipment needs for a formal Dispersed Oil Monitoring Plan (DOMP) to document hydrocarbon water column concentrations, potentially exposed organisms (zooplankton), and the impacts of oil spills with and without dispersant use. Protocols have been developed to provide a rapid semi-quantitative field method for measuring enhanced entrainment into the water column after dispersant use – primarily to inform response personnel about dispersant effectiveness (Henry *et al.*, 1999); however, this approach does not readily address potential impacts to the water column. A significant challenge in the implementation of any plan to evaluate impacts is to locate and sample the dispersed oil plume over time. Repeated sampling of the same plume(s) is needed to determine the exposure of water column organisms. These measurements are essential to the evaluation of environmental trade-offs justified as a decision to use dispersants under certain circumstances. Natural Resource Damage Assessment (NRDA) efforts will be absent critical quantitative and qualitative information with which to verify model results without a sound and pre-planned methodology for collection of water column data.

To address these issues CA OSPR funded and was an active participant in an initial series of fluorescein dye experiments executed by a multidisciplinary team involving members from Scripps Institution of Oceanography (SIO), Payne Environmental Consultants, Inc. (PECI), and Applied Science Associates, Inc. (ASA), with unfunded in-kind contributions from the Marine Spill Response Corporation (MSRC) and the U.S. Coast Guard (USCG). The GOAL of these studies was to develop and test the operational framework for repeated sampling of dispersed oil plumes as outlined in the DOMP. The National Oceanic and Atmospheric Administration/ University of New Hampshire (NOAA/UNH) Coastal Response Research Center (CRRC) then provided additional funds to significantly expand and augment those efforts.

Fluorescein dye plumes (initially about 500 m in diameter after all the dye was released) were tracked and sampled on eight dates, during the period from 8 November 2005 through November 2006, to measure transport and spreading of neutrally buoyant constituents and water as would influence submerged oil droplet transport. Seven experiments were completed off San Diego CA, and a partial data set of observations was collected on a dye release 9 August 2006 off San Francisco. The USCG Pacific Strike Team participated in the exercises and provided their equipment including flow-through fluorimeters as utilized in the SMART (Special Monitoring of Applied Response Technology) protocols. In the San Diego experiments, drifters (drogued at several depths – supplied by University of California Santa Barbara researchers) were deployed to track the plumes and allow their observed trajectories to be compared with Coastal Ocean Dynamics Applications Radar (CODAR, manufactured by CODAR Ocean Sensors, Palo Alto, CA) [a High-Frequency-Radar (HF-Radar) system] velocities and field observations of the dye movements. A Seabird CTD profiling instrument (directed by Dr. Terrill of SIO) was deployed to determine the mixed layer depth, an important variable for vertical dispersion. Vertical and horizontal profiles of dye concentrations, as measured by fluorescence, were made and used to determine the depth of penetration of the dye into the water column over time as well as horizontal dispersion rates. Aerial photos taken from OSPR twin engine aircraft were used to track the movements and spreading of the dye over time.

Modeling analyses were performed to evaluate the ability of current data based on HF Radar and/or drifters to hindcast and potentially predict movements of a neutrally buoyant plume in the mixed layer. A surface wind drift algorithm was tested to evaluate its ability to predict vertical wind-forced shear. Horizontal and vertical dispersion rates were estimated from measurements of the horizontal expansion of georectified images from aerial photographs and from dye concentration data.

While several different oceanographic weather states were encountered during the experiments, it is recognized that one cannot extrapolate from this limited set of measurements to all potential environmental scenarios. Thus, these measurements and algorithm developments were used to further the approach. That is, the purpose of this project was not just to complete seven (or eight) observations in the field, but to develop the methodology to measure small-scale diffusivities and use them in oil-spill models for other times and locations, and to the extent possible, correlate horizontal and vertical diffusivity to observed or measured sea-state (wind conditions, swell height, direction, and frequency) as well as advective transport by larger-scale currents. This information will be useful for model development, which will be transferable to other locations and investigators.

Seven separate 550-gallon fluorescein dye releases were completed off Point Loma (San Diego, CA) under OSPR (8 November 2005; 21 and 22 March 2006) and CRRC (21 and 22 June 2006; 1 and 2 November 2006) support. In addition, photography and some oceanographic data were collected for a dye release during the Safe Seas exercise off San Francisco (9 August 2006). Publicly available information and photographs from the cruises are available at <http://cordc.ucsd.edu/projects/ospr/>.

The dye deployments were conducted at or near a site (Figure 1-1) approximately 3.7 nmiles southwest of Point Loma, San Diego, CA [Primary location: 32° 37' N, 117° 17' W]. Water depth is approximately 40 fathoms (240ft, 73m). EPA federal permits were obtained prior to the dye releases for conducting these studies in federal waters. Figure 1-2 shows the approximate location of the Safe Seas exercise off San Francisco, California.



Figure 1-1. Dye release site offshore San Diego, California.

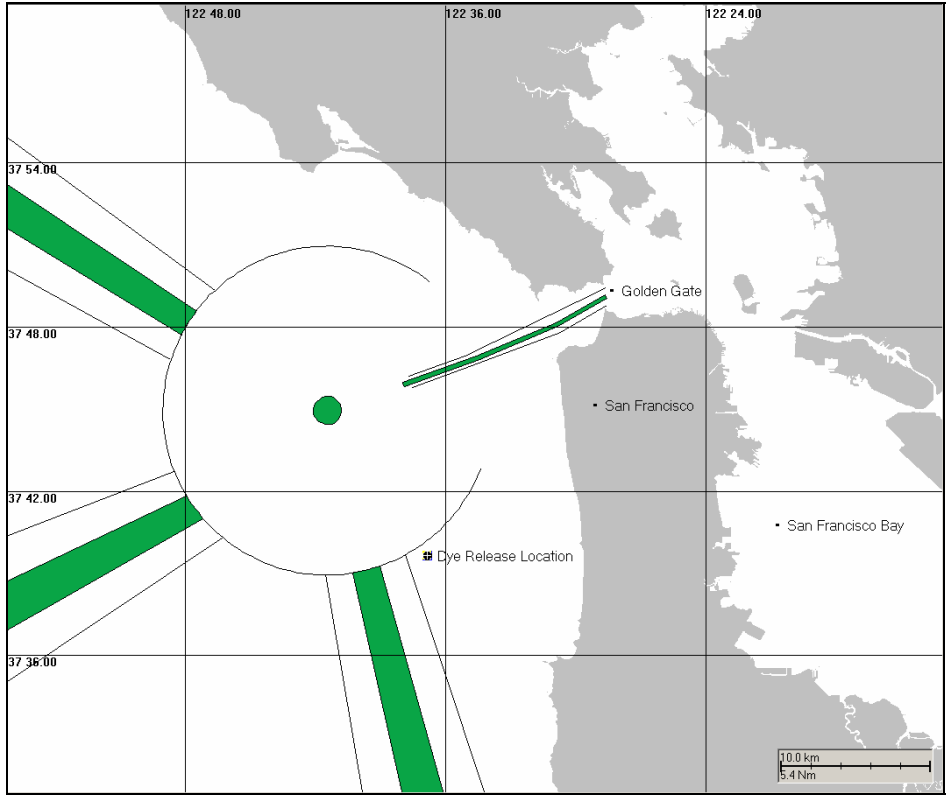


Figure 1-2. Dye release site offshore San Francisco, California.

2. Objectives

The specific objectives of the project were to:

1. Develop understanding of small-scale transport processes important to fate and transport modeling used in oil impact analysis, (i.e., near-surface transport and dispersion (mixing), based on literature review and field studies);
2. Provide detailed measurements of dispersion of dye, from which horizontal and vertical diffusivities are calculated (i.e., with greater sampling frequency and resolution than is frequently performed);
3. Develop algorithms quantifying small-scale transport processes based on measurable oceanographic and meteorological data that can be included in oil fates models;
4. Evaluate the efficacy and reliability of HF Radar and drifters for providing near-surface current input data to oil spill models such as SIMAP (French McCay 2004) by comparison of predicted trajectories with dye movements;
5. Investigate methods for assimilating HF Radar and drogued drifter data into existing oil spill models such as SIMAP (French McCay 2004);
6. Evaluate model-predicted transport and dispersion through comparison of measured dye concentrations over three dimensional space and time as a test of algorithms that may be incorporated into SIMAP and other oil transport and fate models which use bulk coefficients to parameterize mixing;
7. Describe uncertainty of these algorithms and estimates; and
8. Publish the data sets and algorithms for use in other circumstances, locations, and models.

3. Methods

3.1 Preparation for and Performance of Field Experiments

Before each cruise, a detailed cruise plan was developed that reviewed the objectives and approach, identified protocols and sampling procedures, specified personnel roles and contact information, and provided locations and timing for the dye release and sampling. These cruise plans were distributed to all involved personnel several days in advance of each cruise, and logistics were discussed in a pre-cruise meeting the day before each field experiment to work out final details, mitigate any problems arising related to equipment or environmental conditions, synchronize watches and internal clocks in all computers and instruments, prepare premixed dye concentrates, and complete instrument calibrations, as necessary.

Methods for the experiments off Point Loma are described below, with specifics for the Safe Seas exercise on 9 August 2006 discussed separately, as appropriate.

3.1.1 Permitting

The permitting process for this project began with providing the Research Plan and detailed Scope of Work to the U.S. Region 9 Environmental Protection Agency (EPA) office for environmental review under the Marine Protection, Research and Sanctuaries Act (MPRSA, 33 USC 1411 et seq.) and the EPA Ocean Dumping Regulations (40 CFR 220-228). The EPA found that the project was “not expected to result in any adverse impact to the local marine environment... and that the proposed study and work may proceed as scheduled” (Ota, 2006). With this finding and additional input provided by PECI and CA OSPR, NOAA was able to proceed with its required review under NOAA Administrative Order (NAO) 216-6, Environmental Review Procedures, which specify that prior to contract award, all proposed projects be reviewed with respect to environmental consequences on the human environment as required by the National Environmental Policy Act (NEPA). The internal NOAA review found that as proposed, the field experiments would hold “no potential for significant environmental impacts.” “As such, it [the project] should be categorically excluded from the need to prepare Environmental Assessment or Environmental Impact Statements by section 6.03.c.3(d), Administrative or Programmatic Functions, which include basic and applied research and research grants.”

These permitting activities are briefly mentioned here to remind future investigators of the potential project delays that can occur with field programs involving any type of chemical release. Such delays may result in unbudgeted costs, which can be significant, depending on the permitting complexity and the number of different agencies involved (Payne *et al.*, 2005). For this project, it took over two months from the initial project award notification until these reviews could be completed, the contract signed, and contractually-authorized work initiated.

3.1.2 Dye Deployment

Point Loma Experiments

A series of seven fluorescein dye releases were completed off the coast of San Diego, CA (Table 3-1). In these studies, the dye was sprayed on the water surface at an average water depth of 40 fathoms (73m) in federal waters three miles southwest of Point Loma, San Diego (Figure 1-1). The 10.4 m (34 ft) MSRC vessel, *Response 2*, was utilized for all the controlled spraying applications at sea.

Table 3-1. Dye deployment cruises off Point Loma, San Diego.

Date	Location	Dye/Drifter Deployment Vessel	Drogue Depths (m)	Sampling Vessel	Sponsoring Organization
November 8, 2005	32.620793° N 117.289783° W	MSRC <i>Response 2</i>	1	SIO Whaler	CA OSPR
March 21, 2006	32.593133° N 117.270197° W	MSRC <i>Response 2</i>	1	USCG Munson	CA OSPR
March 22, 2006	32.601306° N 117.281688° W	MSRC <i>Response 2</i>	1 and 5	USCG Munson	CA OSPR
June 21, 2006	32.599452° N 117.283533° W	MSRC <i>Response 2</i>	2 and 4	USCG Munson	NOAA/UNH CRRC
June 22, 2006	32.600128° N 117.283021° W	MSRC <i>Response 2</i>	2 and 4	USCG Munson	NOAA/UNH CRRC
November 1, 2006	32.61684° N 117.28322° W	MSRC <i>Response 2</i>	2 and 4	SIO <i>Saikhon</i>	NOAA/UNH CRRC
November 2, 2006	32.61352° N 117.28108° W	MSRC <i>Response 2</i>	2 and 4	SIO <i>Saikhon</i>	NOAA/UNH CRRC

For each cruise, communications between the surface vessels and the observation aircraft had to be established before the dye was released to ensure that the aircraft was in the vicinity ready to begin photo-documentation and that sufficient ceiling was available to allow the aircraft to fly at progressively higher altitudes as the plume spread. This allowed the evolution of the plume to be photographed over time, while keeping the dye within a single photographic image. When this was not possible, it was necessary to take several images of the plume during each overflight, and paste them together in a mosaic pattern during later data processing.

During the experimental studies off San Diego, the non-toxic dye was released as a 400 or 4,000 ppm concentrate from two 2.4 m (8 ft) spray booms attached to two 1041 L reservoir tanks on the stern of the *Response 2*. The spray booms were fixed about 35 cm apart and were lowered parallel to the water surface on an outrigger deployed from the starboard side of the spray vessel (Figure 3-2). For each experiment, a total of 2,082 L (~550 gallons) was discharged over a 16-24 minute period as the application vessel made ever-increasing diameter turns (to starboard) in a growing spiral pattern to avoid transiting through or over the freshly applied dye. A positive displacement pump plumbed into the base of each 1,041 L reservoir tank was used to deliver the dye to the spray booms at an even rate. Power for the pumps was provided by a portable 120 volt AC generator.



Figure 3-2. Fluorescein dye release from the spray booms on the starboard side of the MSRC *Response 2* (left) and the appearance of the dye mixing into the water surface six minutes after release on 22 June 2006 (right).

Safe Seas Experiment

The fluorescein dye release off the coast of San Francisco during the Safe Seas exercise on 9 August 2006 was sprayed on the water surface from a PVC pipe held over the side of the vessel. The initial shape of the dye was not a circle, as would be desirable, but more in an irregular pattern resembling a snake (See Appendix B.9, Figure B.9-1).

3.1.3 Dye Concentrate Preparation and On-Board Mixing

Point Loma Experiments

Keyacid Fluorescein Powder (Item No. 801-073-51) from Keystone Aniline Corporation (Chicago, IL) was used for all the dye deployment experiments. To facilitate mixing and transfer of the powdered dye to the *Response 2*, a concentrated slurry (still containing some solids) of the dye was first premixed in two carboys using fresh water as shown in Table 3-2. The concentrated slurry from each of the two carboys was then transferred into one each of two 1,041 L (275 gal) reservoir tanks on the rear deck of the *Response 2*, and the carboys were rinsed with at least seven carboy-volumes of fresh water to ensure quantitative transfer. The initial slurry and freshwater rinse volumes were calculated and carefully measured to ensure that the final density of the mixed dye (after filling each of the reservoir tanks to 1,041 L with seawater from the MSRC dock) would have the nominal densities shown in the table. After blending the concentrated dye slurry, freshwater rinses, and seawater at the MSRC dock, the contents were thoroughly mixed by the rocking action of the boat during transit to the release site 3 nautical miles west-southwest of San Diego. Upon arriving on station, there were no longer any solids in the dye concentrates contained in the reservoir tanks.

Table 3-2. Weight of fluorescein dye and freshwater/seawater volumes used for each experiment.

Date	Fluorescein kg	Freshwater Vol. L	Seawater Vol. L	Target Density kg/m ³
11/08/2005	0.8333	34.5	2,048	1,024
03/21/2006	9.072	375	1,707	1,024
03/22/2006	9.072	375	1,707	1,024
06/21/2006	9.072	748	1,330	1,020
06/22/2006	9.072	748	1,330	1,020
11/01/2006	9.072	748	1,330	1,020
11/02/2006	9.072	748	1,330	1,020

Based on visual observations from the *Response 2* during each dye deployment, it appeared that our target dye density of 1,020-1,024 kg/m³ was appropriate because the dye did not form a surface microlayer and instead immediately mixed into the upper 0.5-1 m of the water column. CTD and fluorescence data then indicated that the dye mixed into the upper mixed layer over a 20 minute period (additional details are presented below and in French McCay *et al.*, 2007). From the immediate color change (from dark red to fluorescent green and our knowledge of the standard solutions prepared for fluorometer calibrations – Sections 3.1.10 and 4.1) along with the observed mixing, we estimate an initial dilution of at least 1:2500 into the receiving seawater with a typical density of 1,025 kg/m³. Thus, even though the initial dye concentrate may have had a (maximum) density anomaly of 5 sigma-t (compared to the receiving water), it was observed to rapidly mix within minutes to an estimated density anomaly (based on the area covered and the observed mixing depth) of 0.0016 sigma-t. This value is insignificant given the energetics of mixing present at the upper ocean. In all of the experiments, the diluted dye behaved as if it were neutrally buoyant, although there was also evidence of Langmuir circulation cells and near-surface current shear controlling the dye distribution in the upper mixed layer (see Section 4.3, Appendices B and G, and French-McCay *et al.*, 2007). On the other hand, if the powdered fluorescein dye were simply mixed directly into seawater, the resulting mixture would have been too dense, so the weight of the dry powdered dye had to be offset with the indicated volume of fresh water.

In the November 2005 experiment, the desired dye concentration was 400 ppm, but it was not possible to follow the dye plume for more than 2-3 hours. Therefore, for all subsequent experiments, a target dye concentration of 4,000 ppm was used.

Safe Seas Experiment

The fluorescein dye release off the coast of San Francisco during the Safe Seas exercise was prepared by Louisiana State University (LSU) scientists in a similar manner to the Point Loma experiments (similar dye:seawater:freshwater ratios were used).

3.1.4 Photography

Observations from the California Department of Fish and Game fixed-wing aircraft (twin engine, Partenavia) were used to orient the sampling effort and photo document the movements of dye relative to the drifters. In the first field experiment completed in November 2005, the pilot and two observers were able to record the deployment and drift of the dye and drifters, and take multiple digital pictures. Photos were made using the visual light spectrum from a hand-held digital camera, as well as a multi-spectral camera (DMSC-MK2 sensor made by SpecTerra Ltd., Australia; http://www.oceani.com/products_service/aerial_sensor_specs.html; operated by Ocean Imaging, Inc.) fixed to the plane and pointing downward through a viewing window. During all subsequent flights a Nikon digital camera fixed to the plane and pointing downward through the viewing window was used.

Dye Plume Shape Extraction Methods and Georeferencing

The aerial photographs taken during the 2006 dye experiments were processed to determine the size, position and orientation of the dye plume over the course of each experiment. The image files were geo-referenced using ESRI's ArcView Geographic Information System (GIS) software, assuming the GPS location was at the center of the image, that the plane was perfectly level, and estimating the ground size of the image and length scale from recorded altitude at the time of the photograph. Heading data for the plane were also recorded during the experiment and used to rotate the images appropriately after they were geotransformed. During the 21 March 2006 experiment, location and heading information was not digitally appended to the images and was instead transcribed to an excel worksheet. This process introduced some error and is likely responsible for the higher degree of "jumpiness" observed in the dye plume shapes from that day (see discussion of results below). However, the dimensions (area, major axis and minor axis) are the basic data used for analysis of dye dispersion rates, and these are not affected by the absolute position.

All georeferencing was performed using the UTM zone 11N coordinate system. This provided more accuracy during calculations and transformations as latitude/longitude conversions were avoided. The following steps were taken:

1. Given field of view (f) and altitude(h) the following equation was used to calculate the swath width (sw) of the image (assumed perpendicular to the waters surface):

$$sw = 2 * h * \tan\left(\left(\frac{\pi}{180}\right) * \left(\frac{f}{2}\right)\right) \quad (1)$$

2. The swath width can then be divided by the number of pixels in the horizontal (in this case 3008) to calculate the pixel size (p) for the image.
3. Given the pixel size, the vertical height of the image can be calculated by multiplying p by the number of pixels in the vertical.
4. It was assumed that the position (latitude, longitude) recorded for each image represented the position of the center of each image. Using the UTM 11N projection (which provides coordinates in meters to simplify measurement), the four sides of the

image were calculated using the following equations, with x_i being the central longitudinal coordinate, y_i being the central latitudinal coordinate, y being the image “height” and x being the image “width”:

$$\begin{aligned}
 \text{rightedge} &= (x_i + \frac{x}{2}) \\
 \text{leftedge} &= (x_i - \frac{x}{2}) \\
 \text{topedge} &= (y_i + \frac{y}{2}) \\
 \text{bottomedge} &= (y_i - \frac{y}{2})
 \end{aligned}
 \tag{2}$$

5. The result is the production of 6 values (centerX, centerY, right, left, top and bottom) for each image. The values were exported to text files (one for each value type), as were the name and heading (if available) value types.
6. A small custom application was used to automatically generate individual text files for each image based on the text files produced in step 5. Each text file was named for the corresponding image and contained 5 rows of data. Each row contained transformation data in the format: fromX, fromY, toY, toX. The files have a transformation pair for each of the 4 corners and the center point of the image. If heading data are available, there is a 5th column in the file which contains header information.
7. The transformation files were fed into an automatic georeferencing script (custom) which allowed batch-georeferencing of the images and export to geotiff files. The files are transformed spatially (moved and resized based on the transform points in the individual text file) first and then rotated.

Once the images were georeferenced, image processing software (ENVI 4.3) was used to extract the dye plume from each image and create a “shape file” (i.e., a trace of the outline, in the commonly used format employed by ESRI’s and other commercial GIS software systems) representing the extent of the dye plume. The software performed a “band math” operation to create a single band image, which showed the dye in sharp contrast to the surrounding water. This intermediate image was then “classified” by the software to extract the initial dye shape file. The shape file was then post-processed to remove noise and calculate the area, minor axis, and major axis for the plume over the course of the experiment. Figure 3-3 shows the workflow.

The dye images were also interpreted to show the variable intensity of the dye, as integrated by the aerial photograph. The data were scaled arithmetically into 10 intensity “bins” of equal range, by dividing the maximum intensity observed on a given experimental date by 10.

Dye Plume Measurements and Estimation of Advection and Diffusion Rates

The georectified images were used to describe the experiment, document spreading of the dye plume in the cross- and down-wind directions (which corresponded to either the major and minor axes in all experiments except for 22 March 2006 where the major axis was at an angle to the wind), and estimate horizontal advective movements and turbulent dispersion of the dye. The

georectified aerial photo images (as shape files) and centroids (spatial centers weighted by mass) of each image were mapped to measure advection, and compared to drifter movements, HF-Radar predictions of current transport, and estimated wind drift using algorithms developed from existing hydrodynamic studies (and used in the SIMAP model). Methods for estimation of the dispersion rates are in Section 3.2.1 below.

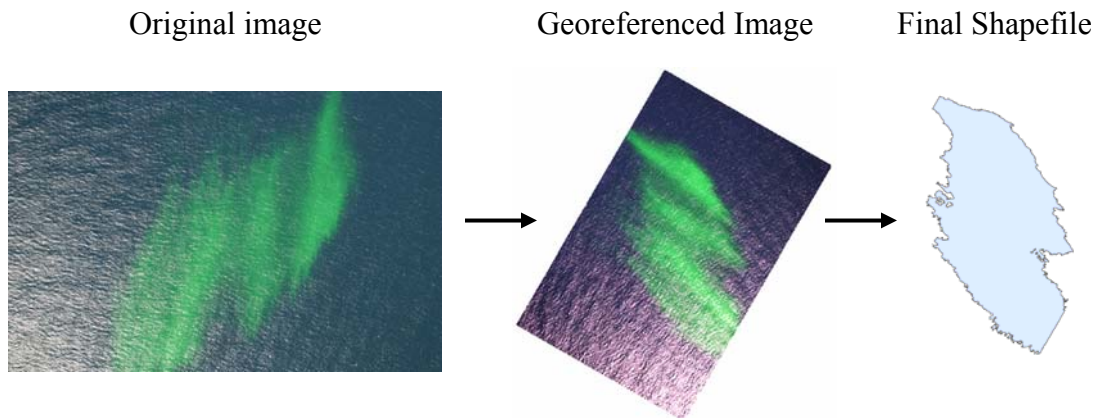


Figure 3-3. Aerial photograph processing steps.

3.1.5 Geographical Position Data

Garmin WAAS-enabled Global Positioning System (GPS) navigational instruments were used to determine position and time of dye/drifter deployments and sampling efforts aboard all research vessels. All units were set to internally log vessel position at 10 second intervals over the entire sampling effort. For a typical transit speed of 1.5m/s, this resulted in a new position every 15m. In addition, position, time, and depth were manually recorded at each sampling location for the beginning and end of each horizontal or vertical profile, or any other sampling activity. Data from horizontal and vertical profiles of *in situ* fluorescence were combined using time and position data in order to characterize the movement of dye tracer at the surface and at depth.

Garmin GPS navigational instruments were also used to determine position and time of aerial photos and the path of the plane performing that surveillance. Latitude, longitude, and altitude were either combined with photos using time stamps or directly recorded with the digital image by the Nikon camera aboard the OSPR aircraft.

3.1.6 High-Frequency Radar (CODAR)

Point Loma Experiments

Three HF-Radar SeaSounder units operating at 24.80, 25.27 and 25.60 MHz (manufactured by Coastal Ocean Dynamics Applications Radar Ocean Sensors, Palo Alto, CA) are currently installed around the San Diego area at Point Loma, the south end of the Tijuana Estuary, and South Coronado Island (see Graber *et al.*, 1997 and Ohlmann *et al.*, 2007, for additional details). The depth of integration at this frequency range is ~0.25-0.5 m. Radial velocity components are recorded every 10 minutes for sectors that are 1.5 km in range by 5° in bearing using measured antenna patterns. Hourly radials are computed from the 10 minute data for each unit. Data from these systems are automatically processed on site before being transmitted, via wireless networks, in near real-time to SIO. Once at SIO, automated processing combines data from all available sites and hourly maps of zonal (u) and meridional (v) current velocities are produced at 1 km resolution. Current velocity data and maps are typically available within 15 minutes of measurement at remote sites. Data used in this analysis were filtered and objectively mapped (5-min maps of zonal (u) and meridional (v) current velocities -- also produced at 1 km resolution) as described in Kim *et al.* (2007).

Safe Seas Experiment

Ocean surface current maps from the high frequency (HF) radar installation, Central and Northern California Ocean Observing System (CeNCOOS), San Francisco Bay Region, were obtained for 9 August 2006 from Dr. Newell (Toby) Garfield of San Francisco State University via the Coastal Ocean Currents Monitoring Program - N. California Romberg Tiburon Center - San Francisco State University website for the Central Coast data: <http://online.sfsu.edu/~regan/COCMPData/CentralCoast/Ascii/Totals/>. Descriptions of the CODAR system for that region are available on the website.

3.1.7 Drifters

Point Loma Experiments

Drifters drogued at 1-, 2-, 4-, or 5-meters (Table 3-1) were released from the *Response 2* before, during, and (in some cases around the edge of the dye) after it was released. Drifter data used in this study were collected with a set of 10 Microstar drifters (Figure 3-4) that are GPS-located, reusable, cellular instruments developed specifically for high-resolution near-shore use (Ohlmann *et al.*, 2005). Physically, the drifters are comprised of a corner-radar-reflector type drogue attached to a surface float that housed the electronics. The roughly 85-cm diameter drogues were centered at the different depths in Table 3-1 during separate cruises in an effort to empirically determine the optimum depth for tracking the subsurface dye. Initially the drifters were drogued at a depth of 1 m. When it appeared that all drifters moved ahead of the dye, drogue depths were changed to 2-, 4-, and 5-meters, in attempt to get the drifters to better move with the dye patch.



Figure 3-4. Drogue (kite) tied with a 1-, 2-, 4-, or 5-m tether to the drifter floats/transponders (left) and release of a drogued drifter/transponder into the dye plume from the MSRC *Response 2* on 8 November 2005 (right).

The surface float is ~ 20 cm in diameter giving a drag-area-ratio greater than 41 (Niiler *et al.*, 1995). The drifters operate by determining their position every 10 minutes with the Global Positioning System (GPS), giving spatial accuracy to a few meters, which was sufficient for monitoring drifter and plume advection. Drifters were not used for estimating dispersion coefficients. Position data were transmitted in near real-time using the Mobitex terrestrial cellular communications system, a text messaging type network. Spatial accuracy of GPS and near real-time data availability made it possible to locate and recover the drifters even if they were not immediately visible from the water surface or the OSPR aircraft.

Safe Seas Experiment

Drifters were not available for deployment in the area of the dye release for this experiment.

3.1.8 Meteorological Measurements

Standard meteorological measurements were made at several established weather stations maintained by NOAA and SIO in the vicinity of San Diego and San Francisco (reported on the NOAA National Data Buoy Center [NDBC] website). Measurements include wind speed and direction (at <10-minute intervals and synthesized as hourly means), air and water temperatures, and wave conditions. Data were downloaded off the web in real time during and just after each field experiment. Estimates of the accuracy of these measurements are available on the NDBC website and in cited references.

In addition, for the San Diego experimental sites, hourly wind speeds and directions were obtained from the Coupled Ocean/Atmosphere Mesoscale Prediction System (COAMPS[®]) model (developed by the Marine Meteorology Division [MMD] of the Naval Research Laboratory [NRL] – see Appendix E.1 for additional information).

3.1.9 *In situ* Measurements of Water-Column Stability and Plume Behavior – Point Loma Experiments

Immediately after the dye was released and the drogued drifters were deployed in the center and around the edge of the plume, the MSRC *Response 2* moved to the side of the experimental zone and remained on station occasionally circumnavigating the plume while obtaining GPS track data. At the same time, detailed across- and down-plume profiling was initiated by the smaller sampling vessels identified in Table 3-1. These vessels had a draft ranging from 12-18", and conducted transects at speeds between 1-2 knots to minimize wake induced stirring of the dye plume. Close examination of the aerial images did not reveal any vessel induced perturbations in the dye patch, and the initial mixing of the dye immediately after surface application suggested that the ocean mixing was much stronger than what may be induced by the sampling vessels.

Transects through the dye plumes were conducted to roughly follow the major and minor axes of the plumes after each deployment. Typical transect speeds were 1-2 knots. Separate instruments were used for *in situ* dye tracking of UV/fluorescence over the horizontal and vertical space due to limitations of each system to sample these specific environments. All three systems were deployed from the same sampling vessel during each cruise (Table 3-1).

CTD Measurements

Fixed-position vertical profiles were sampled by SIO using a CTD (conductivity, temperature, and depth) package in order to vertically profile the water column, determine the density structure (from which mixed layer depth may be inferred), and determine the general characteristics of the water column based on the following sensors:

- Conductivity using Sea-Bird, SBE 37-SM
- Temperature using Sea-Bird, SBE 37-SM
- Depth using Sea-Bird, SBE 37-SM pressure sensor manufactured by Druck, Inc.
- Fluorescence of fluorescein dye using Wet Labs, ECO FL-UR fluorometer
- Beam Attenuation using Wet Labs, C-Star transmissometer

The CTD was deployed from either the SIO or USCG sampling vessels (Table 3-1) during all the southern California studies to determine the mixed layer depth, an important variable in dispersant monitoring. The CTD was deployed to a depth of 30 m in the study region prior to dye release, and then to a depth of 10 m several times in the middle and adjacent to the dye plume during transects completed during each experiment.

The CTD was calibrated by the factory prior to deployment (conductivity, temperature, and depth), with additional five-point fluorescence intercalibration with the USCG Turner A-10 Fluorometers as described in Sections 3.1.10 and 4.1 (Instrument Calibration and

Intercalibration) and the project-specific Quality Assurance Plan (QAP, Revision 2, February 2006). Instrument accuracy and resolution were based on manufacturer specifications:

- Conductance: sensor accuracy 0.003 mS/m, sensor resolution 0.0001 mS/m, required resolution for data interpretation 0.01 mS/m.
- Temperature: sensor accuracy 0.002 °C, sensor resolution 0.0001 °C, required resolution for data interpretation 0.001 °C.
- Pressure: sensor accuracy 1 db, sensor resolution 0.02 db, required resolution for data interpretation 0.5 db.
- Fluorescein fluorometer: excitation/emission 470/570 nm, sensor resolution 0.5 counts, sensor sensitivity 1 ppb, range 4000 ppb, linearity 99%R².

Time and position information collected during each experiment was transcribed into log files. Separate files were created for CTD cast position data and horizontal transect position data. Files are located in <ftp://ftp.mpl.ucsd.edu/pub/CORDC/outgoing/OSPR/YYYYMonth/LOGS>

USCG SMART Sampling at 1, 2, and 5 m

Horizontal profiles were taken by the USCG Pacific Strike Team using dual Turner Design model 10-AU, continuous flow systems at two discrete depths to measure dye fluorescence every second during the entire dye tracking survey (i.e., SMART Protocols). All data were continuously recorded on PC-based data loggers on board the sampling vessel. Instrument calibration procedures are presented in Section 3.1.10.

SIO High Resolution Profiling Fluorometer

A Wet Labs ECO FL-UR fluorometer was towed behind the sampling boat in an undulating mode between depths of 1 and 10 m controlled by a programmable down-rigger powered by a 12 volt battery (Figure 3-5). This system utilized an internal logging, *in situ* fluorometer, Wetlabs FLURRT, set to sample at ~3 Hz. A pressure sensor within the fluorometer allowed the depth of the measurement to be computed, and the system was time-synchronized with the vessel mounted Global Position System (GPS) so that data from undulating transects could be positioned to earth coordinates. The plumes were mapped by operating the sampling vessel along the long axis and across the growing dye plumes to track their evolution in space and time with a minimum of measurement-induced disturbance. Data from these transects were synchronized with the GPS position and analyzed to provide vertical-section views of the dye concentrations.

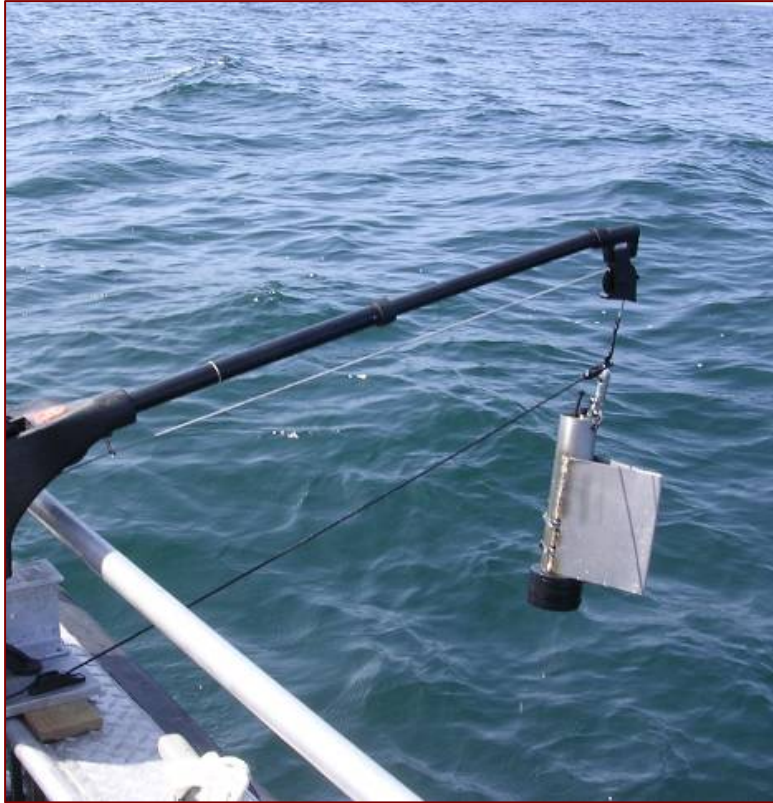


Figure 3-5. The Wet Labs ECO FL-UR fluorometer (with fin for proper orientation in the water when under way) and programmable downrigger to raise and lower the unit to preset depths over time.

3.1.10 Instrument Calibration and Intercalibration

Before and after each dye deployment cruise, the USCG Turner Designs model A-10 fluorometers used for the SMART Protocol measurements and the SIO Wet Labs model ECO FL-UR *in situ* fluorometers were subjected to five-point calibrations with fluorescein dye as outlined in the project-specific Quality Assurance Plan (QAP, Revision 2, February 2006).

Instrument calibrations and standardization:

- Full (five-point) fluorometer calibrations were performed for both the Turner Design 10-AU and Wet Labs *in situ* fluorometers two times during each field experiment. Usually this calibration was completed the day before the first of each two-day cruise event, and the morning after the second cruise. Five-point calibrations were completed by plotting instrument response vs. standard concentrations to ensure the accuracy of field measurements and provide assurance that the sensors were performing within the expected ranges during deployment. Standard fluorescein concentrations include 0, 0.25, 2.5, 25, 250 and 2,500 ppb. This suite of standards encompassed the linear range of both instrument types and allowed overlap in the middle part of the respective operating ranges.

- Instruments were also subjected to a battery and response check before each deployment to ensure data collection during profiles. Response checks were also completed for post-processing measurement validation.
- All calibration, maintenance, and service records were kept on file including any daily operational problems.
- Data collection rates for fluorometers were set to 1 second sampling times. The internal loggers record the time and sample value during each sample collection, and instrument clocks were set to a common time reference before each field experiment so that direct comparison of samples could be assumed based on time of a specific measurement.

Performance evaluation:

- Initial fluorometer evaluations were based on five-point instrument calibrations before each field experiment. Based on past *in situ* instrument performance there has been little drift (per manufacturer's specifications) for this type of equipment. Calibration runs were rejected and repeated if linear regression $r^2 < 0.90$.
- Post performance evaluations were completed for all data collected from the field sampling efforts and included evaluations of the measurements from the nearest neighbor during sampling and from overlapping measurements of sensors.

3.1.11 Communications

At-sea communications were accomplished using handheld California Department of Fish and Game radios, marine band radios, air band radios, and cell phones. This ability to use multiple modes of communication proved critical in all field experiments, as at times one or more forms of communication were unavailable.

3.1.12 Personnel Safety During Marine and Aerial Operations

All personnel were required to wear Personal Floatation Devices (PFDs) at all times when working on board MSRC, SIO, or USCG vessels (even at the dock). Hard hats were required during any operations with overhead cranes and booms. Steel-toed boots were required on MSRC vessels. All personnel complied with USCG regulations regarding on board operations and the release of any plastics or trash from any vessel. Safety and operational briefings were provided by MSRC, SIO, and/or USCG personnel before leaving the dock.

Only DFG personnel and preapproved non-DFG persons were permitted on board of DFG aircraft. Pre-flight safety instructions were given, and required DFG documents were signed before takeoff. All flight operations were operated in accordance with the DFG Air Operations Manual.

3.2 Modeling

The modeling analyses are described in Section 5. However, the data were processed for those analyses as describe in the sections below.

3.2.1 Photographic Images

The georectified aerial photo images (as shape files) were used to estimate dye plume expansion and horizontal dispersion. Linear growth of the down- and cross-wind dimensions of the plume over time (t), as measured from the images, was used to estimate horizontal dispersion coefficients, D_x and D_y in the downwind (x) and crosswind (y) directions, employing the methods described in Elliott *et al.* (1997; see also Csanady, 1973) where D_x and D_y are related to the variance (σ_x^2 or σ_y^2) of the Gaussian-shaped relationship between concentration and the length scale:

$$\sigma_x^2 = 2 D_x t \quad (3)$$

$$\sigma_y^2 = 2 D_y t \quad (4)$$

The values of σ_x^2 and σ_y^2 were estimated from the dimensional measurements of the dye plume images (as georectified shape files). The depth of view of the photos appeared to be to the depth of the dye plume (order 10m), as the visual edges of the dye corresponded with the edges defined by the concentration measurements using fluorescence. The edges of the dye plume, as defined by the image processing above, were assumed to cover 95% of the dye below the water surface, a reasonable assumption given the steepness of the gradients observed at the edges. (Measured fluorescence-based concentrations in transects also supported these assumptions.) Thus, the downwind length was assumed equivalent to $4\sigma_x$, and the crosswind length equivalent to $4\sigma_y$.

Following Elliott *et al.* (1997), trends of σ_x^2 or σ_y^2 over time were examined to determine if they were linear, such that D_x and D_y were constant in time, and so D_x and D_y could be estimated by linear regression of σ_x^2 or σ_y^2 on t . The trends were in fact linear with slopes providing estimates of $2D_x$ and $2D_y$. The regressions included intercepts, since the dye was not initially a point source, rather having an initial area and values of σ_x^2 or σ_y^2 at $t=0$.

Analogous calculations were made using the radial dimension of the plume, i.e., the square root of ($\sigma_x \sigma_y$). This would be useful for models where isotropic turbulence is assumed, i.e., where D_y is assumed equal to D_x .

Elliott *et al.* (1997) suggested that if D_x or D_y varied (decreased) over time, D_x or D_y versus t could be fit to a power curve, based on:

$$\sigma_x^2 = a_x t^{m_x} \quad (5)$$

$$D_x = (m_x a_x / 2) t^{m_x - 1} \quad (6)$$

$$\sigma_y^2 = a_y t^{m_y} \quad (7)$$

$$D_y = (m_y a_y / 2) t^{m_y - 1} \quad (8)$$

However, D_x and D_y (as well as $D_x = D_y$ based on radial spreading) were found not to vary over time in these experiments (see Section 5.3.4).

The dye images were also interpreted to show the variable intensity of the dye, as integrated by the aerial photograph. The images show evidence of Langmuir circulation, with cells sizes of varying scale. Langmuir cells are a series of alternating vortices of flow oriented roughly parallel to the direction of the wind. The surface flow moves downwind and to the right or left in alternating bands. A small convergence line forms between adjacent bands where the flow comes together and divergence zones form at the boundary between bands where the flow tends to separate (Langmuir, 1938; Smith, 1992). The dye intensities showed bands along divergences and convergences. Measurements of Langmuir cell dimensions were estimated from the images.

3.2.2 Mixed Layer Properties

The surface mixed layer depth and density structure are important determinants of the vertical dispersion rate. In general, the higher the slope of the density gradient with water depth, the more stable the water column and the slower the dispersion. The mixed layer depth is commonly derived from oceanic profile data using a threshold difference method. The depth at which density (σ_t) is more than 0.01 kg/m^3 from the surface value is often used to define the surface mixed layer in physical oceanographic studies (Thompson and Fine, 2003). However, this small density change consistently occurred at all depths in the waters where experiments were performed, whereas density profiles typically showed a dramatic increase in slope with depth where the density change was 0.2 kg/m^3 . Thus, the depth at which density was more than 0.2 kg/m^3 from the surface value was defined as the mixed layer depth in this study. The presence of such a gradient indicates that the “mixed layer” so defined was not in fact thoroughly mixed (and could potentially be called a “mixing layer”), but had some stability. This feature is common in situations of low winds, whereas the effect of solar heating at the ocean’s surface offsets the wind-driven mixing. Thus, stability of the mixed layer water column was examined.

Buoyancy frequency (Brunt-Väisälä frequency), N , a measure of water column stability, was estimated from the mean water density (ρ_w) in the mixed layer and the gradient of density versus depth (z) estimated by linear regression.

$$N^2 = g / \rho_w (\Delta\rho_w / \Delta z) \quad (9)$$

where g is the gravitational acceleration ($9.80665 \text{ m}\cdot\text{s}^{-2}$).

The change in wind drift speed with depth to 3m was calculated as an indication of vertical shear. The Richardson number (Ri) was calculated as an index of the strength of water column stratification. When Ri is small (typically considered so below 0.25), then velocity shear

$[(\Delta U / \Delta z)^2]$, where U is velocity at z] is considered sufficient to overcome the tendency of a stratified fluid to remain stratified, and some mixing will generally occur. When Ri is large, turbulent mixing across the stratification is generally suppressed.

$$Ri = N^2 / (\Delta U / \Delta z)^2 \quad (10)$$

3.2.3 Current Estimates Based on Drifters and HF Radar

The drifter waypoints were mapped to show their movements relative to the dye plume. The vector means of the individual waypoints were used to summarize the drifter speeds, directions and east (u) and north (v) components. The sums of the vectors over the time of the experiment indicated the predicted transport if the drifter data were to be used as input to a transport model.

HF-Radar velocity data (gridded to 1 km resolution and at 5 min intervals) were used as input to the SIMAP model to calculate trajectories for each experiment. As a summary of the transport, the HF-Radar velocity data in the rectangular area defined by the ranges of latitude and longitude where either the dye or drifters moved were averaged over the time of the experiment to indicate mean speed, direction, and predicted transport if the HF-Radar data were to be used as input to any transport model.

3.2.4 Dye Concentration Measurements

Data from transects measuring fluorescence were synchronized with the GPS position and analyzed to provide vertical-section views of the dye concentrations. The vertical dispersion rate was estimated from dye concentrations measured for each transect by fitting a Gaussian curve to the concentration versus depth data and its mirror image. The variance, σ_z^2 , of the dye concentration distribution was computed from:

$$\sigma_z^2 = [\Sigma C_z (z - z_0)^2 \Delta z] / [\Sigma C_z \Delta z] \quad (11)$$

An estimate of the vertical diffusion coefficient, D_z , was obtained for each transect time (t) employing the methods described in Elliott *et al.* (1997) where D_z is related to the variance (σ_z^2) of the Gaussian-shaped relationship between concentration and depth:

$$\sigma_z^2 = 2 D_z t \quad (12)$$

Following Elliott *et al.* (1997), trends of σ_z^2 over time were examined to determine if σ_z^2 increased linearly in time (i.e., D_z was constant in time), and so D_z could be estimated by linear regression of σ_z^2 on t . If D_z varied (decreased) over time, D_z versus t was fit to a power curve, based on:

$$\sigma_z^2 = a t^m \quad (13)$$

$$D_z = (ma/2) t^{m-1} \quad (14)$$

4. Results – Field Data

4.1 Fluorometer Calibrations and Comparison of Along-Plume Data Profiles – Point Loma Experiments off San Diego

The two Turner Design A-10 fluorometers used by the USCG for the SMART Protocol and the two SIO Wet Labs model ECO FL-UR *in situ* fluorometers used in the CTD package and the towed high-resolution profiling system were calibrated against fluorescein dye before and after each cruise event. Figure 4-1 presents representative data from the post-cruise calibration completed after the 22 March 2006 cruise. FLURRT18 was used in the CTD array, and FLURRT19 was the towed fluorometer used for detailed plume profiling with the programmable downrigger shown in Figure 3-5. Smart1 and Smart2 were the two USCG fluorometers used for horizontal transects at 1 and 5 meters, respectively. Clearly, all four fluorometers generated a linear response across the calibration range tested ($R^2 > 0.997$ in all cases), although the relative responses and calibration standard ranges were different. Specifically, the Turner fluorometers were more sensitive at lower concentrations (0 – 100 ppb), and they became non-linear above 200 ppb. The Wet Labs fluorometers were linear over a much wider concentration range (0 – 2,500 ppb), but slightly less responsive and somewhat erratic below 25 ppb. The data generated by the two different units for one instrument type were very comparable, and between the two different instrument systems, we were able to generate accurate data over a wide dynamic range

Because the two different fluorometer “systems” (i.e., Turner vs. Wet Labs) generated response curves with different slopes and intercepts, a scaling factor had to be developed to directly compare the data obtained by the two different systems. Once this was accomplished, however, very similar results were obtained by the two different instrument types. Figure 4-2 shows the SIO/Wet Labs fluorometer profile vs. the USCG SMART Turner fluorometer profile obtained during an along-plume transect on 22 March 2006, with both instruments sampling at the same and constant depth. Very comparable and representative data were obtained as the instrument systems moved in and out of the patchy dye plume, and clearly the data from either system can be used for estimating plume dimensions, dye concentrations, and dilution/mixing over time.

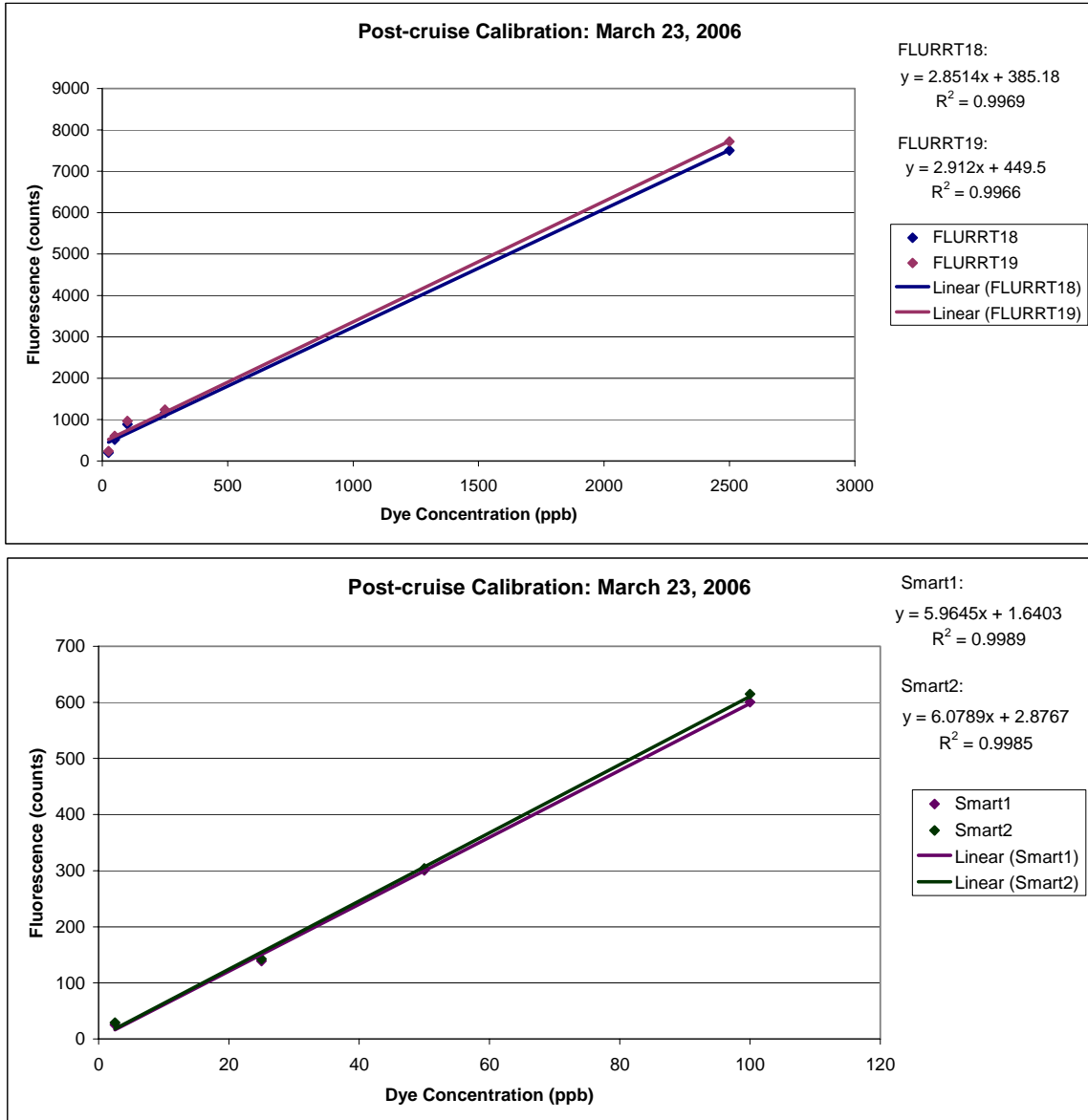


Figure 4-1. Post Cruise Calibration Plots Obtained on the SIO Wet Labs Model ECO FL-UR *in situ* Fluorometers (FLURRT18 and 19) and the USCG SMART Protocol Turner A-10 Fluorometers (Smart 1 and 2) after the 22 March 2006 Dye Studies.

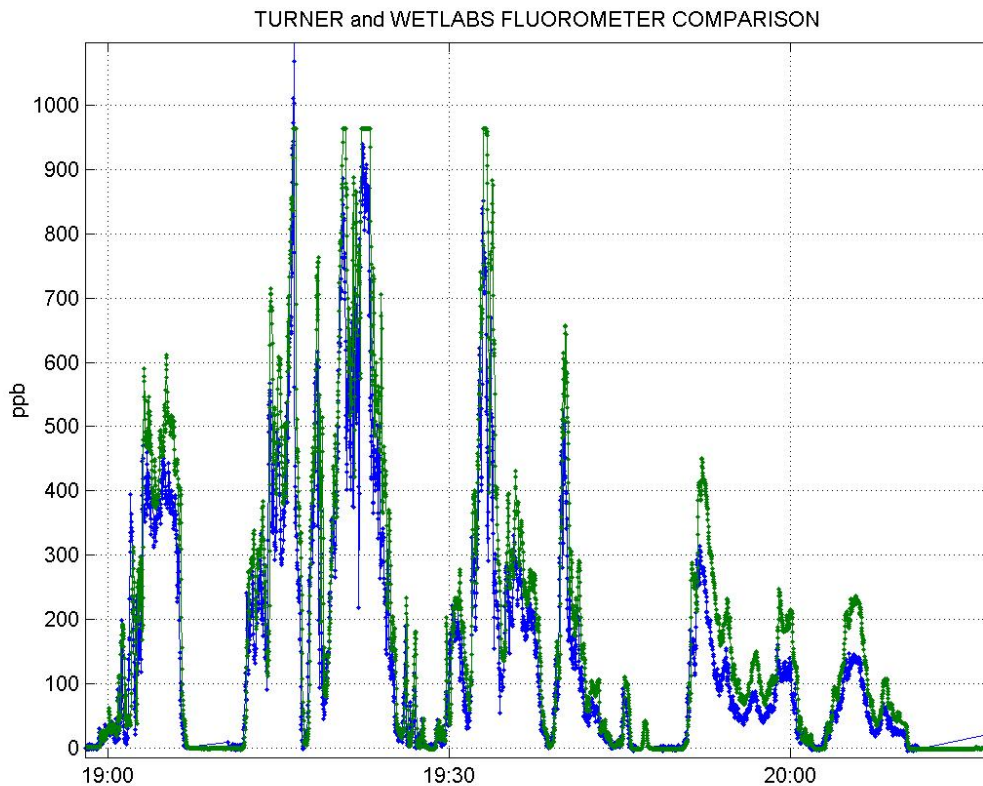


Figure 4-2. Along-plume transect data obtained at a constant depth with the Turner A-10 (green) and Wet Labs (blue) Fluorometers.

4.2 Horizontal Movements and Expansion of the Dye – Point Loma Experiments off San Diego

The locations and times for the seven fluorescein dye experiments completed off the coast of San Diego, CA are in Table 4-1. Summaries of the results are in Sections 4.2.1 to 4.2.7 below, while detailed results and additional figures describing them are contained in Appendices A through G.

Appendix A contains the geographical position (GPS) data for all the CTD sampling stations and selected MSRC *Response 2* ship tracks (circumnavigating the dye plumes over time) and plane tracks from aerial observations/photo documentation. Appendix B contains the photographic image data, including detailed methods, example images, and summaries of the dimensions of the dye over time estimated from the images. All the images and derived products (such as shape files; Appendix B) are available on an ftp site hosted by the Coastal Observing Research & Development Center at SIO (<ftp://ftp.mpl.ucsd.edu/pub/CORDC/outgoing/OSPR>).

Table 4-1. Dye Deployment Cruises off Point Loma (San Diego).

Date	Location	Time Start Dye Release (Local)	Dye Release Duration (min)	Experiment Completion Time (Local)
November 8, 2005	32.620793° N 117.289783° W	10:26	16	16:15
March 21, 2006	32.593133° N 117.270197° W	11:43	25	13:50
March 22, 2006	32.601306° N 117.281688° W	10:04	16	14:45
June 21, 2006	32.599452° N 117.283533° W	12:11	16	16:00
June 22, 2006	32.600128° N 117.283021° W	14:49	15	17:50
November 1, 2006	32.61684° N 117.28322° W	11:52	16	15:30
November 2, 2006	32.61352° N 117.28108° W	11:19	18	15:00

Appendix C contains summaries of the HF-Radar data. Figures of the mean current at hourly intervals during each experiment are available on the SIO FTP site (See Appendix C). Appendix D contains summaries of the drifter movements. Figures describing drifter movements during each experiment are also available on the SIO FTP site (See Appendix D). Appendix E contains wind speed and direction data for wind stations near each experimental site.

Appendix F contains plots of oceanographic data from CTD casts measuring salinity, water temperature, and water density versus depth. CTD casts were taken before the dye release and outside of the plume area in order to characterize the structure of the water column, the pycnocline depth, and the surface mixed layer depth. In the November 2005 and March 2006 experiments, the CTD apparatus was also used to measure fluorescence as a function of depth at specific stations located by longitude and latitude. Thus, the fluorescence data for the November 2005 and March 2006 experiments are presented graphically in Appendix F, along with the CTD data for those dates. In the June 2006 and November 2006 experiments, all fluorescence data were collected with the high resolution profiling fluorometer, which was raised and lowered as the sampling vessel transited the plumes. These data are presented graphically in Appendix G.

The movements of the dye and the shapes and expansion rates of the dye plumes were mapped using shape files from the image processing steps described in Section 3.1.4. Additional details of the methods are in Appendix B.1). The centroids (spatial centers weighted by mass) of each shape file representing an image of the dye plume at a certain time describe the dye movements. Maps of the centroids and data describing the dye dimensions in each image are in Appendix B.

The georeferencing of each image incurred a certain amount of error due to the limitations of the collection method. The magnitude of all general error sources was dependant on the altitude of the plane when the image was captured. The general error sources included:

1. Deviation of camera orientation from perpendicular to ground: This was dependant on the pitch and yaw of the plane, as well as the altitude at the time a particular image was taken. The magnitude of the deviation differed by image and varied from centimeters to kilometers.
2. Location of dye plume within the image frame: This was dependant on how far off center the dye was, the rotation of the image, and the altitude of the plane at the time the image was taken. The approximate magnitude of this error was generally in the 0 – 100's of meters range.

4.2.1 November 8, 2005 Experiment

The georectified aerial photo images (as shape files) mapped to document the plume expansion and movements are compared to drifter locations at corresponding times for the 8 November 2005 experiment (Figures 4-3 and 4-4). The downwind and down-current (parallel to downwind in this experiment) expansion of the plume is evident, as are features related to Langmuir cells along the leading (eastward) edge. (See also Appendix B.2.1, Figures B-5 to B-7.) The wind was from the southeast (168°) at 6.1 m/s (12 kts) based on the nearest NOAA offshore buoy. In La Jolla, the wind was from the south (187°) at 5.4 m/s (11 kts). (Wind records are in Appendix E.)

The 8 November 2005 experiment began at 10:26AM PST and ended approximately 4:15 PM PST. The dye plume expanded and moved primarily to the north and northeast throughout the duration of the experiment. Figure 4-3 contains shape files of the four images of the dye plume, taken at times early in the experiment. Individual images for this experiment are in Appendix B.2.1, along with a close-up view of the four shape files describing the dye positions photographed. The CTD casts and corresponding times in Figure 4-3 represent the dye plume movement for the rest of the experiment. (See also Appendix A.2, Figure A-1.) The drifters followed the same path as the dye (Figure 4-4), but moved faster than the dye, approaching the coast of Point Loma north of the dye at about 4:15PM. All of the drifters used in this experiment were drogued at 1 m. Details of the times for the drifters are in Appendix D.2, as compared with the movements of the dye recorded by the four images and the positions of the CTD casts.

The estimated vectors from the HF-Radar data (Figure 4-5 and Appendix C.1) show northwestward and then northward currents during the experiment, in line with the movements of the dye and drifters (Appendix B.2.1 and Appendix D.1). The total movement indicated by the HF Radar during the time the drifters were in the water was in the same direction but slower than the drifter movements. Unfortunately, the dye concentrations were not high enough to photograph over the entire experiment. However, the CTD cast locations taken in the dye plume

indicate the dye movements. The HF-Radar vectors indicate a trajectory in line with but slower than the dye movements (Appendix C.1, Figure C.1-1). The drifters moved in line with the dye but faster than the dye, ahead of the plume (See Sections 4.5 and 5 for analysis and discussion.)

The dye patch spreading rates, as area versus time and along the down-wind and cross-wind axes, are in Appendix B.2.2. The dye patch spread to about 21,000 m² by an hour after release (Figure B.2-9). The dye patch stretched rapidly in the down-wind direction, to about 230m after one hour (Figure B.2-10). The spreading in the cross-wind direction was very slow; the dye being laid in about a 120-m wide patch, which did not significantly increase in length along the cross-wind axis over the first hour after release (Figure B.2-11).

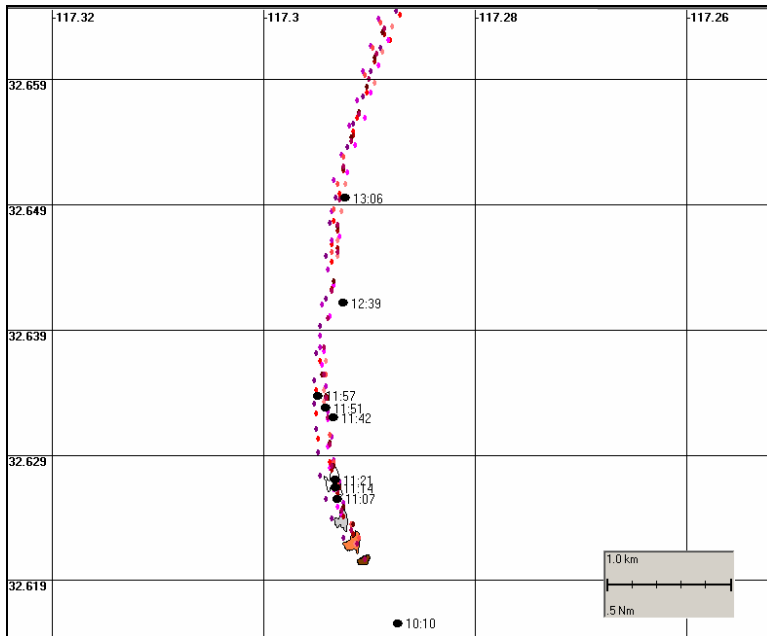


Figure 4-3. Locations of the dye over time in the 8 November 2005 experiment, as interpreted from the aerial photographs. Waypoints of drifter movements (drogued at 1m) are indicated as diamonds (red and purple shades). Black circles and times indicate locations of the dye during CTD casts.

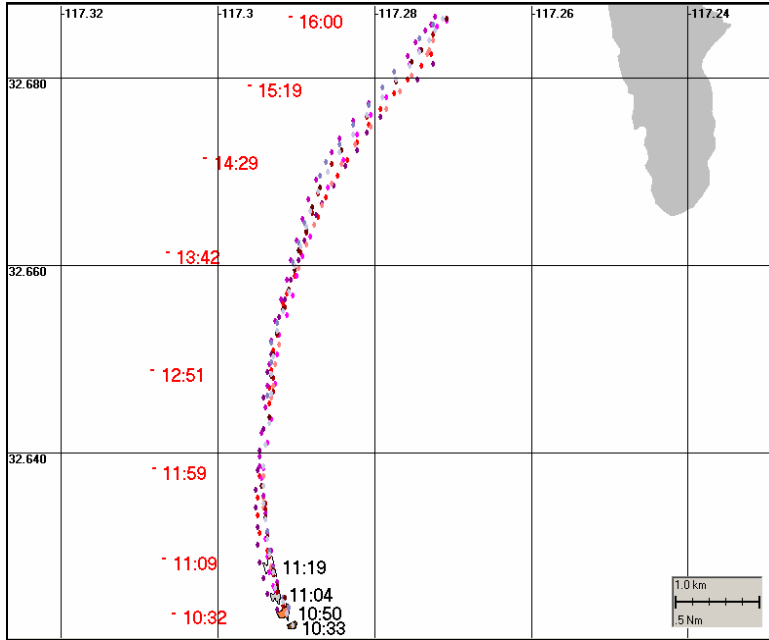


Figure 4-4. Dye plume dimensions and movements over time, and drifter tracks represented by diamonds (all 1-m deployment depth) for the 8 November 2005 experiment. Four images of dye plume are shown with corresponding times (black font). Corresponding times for drifter tracks (diamonds) are in red font.

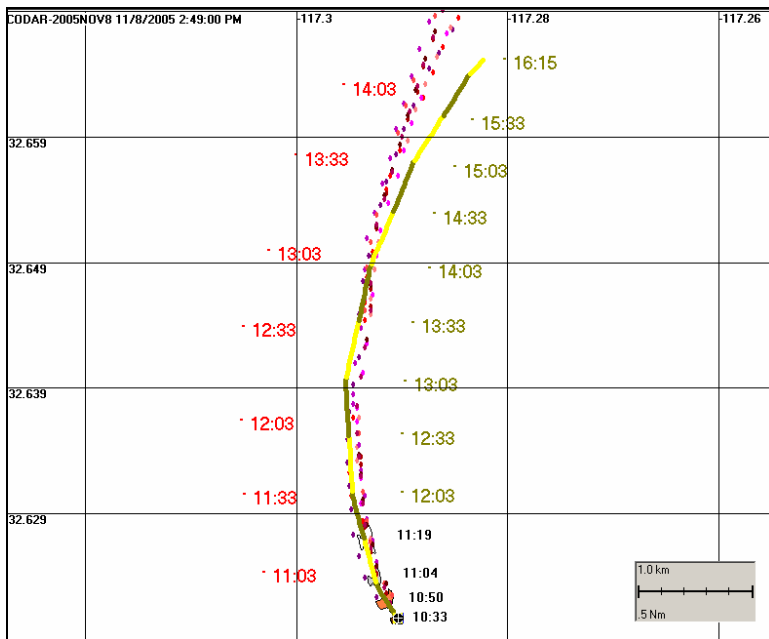


Figure 4-5. Trajectory of a neutrally-buoyant constituent using the HF-Radar vectors up to 16:15 PM (yellow and green line, alternating color by 0.5 hour intervals, with times in green font) compared to drifter movement (red diamonds with times in red font) for the 8 November 2005 experiment.

4.2.2 March 21, 2006 Experiment

The 21 March 2006 experiment began at 11:44AM PST, approximately 3-4 hours after an intense squall passed through the area, and ended at approximately 1:50 PM PST. The wind was from the west-northwest (302°) at 6.5 m/s (13 kts) based on the nearest NOAA offshore buoy. In La Jolla, the wind was from 288° at 5.2 m/s (10 kts), whereas the in COAMPS model for the time and location of the experiment, winds were from 286° at 7.2 m/s (14 kts). (Wind records are in Appendix E.) The sea-state during the experiment was quite confused, with cross-chop and irregular swells from several directions.

The georectified aerial photo images (as shape files) mapped to document the plume expansion and movements are compared to drifter locations at corresponding times for the 21 March 2006 experiment (Figures 4-6 and B.3-1 in Appendix B). Aircraft headings on 21 March 2006 were not recorded digitally. Hand written heading data on these dates were tied to the other digital image information based on time. Thus, particularly on 21 March (Figure B.3-1), the images appeared to “jump” around on the map. In Figure B.3-1, shape file locations that were improperly located (based on being off the track of the drifters with known GPS readings) are plotted as tracings. In the field, the drifters were observed to remain in or just ahead (downwind) of the dye plume. However, while some of the dye positions in Figure B.3-1 are inaccurate, the sizes of the shape files of the images remained relatively accurate (subject only to the error in the aircraft altitude data). Individual images for this experiment are in Appendix B.3.1. Figure 4-6 includes only the images that were lined up with the drifters and so approximately correct in their location.

All of the drifters used in this experiment were drogued at 1 m. Details of the times for the drifters are in Appendix D.2, whereas times and dimensions of each of the images of the dye are in Appendix B.3.2.

In Figure 4-6, the down-current (as indicated by the movement of the drifters) expansion of the plume is evident, as are features related to Langmuir cells along the leading (eastward) edge. (See also Appendix B.3.1, Figures B.3-3 to B.3-4; Appendix B.3.3.) Langmuir cells appeared to be at two scales: more prominent cells about 34 m across from apparent down-welling (indicated by relatively high intensity in Figure B.3-4) and smaller cells about 11 m across. The cells were oriented $19-35^\circ$ to the right of down-wind on average (depending upon wind record used).

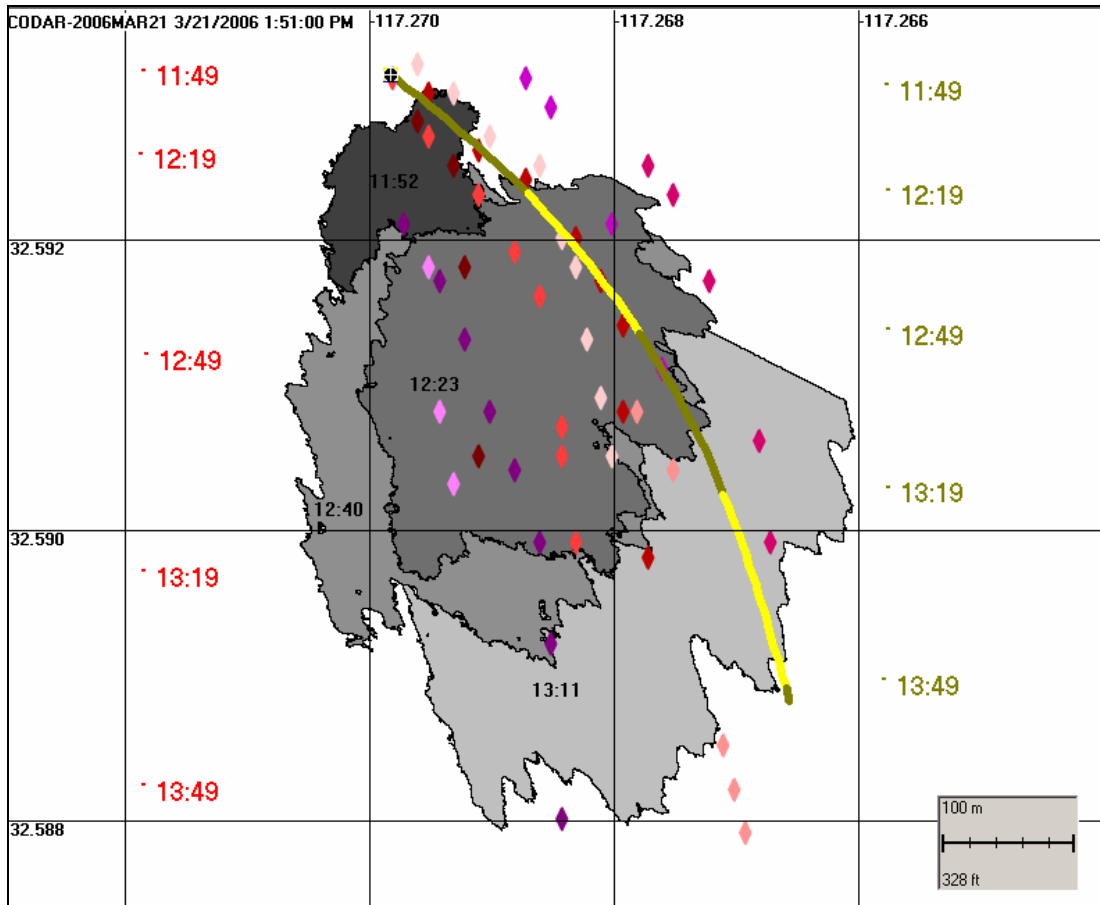


Figure 4-6. Locations of the dye over time in the 21 March 2006 experiment, as interpreted from the aerial photographs. Waypoints of drifter movements (all drogued at 1m) are indicated as diamonds, with times in red font. The trajectory of a neutrally-buoyant constituent using the HF-Radar vectors up to 13:49 (yellow and green line, alternating color by 0.5 hour intervals, with times in green font) may be compared to drifter and dye movements.

The trajectory of a neutrally-buoyant constituent transported by vectors from the HF-Radar data (also in Figure 4-6) shows southeastward current during the experiment, just to the east and nearly in line with the movements of the dye and drifters (see also Appendix C.2, Appendix B.3.1 and Appendix D.2). The total movement indicated by the HF Radar during the time the drifters were in the water was about the same speed as the drifter movements. (See Sections 4.5 and 5 for analysis and discussion.)

The dye patch spreading rates, as area versus time and along the down-wind and cross-wind axes, are in Appendix B.3.2. The dye patch spread to about 200,000 m² by 2.5 hours after release (Figure B.3-5). The dye patch stretched rapidly in the down-wind direction, from 240 m initially to about 660 m after 2.5 hours (Figure B.3-6). The spreading in the cross-wind direction

was slower overall; the dye being laid in about a 230-m wide patch, which increased more rapidly along the cross-wind axis over the first hour to 390 m then more slowly to about 490 m by 2.5 hours after release (Figure B.3-7).

4.2.3 March 22, 2006 Experiment

The 22 March 2006 experiment began at 10:00 PST (18:00 UTC) and ended at approximately 14:45 PST (22:45 UTC). The wind was from the north-northwest (347°) at 5.4 m/s (10 kts) based on the nearest NOAA offshore buoy. In La Jolla, the wind was from the northwest (318°) at 3.7 m/s (7 kts), whereas in the COAMPS model for the time and location of the experiment, winds were from 302° at 4.8 m/s (9 kts). (Wind records are in Appendix E.)

The georectified aerial photo images (as shape files) mapped to document the plume expansion and movements are compared to drifter locations at corresponding times for the 22 March 2006 experiment (Figure 4-7). DFG aircraft headings on 22 March 2006 were not recorded digitally, and instead, hand written heading data on these dates were tied to the other digital image information based on time. Thus, for a few photos, the images appear to “jump” around on the map, and they were not included in Figure 4-7. However, while the dye positions for those few photos were inaccurate, the sizes of the shape files of the images remained relatively accurate. Individual images for this experiment are in Appendix B.4.1.

Seven of the drifters used in this experiment were drogued at 1 m, whereas two were drogued at 5 m. The current, as indicated by the drifters and overall dye movement, was eastward in this experiment (Figure 4-7), whereas the wind was towards the southeast. It was apparent that the drifters drogued at 5 m stayed more in the center of the plume, while the shallower 1-m drogues moved eastward more rapidly and were eventually observed advancing the dye plume. Details of the times for the drifters are in Appendix D.3, whereas times and dimensions of each of the images of the dye are in Appendix B.4.2.

In Figure 4-7, the downwind and cross-wind expansion of the plume is evident, as are features related to Langmuir cells along the down-wind (southeastward) edge. (See also Appendix B.4.1, Figures B.4-3 to B.4-4; and Appendix B.4.3.) Langmuir cells appeared to be at two scales: more prominent cells about 71 m across from apparent down-welling to down-welling (indicated by relatively high intensity bands) and smaller cells about 10 m across. On average, the cells were oriented -34° to the left of down-wind to 10° to the right of down-wind (depending upon wind record used).

The trajectory of a neutrally-buoyant constituent transported by vectors from the HF-Radar data (Figure 4-7) shows southeastward current during the experiment, whereas the drifters and dye both moved to the east (see also Appendix C.3, Appendix B.4.1 and Appendix D.3). The average speed indicated by the HF Radar during the time the drifters were in the water was slower than the drifter movements. The 5-m drifters (blues in Figure 4-7) more closely tracked the speed and direction of dye movement. (See Sections 4.5 and 5 for analysis and discussion.)

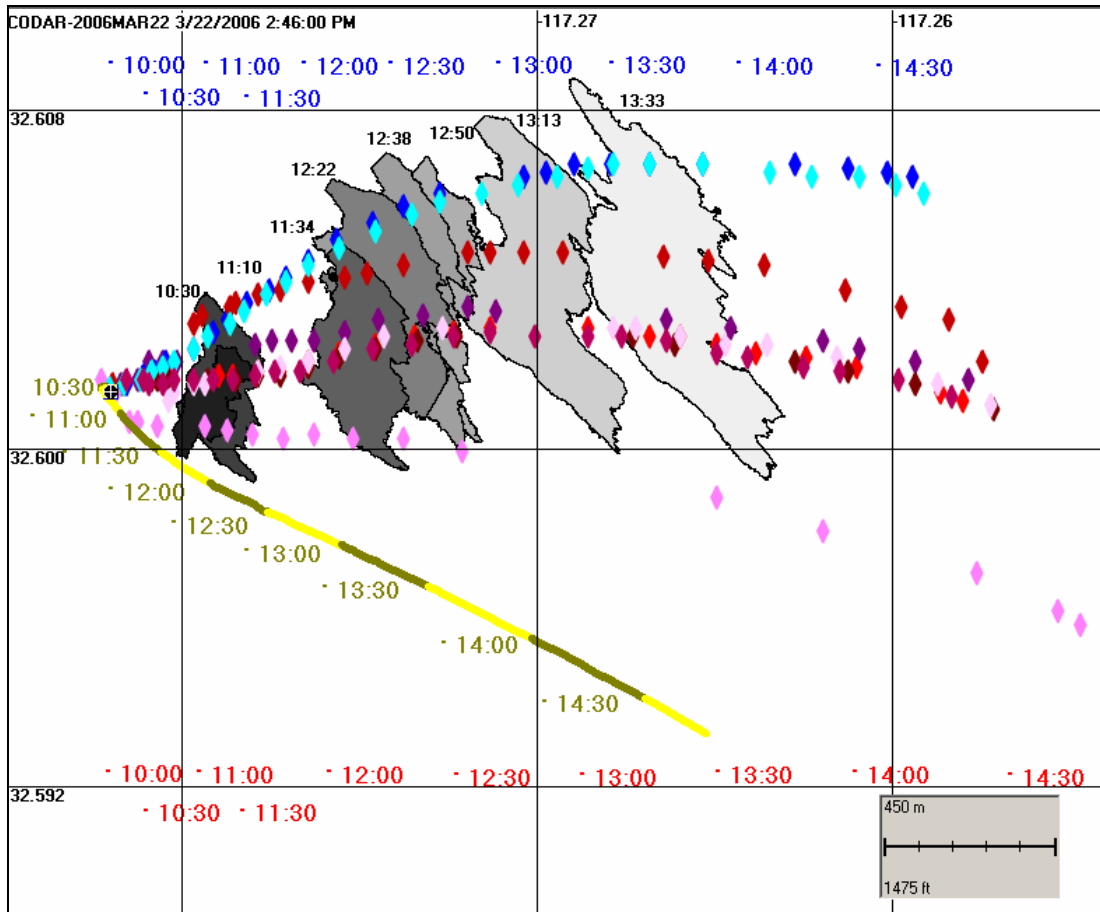


Figure 4-7. Locations of the dye over time in the 22 March 2006 experiment, as interpreted from the aerial photographs. Waypoints of drifter movements are indicated by the diamonds (at 1 m: red diamonds with times in red font; at 5 m: blue diamonds with times in blue font). The trajectory of a neutrally-buoyant constituent using the HF-Radar vectors up to 14:46 PST (yellow and green line, alternating color by 0.5 hour intervals, with times in green font) is shown.

The dye patch spreading rates, as area versus time and along the down-wind and cross-wind axes, are in Appendix B.4.2. The dye patch spread to about 213,000 m² by 3 hours after release (Figure B.4-5). The dye patch stretched rapidly in the down-wind direction, from 140 m initially to about 460 m after 3 hours (Figure B.4-6). The spreading in the cross-wind direction was slower overall; the dye being laid in about a 310-m wide patch, which increased slowly along the cross-wind axis to about 430 m by 3 hours after release (Figure B.4-7).

4.2.4 June 21, 2006 Experiment

The 21 June 2006 experiment began at 12:11 PDT (19:11 UTC) and ended at approximately 16:00 PDT (23:00 UTC). The wind was from the west (254°) at 1.6 m/s (3 kts) based on the nearest NOAA offshore buoy. In La Jolla, the wind was from 256° at 3.5 m/s (7 kts), whereas in the COAMPS model for the time and location of the experiment, mean winds were from 271° at 5.1 m/s (10 kts). (Wind records are in Appendix E.)

The georectified aerial photo images (as shape files) mapped to document the plume expansion and movements are compared to drifter locations at corresponding times for the 21 June 2006 experiment (Figure 4-8). Plane heading data were not recorded for this date. Therefore, heading information was calculated using the aircraft positions at the time of a given image and the time immediately before the image. The orientation of the line connecting the two positions was used as the heading. This resulted in approximate and inaccurate headings and could not be applied to all of the images (i.e., those at the beginning of a pass because of no prior position). Individual images for this experiment are in Appendix B.5.1.

Four of the drifters used in this experiment were drogued at 2 m, whereas five were drogued at 4 m. It was apparent that the drifters drogued at 2 m stayed more in the center of the plume, while the deeper 4-m drogues moved more slowly and were eventually observed slightly behind the dye plume. Details of the times for the drifters are in Appendix D.4, whereas times and dimensions of each of the images of the dye are in Appendix B.5.2.

In Figure 4-8, the downwind and down-current (perpendicular to down-wind in this experiment) expansion of the plume is evident, as are features related to Langmuir cells along the eastward down-wind edge. (See also Appendix B.5.1, Figures B.5-3 to B.5-4)

The trajectory of a neutrally-buoyant constituent transported by vectors from the HF-Radar data (Figure 4-8) shows eastward followed by southeastward current during the experiment, whereas the drifters and dye both moved continuously to the southeast (see also Appendix C.4, Appendix B.5.1 and Appendix D.4). The 2-m drifters (reds in Figure 4-8) indicate the speed and direction of dye movement. The average speed indicated by the HF Radar during the time the drifters were in the water was slower than the drifter movements. (See Sections 4.5 and 5 for analysis and discussion.)

The dye patch spreading rates, as area versus time and along the down-wind and cross-wind axes, are in Appendix B.5.1. The dye patch spread to about 2.5 km^2 by 2.5 hours after release (Figure B.5-5). The dye patch stretched rapidly in the down-wind direction (to the east), from

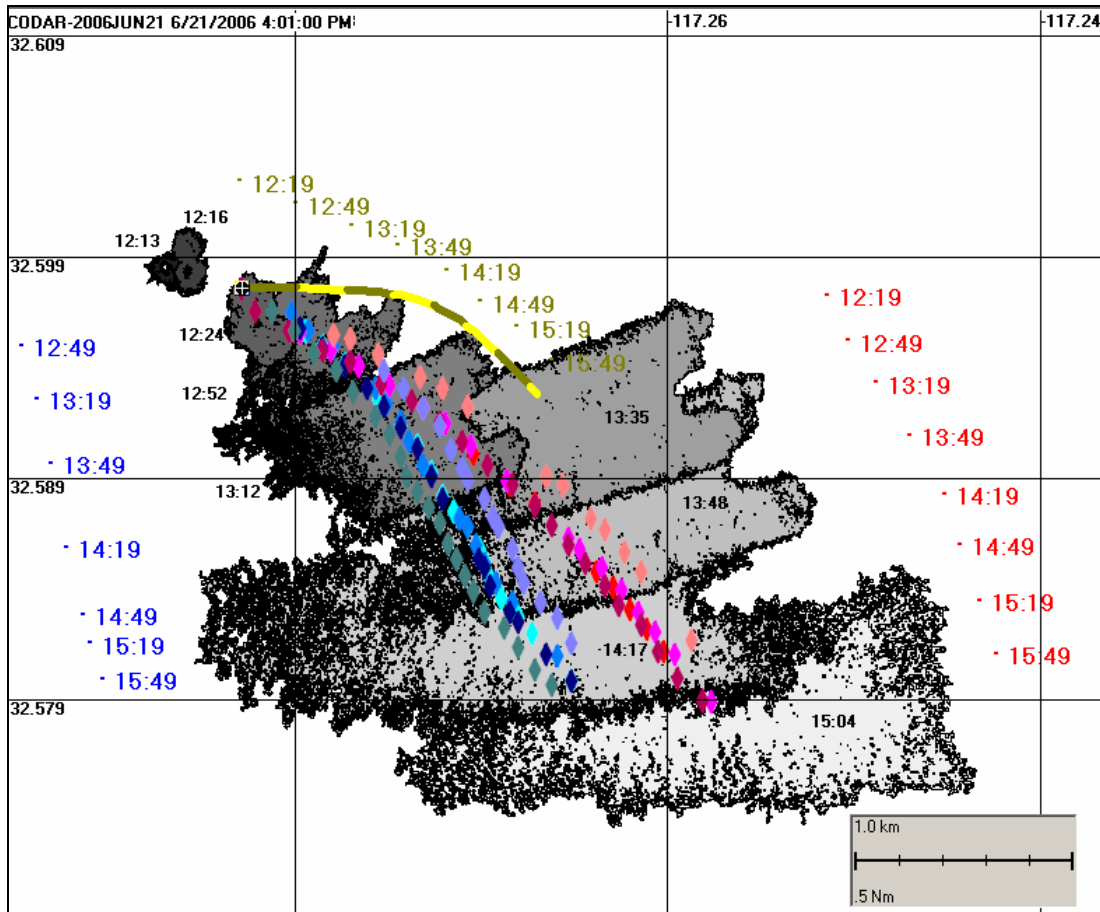


Figure 4-8. Locations of the dye over time in the 21 June 2006 experiment, as interpreted from the aerial photographs. Waypoints of drifter movements are indicated by the diamonds (at 2 m: red diamonds with times in red font; at 4 m: blue diamonds with times in blue font). The trajectory of a neutrally-buoyant constituent using the HF-Radar vectors up to 16:00 PDT (yellow and green line, alternating color by 0.5 hour intervals, with times in green font) is shown.

450 m initially to about 3,500 m after 2.5 hours (Figure B.5-5). The spreading in the cross-wind (down-current) direction was slower overall; the dye being laid in about a 600-m wide patch, which increased slowly to about 1,200 m by 2.5 hours after release (Figure B.5-7).

4.2.5 June 22, 2006 Experiment

The 22 June 2006 experiment began at 14:49 PDT (21:49 UTC) and ended at approximately 17:50 PDT (00:50 UTC, 23 June). The wind was from the southwest (226°) at 3.1 m/s (6 kts) based on the nearest NOAA offshore buoy. In La Jolla, the wind was from 246° at 3.5 m/s (7 kts), whereas the in the COAMPS model for the time and location of the experiment, winds were from 238° at 4.7 m/s (9 kts). (Wind records are in Appendix E.)

The georectified aerial photo images (as shape files) mapped to document the plume expansion and movements are compared to drifter locations at corresponding times for the 22 June 2006 experiment (Figure 4-9). Individual images for this experiment are in Appendix B.6.1.

Five of the drifters used in this experiment were drogued at 2 m and five were drogued at 4 m. It was apparent that the drifters drogued at 2 m stayed more in the center of the plume, while the deeper 4-m drogues moved downwind more slowly and were eventually observed slightly behind the dye plume. Details of the times for the drifters are in Appendix D.6, whereas times of each of the images of the dye are in Appendix B.6.

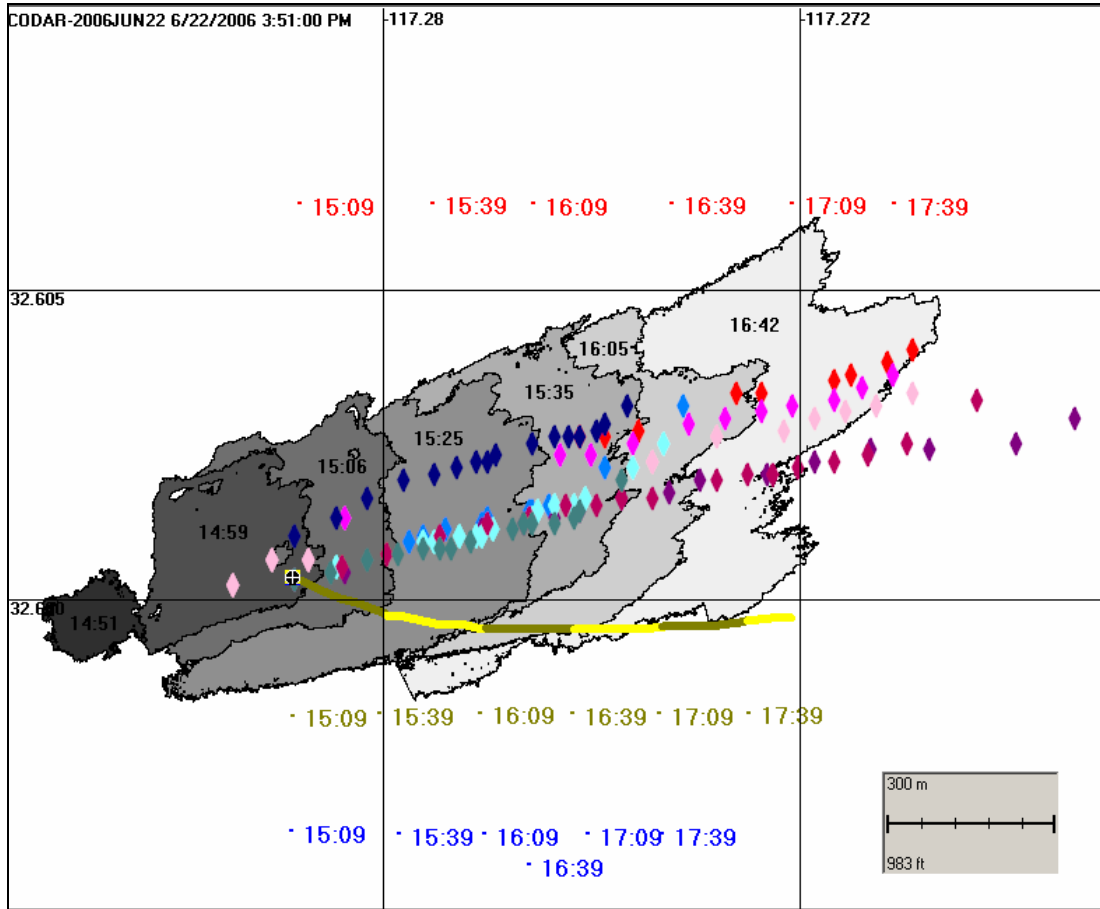


Figure 4-9. Locations of the dye over time in the 22 June 2006 experiment, as interpreted from the aerial photographs. Waypoints of drifter movements are indicated by the diamonds (at 2 m: red diamonds with times in red font; at 4 m: blue diamonds with times in blue font). The trajectory of a neutrally-buoyant constituent using the HF-Radar vectors up to 17:51 PDT (yellow and green line, alternating color by 0.5 hour intervals, with times in green font) is shown.

In Figure 4-9, the downwind and down-current (parallel to down-wind in this experiment) expansion of the plume is evident, as are features related to Langmuir cells along the leading (eastward) edge. (See also Appendix B.6.1, Figures B.6-3 to B.6-4)

The trajectory of a neutrally-buoyant constituent transported by vectors from the HF-Radar data (Figure 4-9) shows eastward current during the experiment, whereas the drifters and dye both moved to the east-northeast (see also Appendix C.5, Appendix B.6.1 and Appendix D.5). The 2-m drifters (reds in Figure 4-9) indicate the speed and direction of dye movement. The average speed indicated by the HF Radar during the time the drifters were in the water was slower than the drifter movements. (See Sections 4.5 and 5 for analysis and discussion.)

The dye patch spreading rates, as area versus time and along the down-wind and cross-wind axes, are in Appendix B.6.1. The dye patch spread to about 290,000 m² by 1 hour after release (Figure B.6-5). The dye patch stretched rapidly in the down-wind direction, from 540 m initially to about 1,200 m after 1 hour (Figure B.6-6). The spreading in the cross-wind direction was slower overall; the dye being laid in about a 380-m wide patch, which increased to about 520 m by 1 hour after release (Figure B.6-7).

4.2.6 November 1, 2006 Experiment

The 1 November 2006 experiment began at 11:50 PST (19:50 UTC) and ended at approximately 15:30 PST (23:30 UTC). The wind was from the northwest (307°) at 4.7 m/s (9 kts) based on the nearest NOAA offshore buoy. In La Jolla, the wind was from 325° at 5.4 m/s (10 kts), whereas in the COAMPS model for the time and location of the experiment, winds were from 301° at 5.5 m/s (11 kts). (Wind records are in Appendix E.)

The georectified aerial photo images (as shape files) mapped to document the plume expansion and movements are compared to drifter locations at corresponding times for the 1 November 2006 experiment (Figure 4-10). Individual images for this experiment are in Appendix B.7.1.

Four of the drifters used in this experiment were drogued at 2 m, and four were drogued at 4 m. It was apparent that the drifters drogued at 4 m stayed more in the center of the plume, while the shallower 2-m drogues moved more rapidly and were eventually observed advancing (and downwind of) the dye plume. Details of the times for the drifters are in Appendix D.6, whereas times and dimensions of each of the images of the dye are in Appendix B.7.2.

In Figure 4-10, the downwind expansion of the plume is evident, as are features related to Langmuir cells along the leading (eastward) edge. (See also Appendix B.7.1, Figures B.7-3 to B.7-4; Appendix B.7.3.) Langmuir cells appeared to be at two scales: more prominent cells about 68 m across from apparent down-welling to down-welling (indicated by relatively high intensity) and smaller cells about 29 m across. On average, the Langmuir cells were oriented to 0-25° to the right of down-wind (depending upon wind record used).

The trajectory of a neutrally-buoyant constituent transported by vectors from the HF-Radar data (Figure 4-10) shows southwestward followed by southward current during the experiment, whereas the drifters and dye both moved to the southwest for a shorter time, then backed to head towards the southeast (see also Appendix C.6, Appendix B.7.1 and Appendix D.6). The average speed indicated by the HF Radar during the time the drifters were in the water was much faster

than the drifter movements, and this phenomenon was only noted during the November experiments. The 4-m drifters (blue in Figure 4-10) indicate the speed and direction of dye movement. (See Sections 4.5 and 5 for analysis and discussion.)

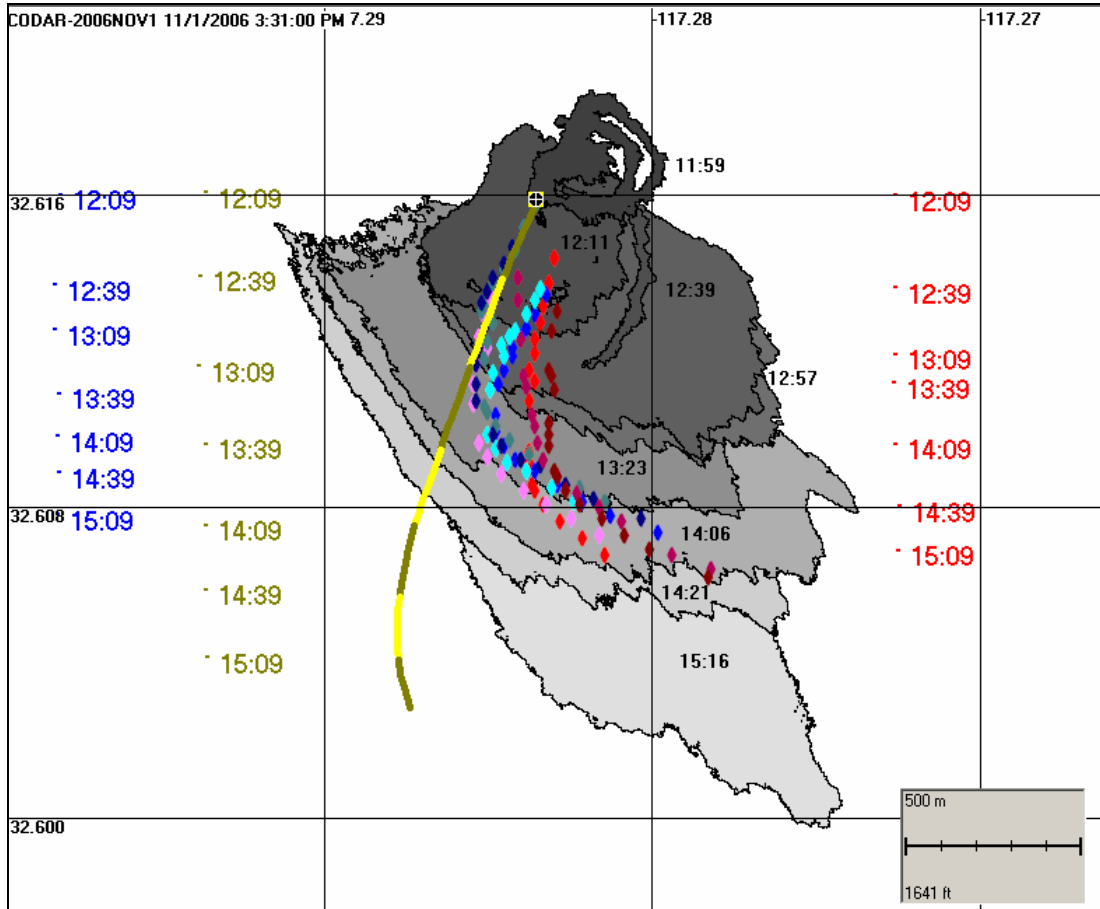


Figure 4-10. Locations of the dye over time in the 1 November 2006 experiment, as interpreted from the aerial photographs. Waypoints of drifter movements are indicated by the diamonds (at 2 m: red diamonds with times in red font; at 4 m: blue diamonds with times in blue font). The trajectory of a neutrally-buoyant constituent using the HF-Radar vectors up to 15:31 PST (yellow and green line, alternating color by 0.5 hour intervals, with times in green font) is shown.

The dye patch spreading rates, as area versus time and along the down-wind and cross-wind axes, are in Appendix B.8.1. The dye patch spread to about 1.0 km² by 3 hours after release (Figure B.8-5). The dye patch stretched in the down-wind direction, from 800 m initially to about 2,000 m after 3 hours (Figure B.8-5). The spreading in the cross-wind (initially down-current) direction was slower overall; the dye being laid in about a 600-m wide patch, which increased slowly to about 800 m by 3 hours after release (Figure B.8-7).

4.2.7 November 2, 2006 Experiment

The 2 November 2006 experiment began at 11:19 PST (19:19 UTC) and ended at approximately 15:00 PST (23:00 UTC). The wind was from the northwest (325°) at 6.0 m/s (12 kts) based on the nearest NOAA offshore buoy. In La Jolla, the wind was from 333° at 3.9 m/s (8 kts), whereas in the COAMPS model for the time and location of the experiment, winds were from 318° at 5.8 m/s (11 kts). (Wind records are in Appendix E.)

Technical issues resulted in a complete loss of all positional (altitude, location, and heading) data from the OSPR aircraft during the 2 November 2006 experiment (see Appendix B.8). As such, only estimated altitudes could be used to scale the images. Positional data were ultimately obtained from flight tracking (following) programs at the Federal Aviation Administration (FAA), making georeferencing possible.

The georectified aerial photo images (as shape files) mapped to document the plume expansion and movements are compared to drifter locations at corresponding times for the 2 November 2006 experiment (Figure B.8-2). Figure B.8-2 shows images at locations not co-located with the drifters, although the drifters were in fact observed to be tracking the plume. The application of the FAA positional data resulted in the dye images being consistently displaced about 612 m to the northwest (315° , i.e., 433 m west and 433 m north), based on the known locations of the dye just after release as compared to drifters placed in the center of the dye. This appears to be a round off error in the FAA record. As a result, the dye shapes were moved 612 m in the direction of 135° T (433 m east and 433 m south) before plotting in Figure 4-11. Thus, while the dimensions of the dye plume are fairly accurate (subject to an error in altitude of up to 250 ft), the locations are only approximate. Individual images for this experiment are in Appendix B.8.1.

Four of the drifters used in this experiment were drogued at 2 m, and four were drogued at 4 m. It was apparent that the drifters drogued at 4 m stayed more in the center of the plume, while the shallower 2-m drogues moved more rapidly and were eventually observed advancing downwind of the dye plume. Details of the times for the drifters are in Appendix D.7, whereas times and dimensions of each of the images of the dye are in Appendix B.8.2.

In Figure 4-11, the downwind and down-current (roughly parallel to down-wind in this experiment) expansion of the plume is evident, as are features related to Langmuir cells along the leading (eastward) edge. (See also Appendix B.8.1, Figures B.8-3 to B.8-4; and Appendix B.8.3.) Langmuir cells appeared to be at two scales: more prominent cells about 40 m across from apparent down-welling to down-welling (indicated by relatively high intensity) and smaller cells about 15 m across. On average, the cells were oriented -7° to the left of down-wind to 12° to the right of down-wind (depending upon wind record used).

The trajectory of a neutrally-buoyant constituent transported by vectors from the HF-Radar data (Figure 4-11) shows southwestward followed by southward near-surface current during the experiment, whereas the drifters and dye both moved to the south and then to the southeast (see also Appendix C.7, Appendix B.8.1 and Appendix D.7). As observed on the previous day (and only during the November experiments), the average speed indicated by the HF Radar during the

time the drifters were in the water was much faster than the drifter movements. The 4-m drifters (blue in Figure 4-11) best indicated the speed and direction of dye movement. (See Sections 4.5 and 5 for analysis and discussion.)

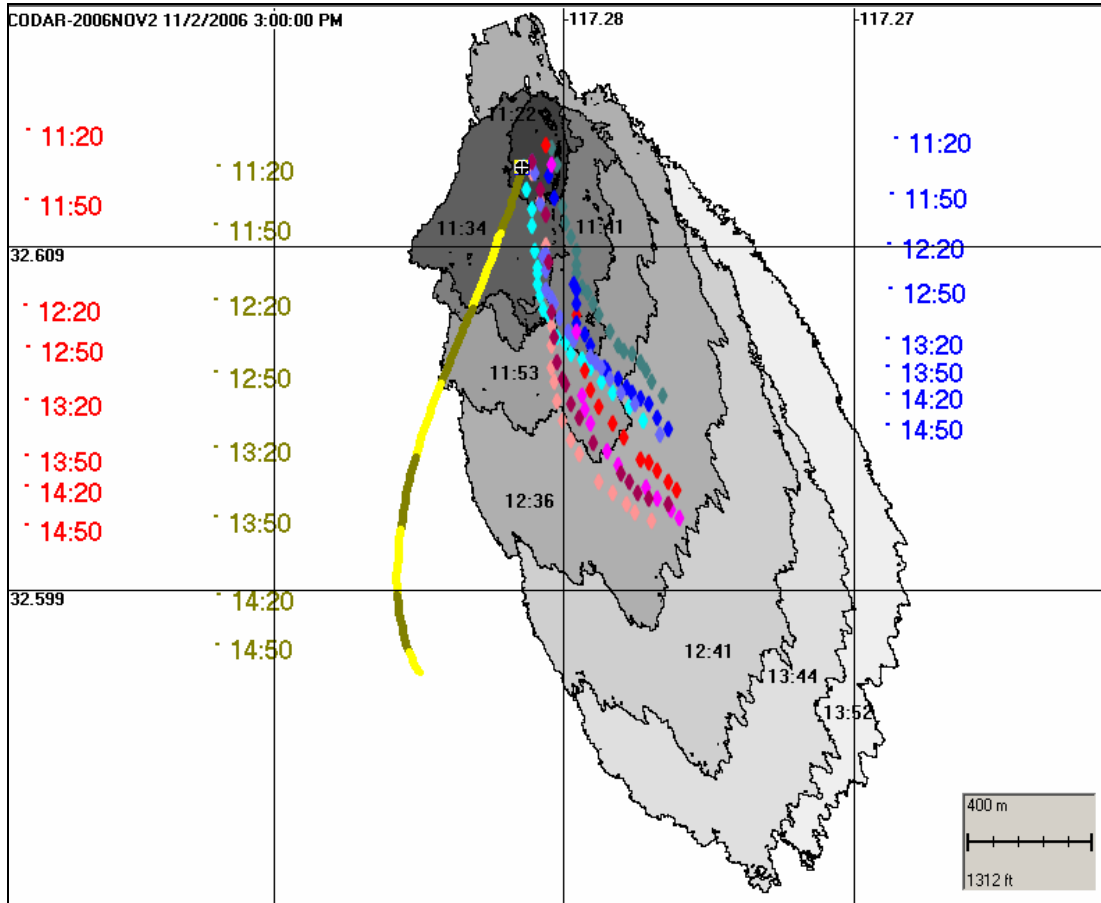


Figure 4-11. Locations of the dye over time in the 2 November 2006 experiment, as interpreted from the aerial photographs. Waypoints of drifter movements are indicated by the diamonds (at 2 m: red diamonds with times in red font; at 4 m: blue diamonds with times in blue font). The trajectory of a neutrally-buoyant constituent using the HF-Radar vectors up to 15:00 PST (yellow and green line, alternating color by 0.5 hour intervals, with times in green font) is shown.

The dye patch spreading rates, as area versus time and along the down-wind and cross-wind axes, are in Appendix B.8.2. The dye patch spread to about 1.9 km² by 3 hours after release (Figure B.8-5). The dye patch stretched rapidly in the down-wind direction in the first 1.5 hours, from 850 m initially to about 2,400 m, and then slowly to 2,800 m by 3 hours after release (Figure B.8-5). The spreading in the cross-wind direction was slower overall; the dye being laid in about a 580-m wide patch, which increased slowly to about 1,100 m by 3 hours after release (Figure B.8-7).

4.3 Vertical Penetration of the Dye – Point Loma Experiments off San Diego

Appendix F contains plots of oceanographic data from CTD casts measuring salinity, water temperature, and water density versus depth. CTD casts were taken before the dye release and outside of the plume area in order to characterize the structure of the water column, the pycnocline depth, and the surface mixed layer depth. In the November 2005 and March 2006 experiments, the CTD apparatus was also used to measure fluorescence as a function of depth at specific stations located by longitude and latitude. Thus, the fluorescence data for the November 2005 and March 2006 experiments are presented graphically in Appendix F, along with the CTD data for those dates.

In the June 2006 and November 2006 experiments, all fluorescence data were collected with the high resolution profiling fluorometer, which was raised and lowered as the sampling boat transited the plume. Thus, the June and November 2006 data are in the form of continuous profiles of varying depth. These data are presented graphically in Appendix G. The CTD data for June 2006 and November 2006 are in Appendix F. Only a few CTD casts were made in those latter experiments, with the objective of characterizing the water-column stratification before and after the dye releases.

Dye penetration and the depth of the surface mixed layer (as defined by a density difference from the water surface of 0.2 kg/m^3 , see Section 3.2.2) are listed in Table 4.3-1. The dye penetrated to the depth of the mixed layer within a half hour after release, but was not uniform in concentration over the mixed layer. That transport was evidently by Langmuir circulation. (See further discussion of vertical dispersion in Section 5.1.)

Table 4.3-1. Dye penetration and the depth of the surface mixed layer.

Date	8 Nov 2005	21 Mar 2006	22 Mar 2006	21 Jun 2006	22 Jun 2006	1 Nov 2006	2 Nov 2006
Mixed layer depth (m)	9	12	15	10	7	11	8
Dye plume penetration depth (m)	10	10*	10 to 14	6	7	10**	8

* Plume measured for approximately one hour and dye may not have reached maximum depth during sampling.

** Deepest depth sampled but dye is known to have gone deeper since the edge of the plume was not detected at that depth (Fluorescence was still above background at 10 m.)

4.4 Safe Sea Exercise off San Francisco on August 9, 2006

In addition to the planned OSPR- and CRRC-sponsored cruises off Point Loma discussed above, we were invited to participate in the Safe Seas Exercise completed off San Francisco, CA on 8 and 9 August 2006. Our participation was requested rather late in the planning process, and given the time and logistical constraints, our involvement was primarily limited to assisting with dye deployment and dissipation rate measurements. The objectives of our involvement were to:

1. Provide a dye target for aerial application of simulated dispersant (water), and
2. Measure dissipation rates using data from:
 - a. Aerial photography
 - b. *In-situ* fluorometry (to be completed by LSU under separate contract)
 - c. Flow-through fluorometry (to be completed by the USCG SMART Team).

Planned Activities:

Detailed plans for the application of the dye and the field measurements (ship based fluorometry and aerial photography) were developed and agreed upon in advance of the field deployment. These plans were, however, altered several times to accomplish operational requirements. Final details were discussed in three meetings on August 8 that we attended. These were a ship ops meeting on the MSRC *Pacific Responder*, an air ops briefing at the US Coast Guard Air Station, and a safety briefing near downtown San Francisco.

Several challenges to previously agreed upon operations were addressed and the necessary changes incorporated. This included an additional task for the Department of Fish & Game (DFG) aircraft to handle the Air Traffic Control of all airplanes involved in the aerial dispersant application, but this eliminated the co-pilot seat that W. Nordhausen was supposed to occupy for the aerial photography. As a result, it was agreed that the air traffic controller would also assist D. French-McCay in the aerial photography mission and W. Nordhausen would coordinate the ship operations on the *R/V Shearwater* in support of the aerial dye dissipation measurements.

Accomplishments:

The dye release was significantly delayed due the *Pacific Responders'* mission to demonstrate the deployment and recovery of open-ocean boom and skimming equipment prior to the dye release. Vessels transporting VIPs and press were also late on scene, and their observation of the booming and skimming operations further delayed the dye release. The dye release that provided the visual target for the aerial application of dispersants was crucial, and the delayed dye release pushed all other operations back.

Further time pressure to expedite operations was presented to the *R/V Shearwater's* master and forward incident commander by the fact the USCG cutter *Aspen* announced that they would have to leave the site in order to return to San Francisco in time for a press briefing. As a result, the forward IC decided to cancel the previously scheduled fluorometry measurements of the initial

dye concentrations in order to expedite the air ops. We were, however, able to collect some fluorometry measurements following the completion of the aerial spraying of water to simulate dispersant applications.

Observations and Conclusions:

The application of dye was only partially successful, but it did at least provide a target for the simulated dispersant application. The opportunity to attempt to sample for qualitative water column measurement for scientific purposes was greatly appreciated and acknowledged. It must be realized, however, that the priority of this exercise was personnel training and observing aerial dispersant applications. Science clearly was not the main purpose of the overall Safe Seas exercise. As a result, only very limited data were obtained.

Much of the confusion and delays of the aerial operations (and the cancelled initial measurements) could have been avoided if the *Pacific Responder* had not been tasked with the boom deployment and skimming demonstrations prior to the dye release. Also, it appeared as if the air ops chief was not aware of this scheduled requirement, at least prior to the air ops meeting on 8 August 2006, when W. Nordhausen tried to point this out.

4.1.1 Horizontal Movements and Expansion of the Dye – August 9, 2006 Safe Seas Experiment

The 9 August 2006 Safe Seas dye release off San Francisco began at 11:50 PDT (19:50 UTC) and was tracked until approximately 13:30 PDT (20:30 UTC) when the dye became too diffuse to effectively photograph (Table 4.4-1). The wind was from the northwest (305°) at 5.0 m/s (10 kts) based on the nearest NOAA offshore buoy. (Wind records are in Appendix E.)

Table 4.4-1. Dye Deployment off San Francisco during the Safe Seas Exercise.

Date	Location	Time Start Dye Release (Local)	Dye Release Duration (min)	Experiment Completion Time (Local)
August 9, 2006	37.66123° N 122.61412° W	11:50	17	13:30

The aerial photo images were georectified (as shape files) and selected complete images were mapped to document the plume movements and expansion (Figure 4-12 and Appendix B.9).

Unfortunately, the dye was not released in a focused circular area, instead being released from a hose in a curvilinear manner in generally a cross-wind direction (see Figure B.9-1 in Appendix B.9). This made analysis of the dye dimensions difficult, and any data resulting from such an analysis would be difficult or impossible to interpret. Such interpretation was not attempted, both for this reason and because of the lack of drifter data in the area of the dye release.

Selected images of the dye movements for this experiment (which were the most complete image at each overpass of the plane taking the photographs) are shown in Figure 4-12. The trajectory of a neutrally-buoyant constituent transported by vectors from the HF-Radar data (Figure 4-13) shows northward current during the experiment, followed by southeastward current after the tide turned at 14:00 hours (see also Appendix C.8 and Appendix B.9.1). While the HF-Radar trajectory followed the same path as the dye movements, the average speed indicated by the HF-Radar during the time the dye was tracked was slower than the dye movements (compare Figure 4-12 and 4-13). The wind was from 305° (NW) at 5 m/s (10 kt) at the time, which would induce a wind drift opposing the northward movement of the dye. As the dye was likely deeper than the near-surface where the HF-Radar measures current, the HF-Radar likely included a southward component of wind drift, whereas the dye plume was in deeper water where that component was much smaller and evidently currents were moving to the north.

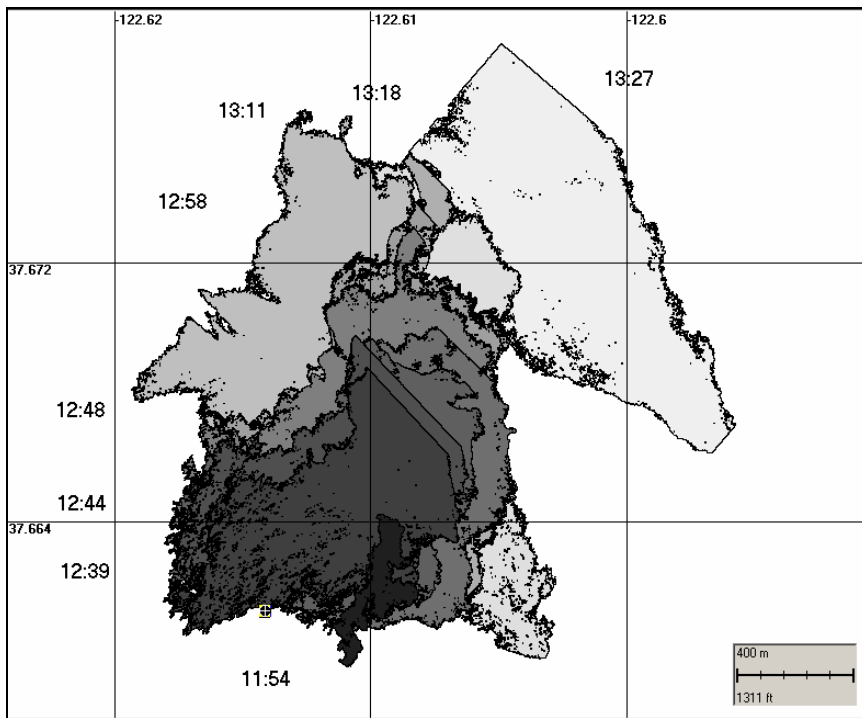


Figure 4-12. Locations of the dye over time in the 9 August 2006 experiment, as interpreted from the aerial photographs.

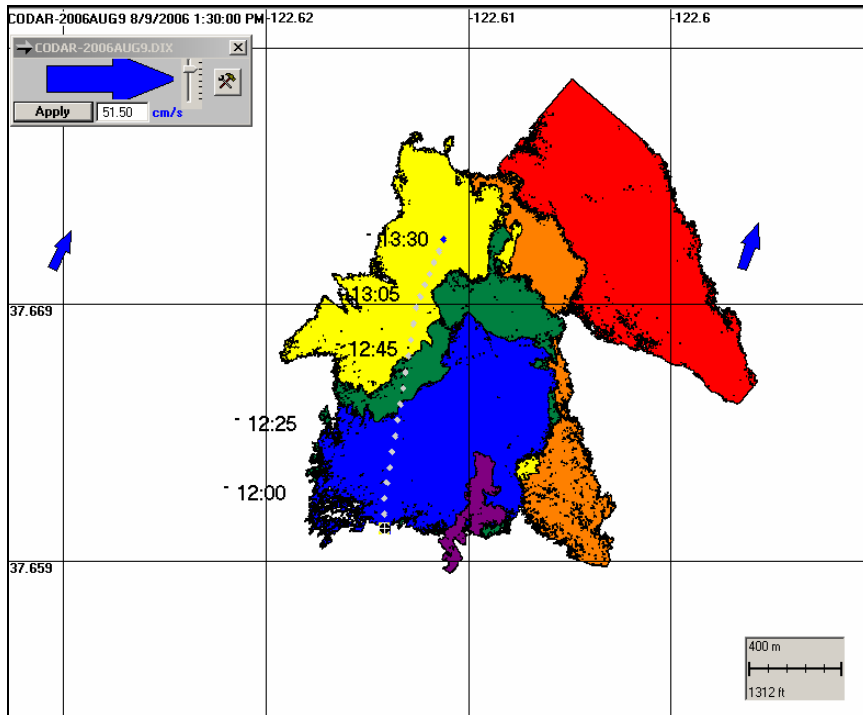


Figure 4-13. Trajectory of a neutrally-buoyant constituent using the HF-Radar vectors up to 13:30 PDT (grey line with times in black font) for the 9 August 2006 experiment overlaid on dye locations based on shape files derived from selected images. The arrow indicates the HF-Radar speed at the end time of the trajectory simulation.

4.4.2 Vertical Penetration of the Dye – August 9, 2006 Safe Seas Experiment

CTD and fluorescence data for the 9 August 2006 experiment are included in Section F.8 of Appendix F. The mixed layer defined by the depth at which density was more than 0.2 kg/m^3 from the surface value was evidently within 1m of the surface (Figure F.8-1 in Appendix F). However, a dramatic change in density occurred at about 11m depth. Thus, one would expect the dye to penetrate to about 11m deep.

The fluorescence profiles for the 9 August 2006 experiment appeared to be dominated by algal fluorescence rather than dye, as the fluorescence was much higher at depth than either in the upper 11 m or near the surface where the dye was released and visually observed. Thus, it is not clear whether or not dye concentrations were actually measured after the dye release, and unfortunately, the data are not useful for that purpose.

4.5 Drifter & HF Radar Direct Comparisons

Velocities measured by drifters and HF-Radar were directly compared in order to assess differences between modeled trajectories produced by the two measurements. Because horizontal shear was observed in both HF-Radar and drifter velocities over all experiments, HF-Radar velocities were interpolated in space and time to each of the shallowest drifter locations for each fix over all experiments. Mean bearings, magnitudes and differences for wind, HF-Radar, and the shallowest drifter velocities are summarized in Table 4.5-1, while supporting figures are available in Appendix C. Wind from station LJPC1 was used for this comparison because it was coherent with wind measured south of the dye release site at Imperial Beach, CA and with COAMPS nowcasts of winds at the dye release site for each experiment.

Overall, better agreement in velocity bearing between HF-Radar and drifter measurements was observed when drifters were drogued at 1m relative to 2m. The best agreement in bearing between HF-Radar and drifter measured velocities was on 8 November 2005 and 21 March 2006 when drifters were drogued at 1m. The reason for the relatively large discrepancy in bearing on 22 March 2006 is likely due to increased horizontal shear as indicated by the large spread of drifter trajectories with similar starting points (Figure 4-7).

Absolute differences in magnitude between HF-Radar velocities and drifter velocities are below 5 cm/s for all experiments with the exception of 8 November 2005, when drifters advected ahead of the dye plume, and 21 June 2006. However, these differences are well within HF-Radar error bounds of 8 – 9 cm/s (Ohlmann *et al.*, 2007), especially since horizontal shear over the spatial averaging area of the HF-Radar isn't accounted for in the drifter velocities. Other discrepancies such as differences in sampling depth in later experiments also play a role in observed differences.

Table 4.5-1. Mean wind, HF-Radar and drifter bearings and magnitudes, and calculated differences over each experiment.

Expt. Date	Drifter Depth (m)	Bearing (degrees, clockwise from North)					Magnitudes (cm/s, wind in m/s)			
		Wind	HFR	Drifter	HFR – Drifter	HFR - Wind	Wind	HFR	Drifter	HFR - Drifter
2005/11/08	1	11.1	11.4	15.8	-4.4	0.3	5.7	22.4	37.4	-15.0
2006/03/21	1	104.0	144.9	159.5	-14.6	40.9	5.0	8.6	8.4	0.2
2006/03/22	1	138.6	124.2	92.3	31.9	-14.4	4.2	10.6	15.1	-4.5
2006/06/21	2	76.4	107.3	130.3	-23.0	30.9	3.5	15.5	25.8	-10.3
2006/06/22	2	69.0	99.4	76.4	23.0	30.4	3.3	9.5	12.7	-3.2
2006/11/01	2	144.8	189.2	154.1	35.1	44.4	5.2	11.5	8.7	2.8
2006/11/02	2	146.8	174.1	154.9	19.2	27.3	4.2	12.4	9.6	2.8

Differences in measurement methods between HF-Radar and drifters contribute to differences observed in measured velocities. HF-Radar velocities are averaged spatially over ~1km, temporally over 1 hour, and vertically over the surface 0.5m. Drifters measure velocities at a

depth of 1 or 2 meters, are Lagrangian, and have an effective temporal average of 10 minutes. These sampling discrepancies are expected to yield differing results in a time-dependent environment with horizontal and/or vertical shear. Additional discussions of the comparison between drifter and HF-Radar results are presented in Section 5.

4.6 Analysis of Continuous Sampling Fluorometer Data

The June and November 2006 experiments included the use of a continuous sampling profiling fluorometer, which enabled detailed analysis of the dye patch's spatial structure and temporal evolution. Exploratory plots for all experiments with the continuous sampling profiling fluorometer are shown in Appendix G. This initial analysis of the data included the determination and designation of along-plume and cross-plume transects from the ship's GPS track. The dye patches roughly resemble ellipses, and the along-plume dimension approximates the major axis while the cross-plume dimension approximates the minor axis. Once these designations were made in the GPS tracks, dye concentrations, represented as $\log_{10}(C/C_{\max})$, were plotted as cross section of the dye plume in both the along- and cross-plume directions. Along-track distances were approximated based on the length of the sampling leg and the GPS track sampling frequency.

Two experiments had particularly well defined sampling transects and were chosen for estimation of the plume's velocity (in the along-plume direction) in low and relatively high vertical shear environments. The 2 November 2006 experiment represents a low shear environment while the 22 June 2006 experiment exhibits behavior consistent with higher shear. Results from these detailed analyses are presented below.

4.6.1 June 22, 2006 Experiment

Using the along-plume sampling designations made in this initial exploration of the data, a least squares best fit to all the along-plume transects was used to define the mean along-plume axis (Figure 4-14). Each sampling transect is then projected onto the mean along-plume axis and along-plume distances are computed from the cross-plume axis shown in the figure. This produces cross sections of the dye concentration along the dye plume with absolute distances required for velocity estimates. With the data translated into the along and cross-plume axes, it is vertically and horizontally binned (by median filtering to remove spikes and reduce noise) in increments of 10m horizontally and 0.5 m vertically. This produces filtered and regularly spaced data in vertical and along-plume dimensions suitable for estimates of maximum concentration profiles (Figure 4-15). These maximum concentration profiles represent the core of the dye patch in the along plume direction. Using the along-plume distance for each maximum concentration profile and the time elapsed between each sampling transect and the first sampling transect, a velocity profile in the along-plume dimension can be estimated from all (but the first) sampling transects. The slope of the mean along-plume velocity profile is then used to estimate vertical shear in the along plume direction (Figure 4-16). These same methods are used in the 2 November 2006 analysis described in Section 4.6.2.

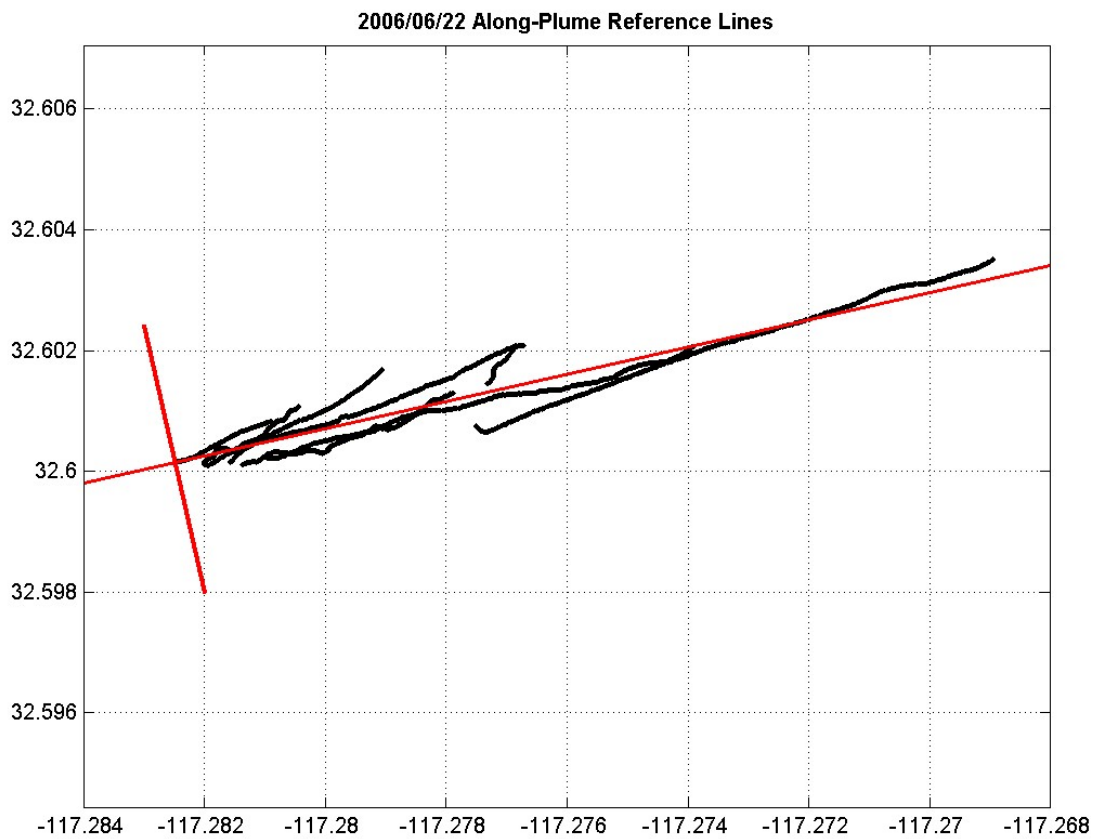


Figure 4-14. All along-plume transects (black) shown with along-plume axis (parallel to transects) and the cross-plume axis (orthogonal to along-plume axis). The cross-plume axis is oriented such that it serves as a starting reference for all of the along-plume transects.

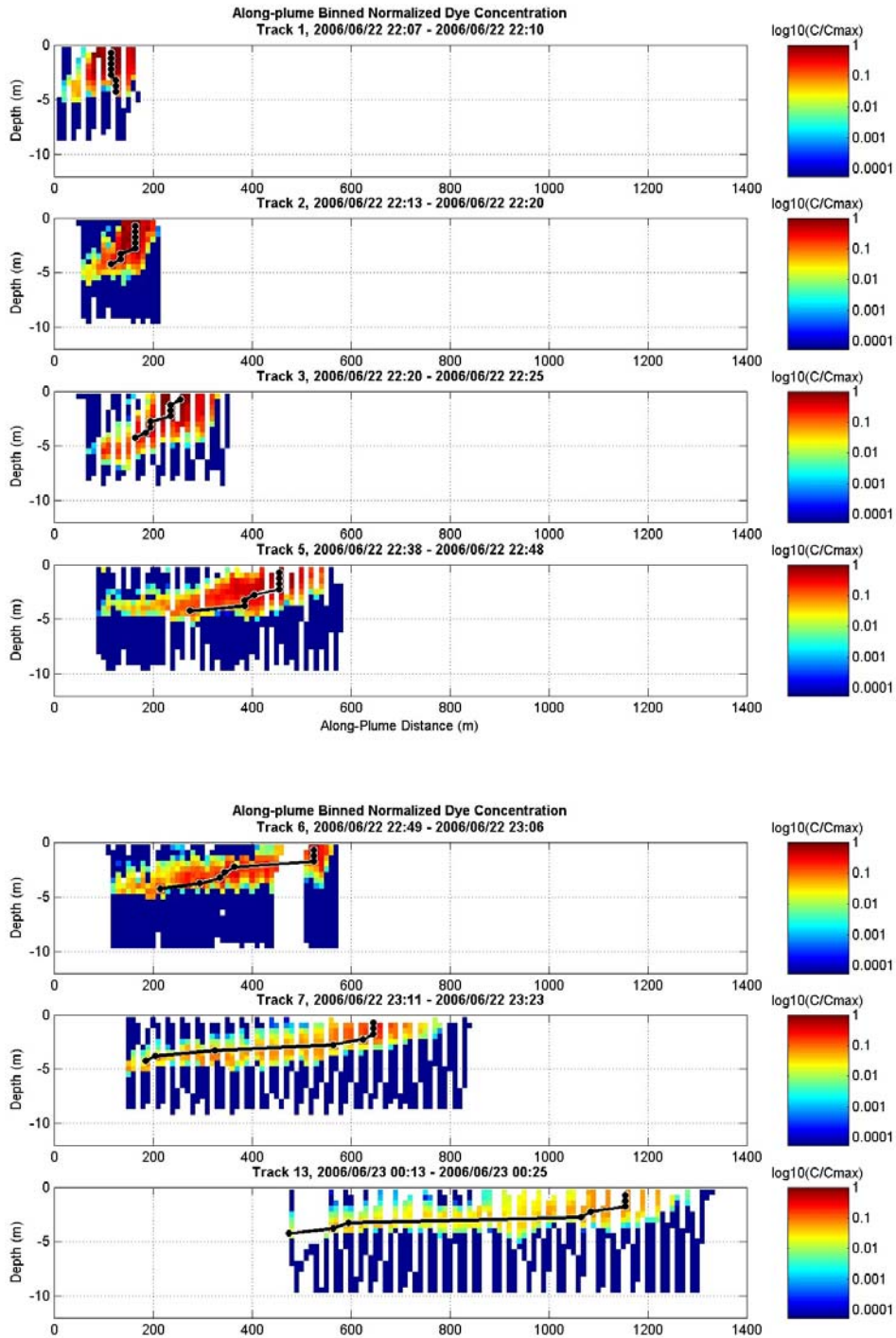


Figure 4-15. Along-plume sampling transects projected onto the along plume axis with absolute distances. Dye concentrations are vertically and horizontally binned (by medial filtering to remove spikes and reduce noise) in increments of 10 m horizontally and 0.5 m vertically. Maximum dye concentration profiles (in black) indicate the core of the dye plume.

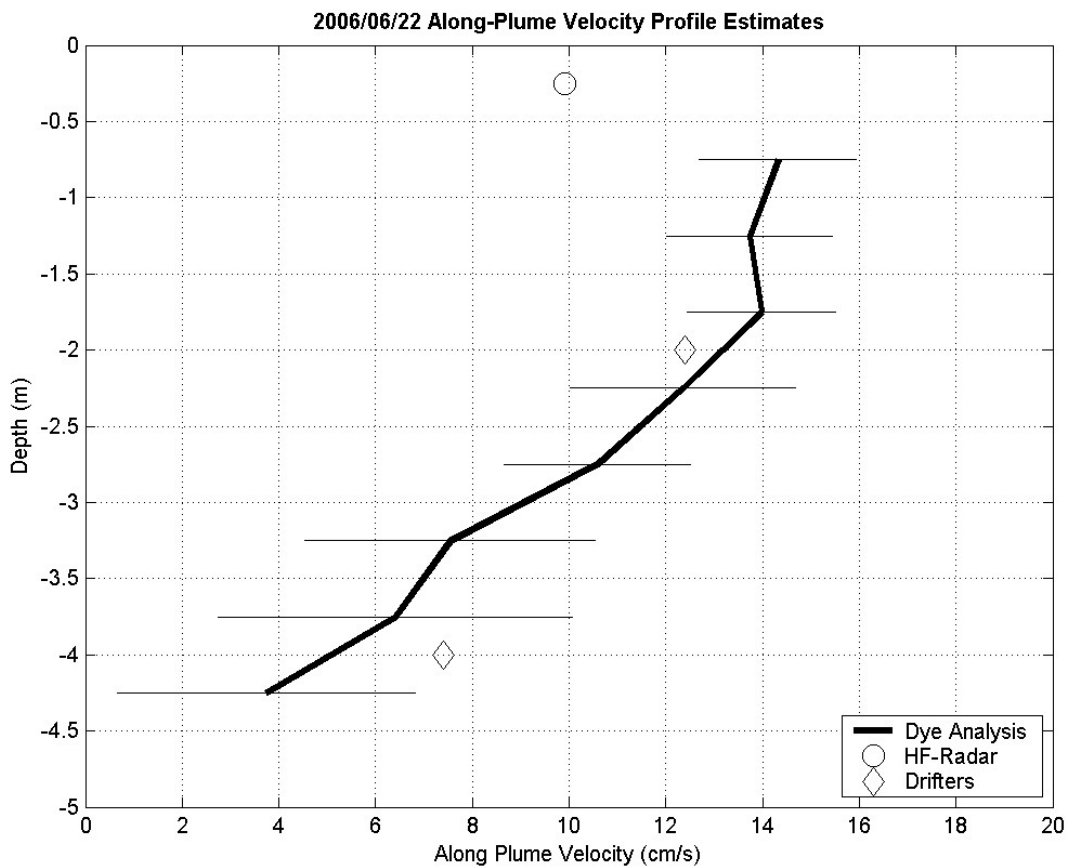


Figure 4-16. The mean velocity profile in the along plume direction is shown with bars indicating envelope of one standard deviation. The vertical shear based on a least square's fit to the profile is 0.031 s^{-1} . Mean HF-Radar (computed at the mean along-plume position) and drifter velocities projected onto the along-plume axis are shown for comparison.

Seven along-plume transects were identified from the sampling track for 22 June 2006. The along-plume axis orientation defined by the least square's fit to all the along-plume transects is 77.3 degrees clockwise from North (Table 4.6-1), which is 9.3 degrees clockwise from the mean wind direction (measured at station LJPC1) over the experiment. The along-plume dye concentration indicates that dye was rapidly dispersed through the mixed layer since the first transect shows dye mixed to 5 m then, 10 minutes later, dye was dispersed to its maximum depth of 6.8 m (Figure 4-15). Over the course of the experiment, the core of the dye plume advected 1 km near the surface and only 150 m at the bottom of the mixed layer. This difference between near surface and deeper velocities is clearly captured in the along-plume velocity profile (Figure 4-16). The vertical shear in the along plume direction estimated from the slope of the velocity profile is 0.031 s^{-1} compared with 0.025 s^{-1} estimated from the drifters drogued at 2m and 4m. While data coverage is insufficient to compare HF-Radar velocities to velocities estimated from the dye analysis, drifter velocities projected onto the along-plume axis fall within one standard deviation of the velocity profile computed from the dye analysis.

Table 4.6-1. Comparison of along-plume velocity profiles and shear estimates from drifters and dye analysis.

Date	Measure	Along-Plume Axis Orientation (degrees*)	Along-Plume Current Magnitude (cm/s)		Along-Plume Shear
			2 m	4 m	
22 June 2006	Dye Analysis	77.3	13.1	5.0	0.031
	Drifters		12.4	7.4	0.025
2 Nov. 2006	Dye Analysis	153.4	9.8	9.1	0.006
	Drifters		9.6	7.2	0.011

* Degrees measured clockwise from true North.

4.6.2 November 2, 2006 Experiment

Following the same analytical methods described in Section 4.6.1, sixteen along-plume transects were identified from the sampling track for 2 November 2006. The along-plume axis orientation defined by the least square's fit to all the along-plume transects is 153.4° clockwise from North (Figure 4-17, Table 4.6-1), which is directly in-line with the mean wind direction (measured at station LJPC1) over the experiment. Dye was rapidly mixed to 6 m then gradually mixed to a maximum of 8.2 m by the end of the experiment (Figure 4-18). The core of the dye plume advected approximately 650 m over the upper 5 m with little vertical shear in the along-plume direction. The along-plume velocity profile clearly shows a low shear environment with a vertical shear estimate of 0.006 s⁻¹. This lower shear relative to the 22 June 2006 experiment is in agreement with an estimated shear of 0.011 s⁻¹ computed from drifters deployed at 2m and 4m (Table 4.6-1). While data coverage is insufficient to compare HF-Radar velocities to velocities estimated from the dye analysis, drifter velocities projected onto the along-plume axis fall within one standard deviation of the velocity profile computed from the dye analysis.

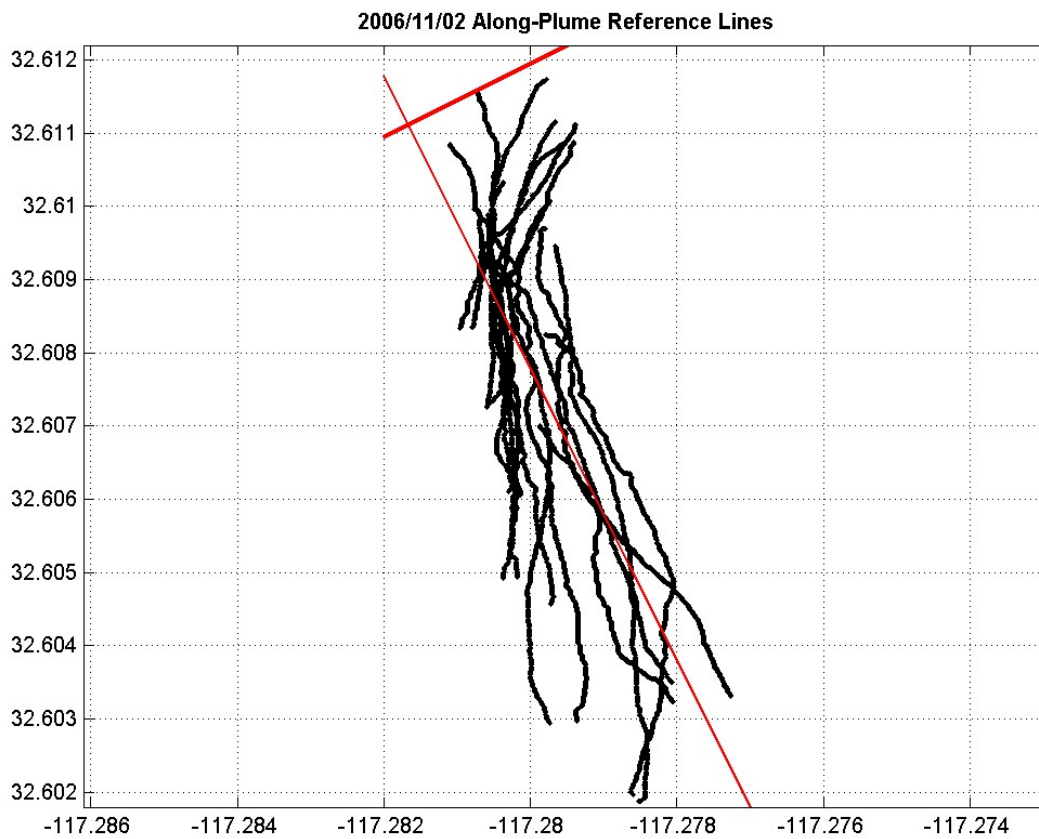


Figure 4-17. All along-plume transects (black) shown with along-plume axis (parallel to transects) and the cross-plume axis (orthogonal to along-plume axis). The cross-plume axis is oriented such that it serves as a starting reference for all of the along-plume transects.

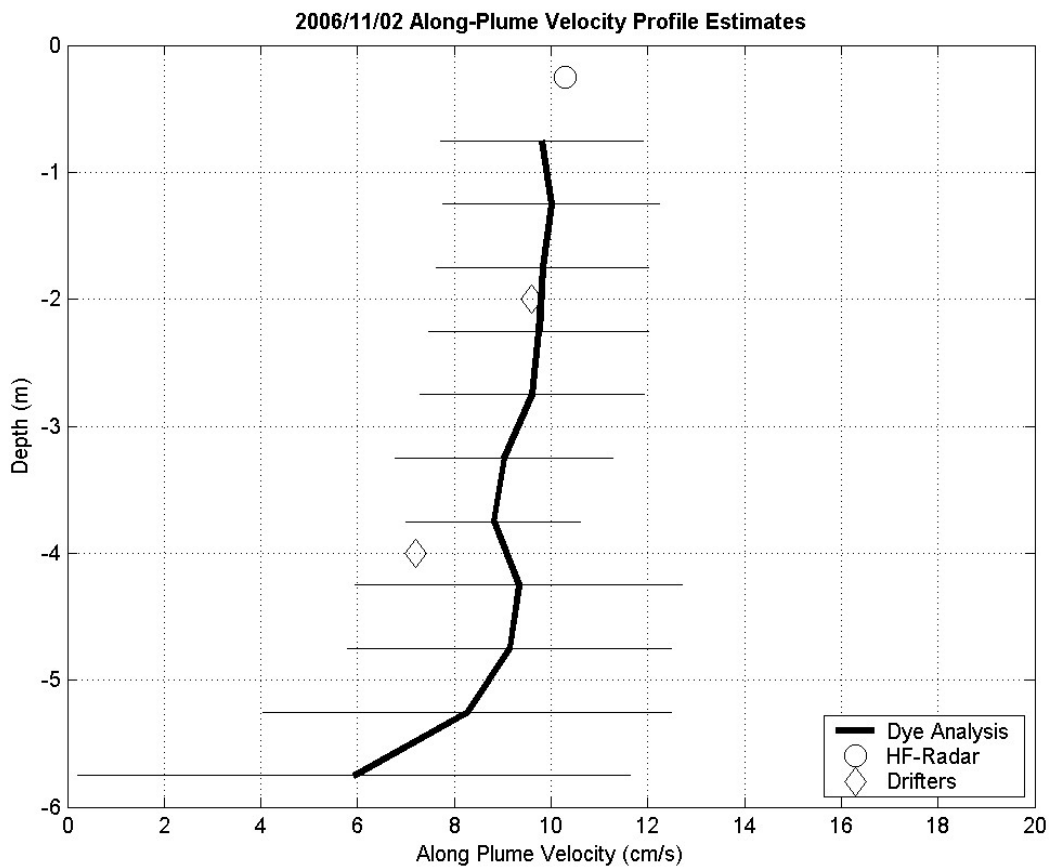


Figure 4-18. The mean velocity profile in the along plume direction is shown with bars indicating envelope of one standard deviation. The vertical shear based on a least square's fit to the profile is 0.006 s^{-1} . Mean HF-Radar (computed at the mean along-plume position) and drifter velocities projected onto the along-plume axis are shown for comparison.

5. Results – Modeling

5.1 Approach

Oil-spill fate and transport modeling may be used to evaluate water column hydrocarbon concentrations, potential exposure to organisms (zooplankton), and the impacts of oil spills with and without use of dispersants. A number of such analyses have been performed using SIMAP (French McCay, 2003, 2004), which uses wind data, current data, and transport and weathering algorithms to calculate the mass of oil components in various environmental compartments (water surface, shoreline, water column, atmosphere, sediments, etc.), oil pathways over time (trajectories), surface oil distributions, and concentrations of the oil components in water and sediments. SIMAP's biological effects model is then used to evaluate exposure, toxicity, and effects on each habitat and species (or species group) in the area of the spill.

Often, currents that transport oil components and organisms are estimated by a hydrodynamic model; however, observational current data, such as from high-frequency-radar (HF-Radar) systems, drifters, or current meters, may also be used. The transport models for such analyses are highly sensitive to the current velocities and turbulent dispersion coefficients input to the models, as are further calculations utilizing the transport results. In this study, we evaluate the usefulness of field-collected data from fluorescein dye studies off San Diego, California, to document movement and dispersion of subsurface oil (dye) over three spatial dimensions and time. We analyzed HF Radar and drogue measurements of near-surface currents, dispersion coefficients based on dye spreading measurements, modeling of wind-forced surface water drift as a function of wind speed and direction (based on published results of fluid dynamics studies), and water density profiles to determine their efficacy and accuracy as inputs for modeling transport of near-surface constituents (such as dissolved hydrocarbons from naturally entrained or chemically dispersed oil).

More specifically, the modeling issue addressed in this study is as follows. Small-scale transport processes need to be resolved in fate and transport modeling used in oil impact analysis in order to evaluate effects on water column biota. These small-scale processes determining current velocities are complex, and as such, it is not feasible to include most of the complexities at appropriately small scales in oil spill modeling applications, both in real time and in hindcast. While three-dimensional hydrodynamic model systems have and might be developed to model the various processes and scales, a considerable location-specific effort would be required to resolve the currents in fine enough scales both spatially and temporally to accurately predict or hindcast movements of oil constituents at the scale needed to evaluate water column effects on biota. Also, there are difficulties in predicting currents with a hydrodynamic model application that does not include all the forcing or enough temporal detail in the forcing functions (e.g., use of boundary conditions based on climatic means rather than date-specific patterns) to capture advection of the appropriate scale.

In modeling oil spill fate, it is common practice to use Lagrangian (particle) trajectory models to predict the transport of so-called spilletts (Lagrangian elements, LEs, etc.), which represent sublots of the spilled oil (e.g., Mackay *et al.*, 1982; Spaulding *et al.*, 1983; Spaulding, 1988; Lehr *et al.*, 1995, 2000; French *et al.*, 1996; Galt, 1998; Reed *et al.*, 1999, 2000; French McCay, 2003, 2004). The current and wind fields used to force these models are either supplied by hydrodynamic and meteorological models or are interpolated/extrapolated current and wind observations. The advective movements of spilletts are typically approximated as the vector sum of the current field plus an empirically based down and cross (leeway) drift in response to wind forcing (called Stokes drift). Allen and Plourde (1999) and Allen (1999) provide empirical leeway drift factors (drift rate, down- and cross wind, versus wind speed) and the associated uncertainties for sixty-three separate classes of objects. Many oil spill models have depended on earlier drift observations summarized in Lange and Hufnerfuss (1978). Youssef and Spaulding (Youssef, 1993; Youssef and Spaulding 1993, 1994) developed a model of surface wind-forced current and Stokes drift, which is employed in a simplified form in SIMAP along with the option of using the even simpler approach of a constant drift rate and leeward drift angle (French McCay, 2004). The advantage of the Youssef and Spaulding model (and similar hydrodynamic models addressing these processes) is that it captures the vertical shear (decrease in speed and change in angle with increasing depth in the first few meters under the surface) of the Stokes drift which has been observed to shear subsurface plumes (French *et al.*, 1997; Youssef and Spaulding 1993, 1994; Cox *et al.*, 2004) as shown by slower movements of subsurface drifters. This vertical shear was observed in the dye experiments off San Diego, and one objective was to determine the usefulness and accuracy of such wind drift algorithms to predict subsurface plume movement and diffusion. The Youssef and Spaulding model was evaluated specifically, but the intent was to assess the approach. It is expected that further development will be necessary to improve the applicability of such a modeling effort in the future.

Another modeling issue is to appropriately parameterize small scale motions termed dispersion or eddy diffusion: those turbulent eddies and motions at spatial and temporal scales smaller than the grid-cell size and time step used in the hydrodynamic model producing the advective current field. Because hydrodynamic model applications need to cover large spatial domains in order to get the appropriate forcing functions correct, they typically have grid cells on the order of 1 km or more. In most oil spills, with the exception of those where natural dispersion is extremely high and involves a large release of oil such as the *North Cape* oil spill (French McCay 2003), the dimensions of the subsurface plumes are smaller than 1 km and very patchy (McAuliffe, 1987; French McCay, 2004; French McCay *et al.*, 2005; NRC, 2005). Even with added chemical dispersant, the plume dimensions would be expected to be small scale (French McCay and Payne, 2001), smaller than the scale captured by the advective current field typically input to oil transport models. Thus, the predicted subsurface concentrations of oil droplets and dissolved hydrocarbons from any oil spill model are dependant on the assumed small-scale turbulence parameters input to the model. These assumptions are infrequently discussed or recognized as to their importance. For example, no mention was made in the Cox *et al.* (2004) report of the assumptions used for the Prince William Sound oil spill modeling (OSCAR simulations). However, the predictions of subsurface concentrations and impacts on water column biota are completely dependent on these assumptions (see for example French McCay, 2003 where sensitivity analysis varying these assumptions was used to calibrate the SIMAP model).

The small scale turbulent motions, more simply called mixing, are caused by a number of physical forces in the surface mixed layer of the ocean: cooling and evaporation-induced convection caused by sinking denser water; wind stress transmitted to turbulence; breaking wave-induced turbulence; Langmuir circulation; wind-driven shear in the water column; etc. (Thorpe, 1995; see summary by Moun and Smyth, 2001). Most of these processes have not been modeled and many are poorly understood. Thus, empirical measurements have been used to parameterize the small scale mixing processes in many applications (Okubo, 1967; Okubo and Ozmidov, 1970). Again, it is the small scale mixing processes that are of critical importance to the prediction of subsurface plume dynamics and dilution if the spatial domain modeled is of similar scale. This priority area for research is identified in the NRC (2005) report, as noted above.

The turbulent motion is typically parameterized in Lagrangian transport models by employing a first-order random walk technique (i.e., randomizing position each time step using horizontal and vertical dispersion coefficients to scale the magnitude of the movements). Recently, Spaulding *et al.* (2006) evaluated the use of the customary first-order random walk technique as opposed to higher-order random walk models (where sequential velocities are correlated rather than random in direction), finding the first-order random walk technique based on the Gaussian diffusion model works as well as higher order models given the uncertainties in needed input assumptions for the higher order models.

An alternative to using hydrodynamic modeling to provide current data needed for transport models, is to use empirical measurement data. The Cox *et al.* (2004) report is one example of a study that demonstrates that high frequency coastal radar systems are useful sources of real time measurements that could provide input to oil spill models (as well as for Search and Rescue modeling and other applications). These systems have the potential of providing high spatial (1.5 to 6 km) and temporal (1 to 3 hr) resolution observations of surface current fields over ranges of 50 to 150 km. Spaulding *et al.* (2005) employed drifter observations to test the usefulness and accuracy of CODAR-generated surface advective fields as input to transport models. In the present project, the dye study data in conjunction with drifter movements, allowed direct measurement of transport and dispersion with which to test the usefulness of HF-Radar data for this purpose, as well as to develop methods (fitting algorithms) for using dye study data to estimate small-scale dispersion that may be applied by NOAA and other oil spill modelers.

The application of dispersants during an oil spill response calls for observations and sampling of the dispersed oil to determine the dispersant efficiency, and protocols have been developed to provide a rapid semi-quantitative field method for measuring enhanced entrainment into the water column after dispersant use (Henry *et al.*, 1999). Additional methods are being developed to measure environmental impacts associated with dispersant applications (Payne *et al.*, 2007). Repeated sampling of the same plume(s) is essential to determine the exposure of water column organisms, to validate models of exposure and effects, and to evaluate environmental trade-offs justified as a decision to use dispersants under certain circumstances. Natural Resource Damage Assessment will be absent critical quantitative and qualitative information with which to verify model results without a sound methodology for collecting water column data. A significant

challenge is to locate and sample the dispersed oil plume over time. Thus, another objective of this project was to demonstrate a methodology for locating and tracking a plume using real-time observations of upper ocean currents.

As described in Section 2, the overall objectives of the project were to:

- Develop understanding of small-scale transport processes important to fate and transport modeling used in oil impact analysis, (i.e., near-surface transport and dispersion (mixing), based on literature review and field studies);
- Provide detailed measurements of dispersion of dye, from which horizontal and vertical diffusivities can be calculated (i.e., with greater sampling frequency and resolution than usually available);
- Develop algorithms quantifying small-scale transport processes based on measurable oceanographic and meteorological data that can be included in oil fates models;
- Test the efficacy and reliability of HF Radar and drifters for providing near-surface current input data to oil spill models such as SIMAP (French McCay 2004) by comparison of predicted trajectories with dye movements; and
- Evaluate model-predicted transport and dispersion through comparison of measured dye concentrations over three dimensional space and time as a test of algorithms that may be incorporated into SIMAP and other oil transport and fate models that currently use bulk coefficients to parameterize mixing.

More specifically, four hypotheses were tested with respect to modeling near-surface transport:

1. Measured wind data combined with surface current maps from an HF-Radar system can be used to hindcast the plume trajectory and/or concentrations.
2. Measured wind data combined with near-surface current observations from drifters can be used to hindcast the plume trajectory and/or concentrations.
3. Measured wind data alone can be used to hindcast the plume trajectory and/or concentrations.
4. Fluorescein dye simulating dispersed neutrally-buoyant or dissolved constituents can be measured repeatedly and used to calibrate and/or validate the computer simulations.

5.2 Model Algorithms

5.2.1 Lagrangian transport model

The transport model in SIMAP (French McCay, 2003, 2004, also earlier version in French *et al.*, 1996) and other oil spill models (Mackay *et al.*, 1982; Spaulding *et al.*, 1983; Spaulding, 1988; Lehr *et al.*, 1995, 2000; Galt, 1998; Reed *et al.*, 1999, 2000) utilize similar algorithms for calculating advective movements and turbulent dispersion. Lagrangian particles (“spilletts”) are used to track the oil movements and weathering. The movements in three spatial dimensions over time are described by vector positions: new vector position of the spillet center is calculated from the old plus the vector sum of east-west, north-south, and vertical components of advective and diffusive velocities:

$$X_t = X_{t-1} + \Delta t (U_t + D_t + R_t + W_t) \quad (15)$$

where X_t is the vector position at time t , X_{t-1} is the vector position the previous time step, Δt is the time step, U_t is the sum of all the advective (current) velocity components in three (spatial) dimensions at time t , D_t is the sum of the randomized diffusive velocities (i.e., dispersion) in three dimensions at time t , R_t is the rise or sinking velocity of whole oil droplets in the water column, and W_t is the surface wind transport (“wind drift”). The magnitudes of the components of D_t are scaled by horizontal and vertical dispersion coefficients (Okubo and Ozmidov, 1970; Okubo, 1971). R_t is typically computed by Stokes law, where velocity is related to the difference in density between the particle and the water, and to the particle diameter. In this study, the dye was assumed neutrally buoyant and R_t was zero.

In SIMAP at each time step, concentrations in the water column are calculated by summing mass within each grid cell of a multilayer grid on the order of 100 (east-west) by 100 (north-south) cells, which are scaled each time step to just cover the dimensions of the plume. This maximizes the resolution of the contour map at each time step and reduces error caused by averaging mass over large cell volumes. Distribution of mass around each Lagrangian particle center is described as Gaussian in three dimensions, with one standard deviation equal to twice the diffusive distance ($2D_x t$ in the horizontal and $2D_z t$ in the vertical, where D_x is the horizontal and D_z is the vertical dispersion coefficient, and t is particle age). The plume grid edges are set at one standard deviation out from the outer-most particle. Concentrations are calculated in each cell and time step and saved to files for later viewing and calculations.

Thus, in SIMAP there are two diffusive scales that may be used, or one is set to zero in simple cases. The advective dispersion, D_t , operates on a larger scale than the local dispersion measured in the dye studies.

5.2.2 Wind drift

In the SIMAP fates model, if the wind drift of the surface wave-mixed layer (wind-induced drift current plus Stokes drift caused by wave motions) is not included in current data supplied to the fates model (typically by a hydrodynamic model, which may include some wind forcing but not Stokes drift), and where fetch is sufficient for waves and Stokes drift to develop, wind drift is added to the advective particle velocity within the oil fates model. Wind drift is at a maximum at the water surface and decreases rapidly with depth. The drift extends deeper into the water column the higher the wind speed. At very low wind speeds, the wind drift is insignificant at 4 or 5 meters, the depth of the deeper drogues on drifters in this experiment. At 1 m, wind drift is significant in most of the experimental periods. Evidence of vertical shear consistent with (general) wind drift theory was seen in the vertical profiles of the dye (Figure 4-15).

The wind drift rate is the ratio of drift speed relative to the wind speed. Drift velocities related to wind speed vectors, u_{wc} and v_{wc} (m/sec), toward the east and north, respectively, are

$$u_{wc} = (C_w/100) u_w \quad (16)$$

$$v_{wc} = (C_w/100) v_w \quad (17)$$

where u_w is the east component of wind speed (m/sec), v_w is the north component of wind speed (m/sec), and C_w is the drift factor (percentage of wind speed).

The drift factor, C_w , may be estimated from empirical data as a constant (e.g., based on observations by Lange and Hufnerfuss, 1978; Wu, 1980; Samuels *et al.*, 1982), where C_w varies between 2.5 and 4.5%. Values typically used in modeling floating oil are 3.0-3.5%. In some models, the uncertainty of the angle and speed of the wind stress and resulting wind drift is included by randomly varying the percentage and angle within the range of potential values (e.g., Galt 1998; Lehr *et al.* 1995). This inclusion of uncertainty is particularly important in forecasts of oil trajectories. If current data based on a hydrodynamic model that includes wind forcing is used as input to a transport model, the wind drift factor should be lower, depending on the parameterization of wind drift included in the hydrodynamics, and uncertainty ranges should reflect this.

The wind drift angle is the angle transported constituents drift clockwise (to the right in the northern hemisphere, use negative values for southern hemisphere) of the wind (down-wind) direction. Drift velocities due to wind, u_{wd} and v_{wd} (m/sec), toward the east and north, respectively, are

$$u_{wd} = u_{wc} \cos \theta + v_{wc} \sin \theta \quad (18)$$

$$v_{wd} = -u_{wc} \sin \theta + v_{wc} \cos \theta \quad (19)$$

where u_{wc} is the drift velocity due to wind (m/sec) toward the east, v_{wc} is the drift velocity due to wind (m/sec) toward the north, and θ is the drift angle (degrees). A mean drift angle of 20° has been observed in several spills in open waters of mid latitudes. The angle increases with latitude. In confined water bodies, the drift angle is typically near zero (French McCay, 2004).

Alternatively, as is done herein and in the SIMAP model, an algorithm developed from a hydrodynamic modeling study of local wind-induced transport in the surface layer of open waters, such as by Youssef (1993) and Youssef and Spaulding (1993, 1994), may be used. Other hydrodynamic modeling efforts (e.g., Leibovich, 1977; Huang, 1979; Weber, 1983; Jenkins, 1986, 1987; Boufadel *et al.*, 2006a,b) could also be used to develop such an algorithm. These hydrodynamic models sum wind-induced drift current and Stokes drift based on wave theory. They employ the equations of motion for the wind-induced drift current, which includes the Coriolis force (effect). Thus, the results are to some degree a function of latitude. Youssef and Spaulding (1993, 1994) assumed a latitude of 60°N when running the model, as they compared the results to field experiments at that latitude. Sensitivity to latitude has not been examined specifically, although observations of drifting objects (Lange and Hufnerfuss, 1978; Wu, 1980; Samuels *et al.*, 1982) seem to be within the same range over a large range of latitudes. One would expect that the principle role of Coriolis force is to change the near surface drift direction, but not its magnitude. The larger the Coriolis force the larger the drift angle. At our 32.6°N study site, the Coriolis force is less than at 60°N , and so the wind drift angle may be over-estimated by the model. In the absence of the Coriolis force (i.e., at the equator) the surface currents would simply be in the downwind direction.

The model results developed by Youssef (1993) and Youssef and Spaulding (1993, 1994), to which the following equations were fit, were based on an assumption of steady state conditions and a fully-developed sea in deep water. Thus, it applies when there is sufficient fetch to have an equilibrium sea state (and absence of swell), and where the wind has blown in the same direction for on the order of 5-6 hours (Youssef and Spaulding, 1993). Since the winds at our study site during the observation periods were primarily diurnal (afternoon sea breeze influence, see Appendix E) with non-equilibrium waves and swell present, the applicability of the model results to the experimental conditions was evaluated.

Youssef's and Spaulding's results show that the wind drift factor at the water surface, C_{wo} , is related to wind speed w (Youssef and Spaulding, 1993, 1994):

$$C_{wo} = 3.9088 - 0.031885 w \quad (20)$$

The wind drift ranges from 4% of wind speed for very light winds to 3% of wind speed at a 30 m/s wind speed. Similarly, the wind drift angle at the water surface, C_{ao} , is related to wind speed w (Youssef and Spaulding, 1993, 1994) by:

$$C_{ao} = 23.627 - 7.97 \log_{10}(w) \quad (21)$$

The wind angle varies from 24° for very light winds to 12° at a 30 m/s wind speed.

The wind drift factor decreases and the angle increases with increasing depth into the water (Youssef, 1993 and Youssef and Spaulding, 1993, 1994). To quantify the current shear as a function of depth (similar to an earlier version of this algorithm, French McCay, 2004), functions were fit empirically to the Youssef and Spaulding model results:

$$C_{wz} = \text{Max}(\{ [k_{w1} - 0.09757 \ln(z)] C_{wo}, 0 \}) \quad (22)$$

$$k_{w1} = 0.19692 \ln(w) - 0.19047 \quad (23)$$

$$C_{az} = \exp(k_{w2}) z^{k_{w3}} \quad (24)$$

$$k_{w2} = 4.999 w^{-0.1233} \quad (25)$$

$$k_{w3} = 0.344 w^{-0.2396} \quad (26)$$

where C_{wz} is the drift factor (percent of wind speed) and C_{az} is the drift angle at depth z and k_{w1} , k_{w2} and k_{w3} are functions of wind speed.

Figure 5-1 shows the relationships of drift speed and angle (relative to downwind) to wind speed. In Figure 5-2, wind drift vectors are averaged over the water column to a given depth, indicating transport of a neutrally buoyant or dissolved constituent in a surface mixed layer of that depth. Note from Figure 5-2 that depth-averaged speed declines rapidly with depth, while the angle approaches 30-50° if the mixed layer is >1 m in depth, the typical situation.

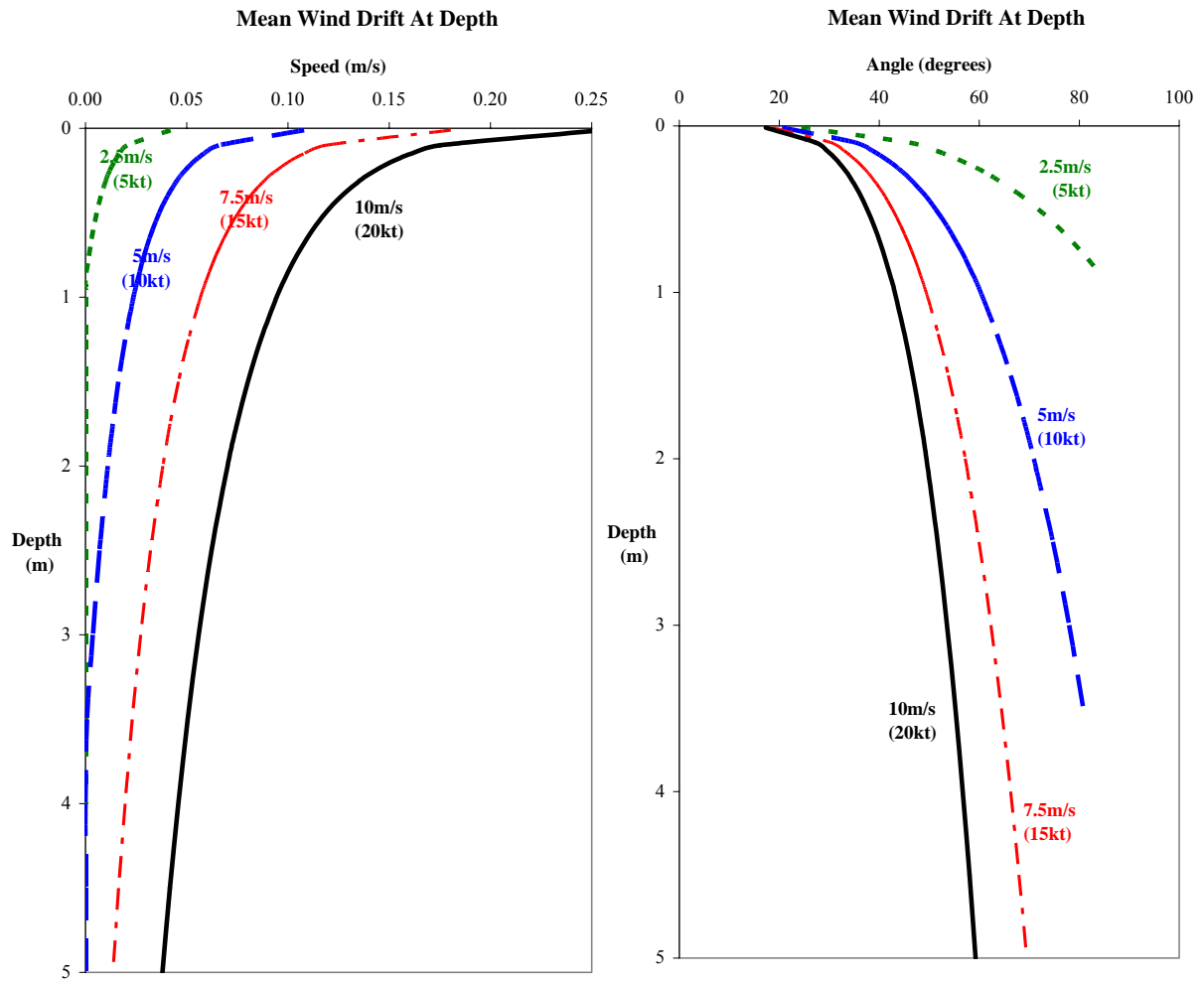


Figure 5-1. Drift speed (left panel) and angle (relative to downwind, right panel) as a function of depth and wind speed.

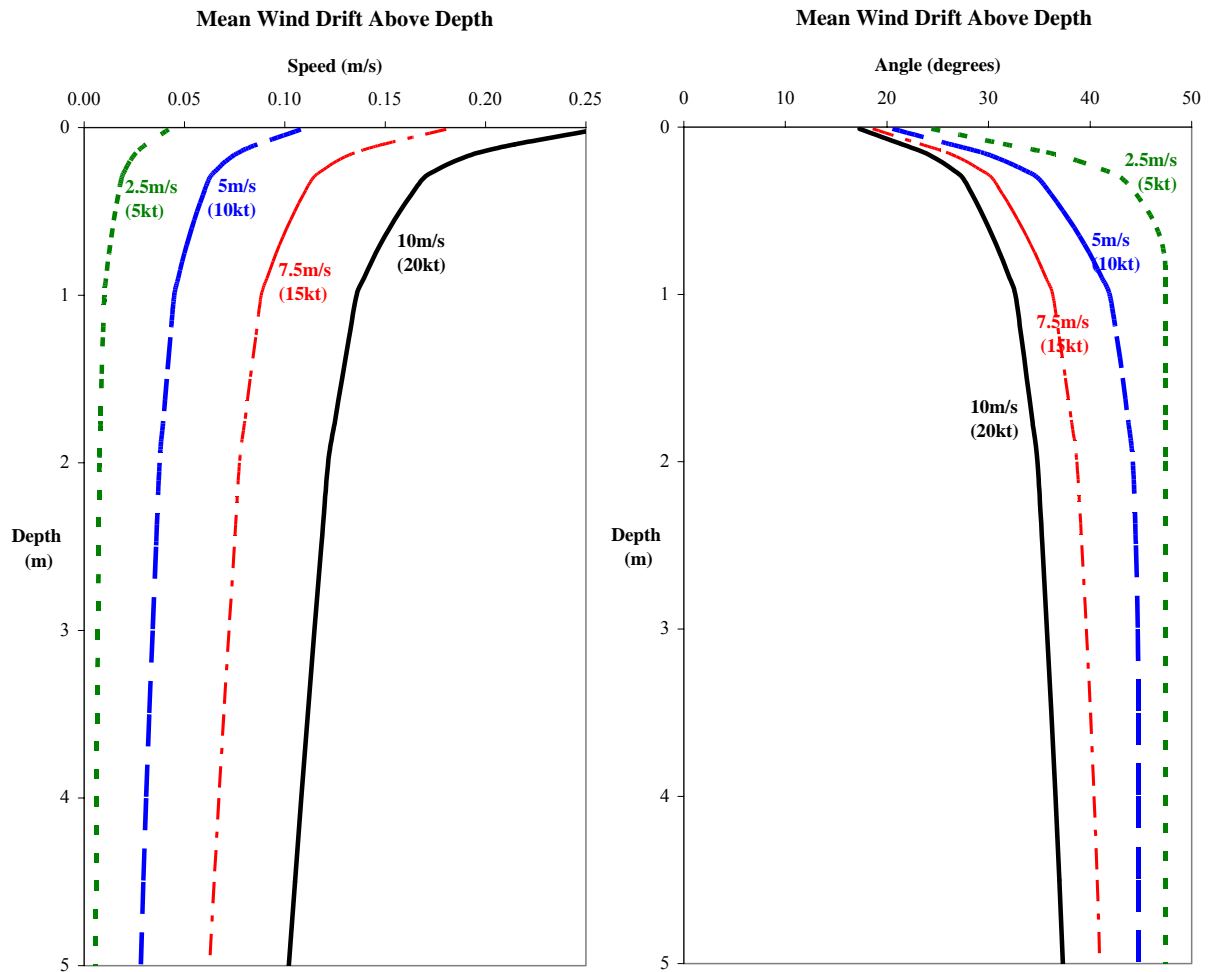


Figure 5-2. Drift speed (left panel) and angle (relative to downwind, right panel) as a function of wind speed, averaged over the water column from 0 m to depth.

5.3 Model Results

5.3.1 Wind Conditions and Mixed Layer Characteristics

Table 5-1 lists wind speed and direction data for the La Jolla station (LJPC1), on the shoreline 30 km north of the experimental site. Winds were generally from the west or northwest in all experiments except for that on 8 November 2005 when the wind was from the southeast. Winds were very light in the 21-22 June 2006 experiments. Winds were from a similar direction but slightly higher at the offshore weather buoy 46086, 70 km west of the experimental site.

The surface mixed layer depths and water column stability during each experiment are also listed in Table 5-1. The dye penetrated to the depth of the mixed layer via Langmuir circulation within a half hour after release, but was not uniform in concentration over the mixed layer. Thus, the “mixed layer” was not entirely mixed in the experimental time frames. In most locations, the dye did not mix deeper than the mixed layer depth by the end of the experiment. It was apparent that the vertical dispersion rate slowed at the base of the mixed layer (as defined here), where a stronger pycnocline impeded vertical mixing.

Table 5-1. Wind and wave conditions, mixed layer depth, water density, and stability characteristics.

Date	8 Nov 2005	21 Mar 2006	22 Mar 2006	21 Jun 2006	22 Jun 2006	1 Nov 2006	2 Nov 2006
Wind direction (deg., from) at LJPC1 ⁺	191	284	319	256	249	325	327
Wind speed (m/s) at LJPC1 ⁺	5.7	5.0	4.2	3.5	3.3	5.2	4.2
Significant wave height (m) at Buoy 46086	1.1	1.5	1.8	1.5	1.2	1.0	1.2
Mixed layer depth (m)	9	12	15	10	7	11	8
Dye plume penetration depth (m)	10	10*	10 to 14	6	7	10**	8
Mean water density in mixed layer (kg/m ³)	1024.3	1025.3	1025.3	1023.2	1023.1	1024.3	1024.1
Density gradient with depth in mixed layer	0.0270	0.0152	0.0172	0.0662	0.0228	0.0172	0.0024
Buoyancy frequency (N , sec ⁻¹) [equation 3]	0.0161	0.0121	0.0128	0.0252	0.0148	0.0128	0.0048
Vertical shear: based on wind-drift speed, averaged in top 3m	-0.027	-0.024	-0.020	-0.015	-0.014	-0.024	-0.020
Richardson Number ($Ri > 0.25$ indicates a stable water column) [equation 4]	0.36	0.26	0.43	2.83	1.19	0.28	0.06

⁺ Averaged over the time drifters were deployed.

* Plume measured for approximately one hour and dye may not have reached maximum depth during sampling.

** Deepest depth sampled but dye is known to have gone deeper since the edge of the plume was not detected at that depth (Fluorescence was still above background at 10 m.)

The mixed layer was relatively stable in the November 2005 and June 2006 experiments, but unstable (or of low stability, $Ri < 1$) in the March 2006 and November 2006 experiments, as shown by the Ri values in Table 5-1. The higher degree of density stratification and shallower mixed layer would be expected in June when surface heating is highest and winds are light. Note that the Ri values in Table 5-1 were calculated using vertical shear based on the wind drift algorithm, whereas the vertical shear measured by the dye (Table 4.6-1) represented the total shear in the upper few meters and included other physical mechanisms.

5.3.2 Advection

The movements of the dye and drifters, and the shapes and expansion rates of the dye plumes were shown in Section 4, Figures 4-3 to 4-11. The 1- and 2-m drifters moved faster than the 4- and 5-m drifters (Table 5-2), indicating the expected decrease in wind drift with depth predicted by wind drift theory. Evidence of vertical shear was also seen in the vertical profiles of the dye (Figure 4-15). For experiments in 5-7 m/s winds where the surface mixed layer was unstable (22 March 2006 and 1-2 November 2006), the drifters drogued at 4-5 m tracked the dye most accurately, whereas drifters drogued at 1-2 m moved downwind just ahead of the dye plume, as predicted by the wind drift algorithm (Figure 5-1). In the 21-22 June 2006 experiments where the surface mixed layer was highly stable and wind drift was slow and shallow (due to light winds), drifters drogued at 2 m tracked the dye closer, with the 4-m drifters slower than the bulk dye movements.

Velocities measured by drifters and HF-Radar were directly compared in order to assess differences between modeled trajectories produced by the two measurements and the ability of the wind drift algorithm to reconcile them. Because horizontal shear was observed in some high-resolution vertical profiling measurements with the *in situ* towed fluorometer (Section 4.6, e.g., Figure 4-15) and with HF-Radar and drifter velocities over all experiments, HF-Radar velocities were interpolated in space and time to only the shallowest drifter locations for each fix over all experiments. Mean bearings, magnitudes, and differences between HF-Radar and the shallowest drifter velocities are summarized in Table 5-2.

Table 5-2. Observed movements of drifters and HF-Radar-measured current (interpolated to each of the shallowest drifter locations for each fix in time).

Date	8 Nov 2005	21 Mar 2006	22 Mar 2006	21 Jun 2006	22 Jun 2006	1 Nov 2006	2 Nov 2006
Drifters at 1m or 2m*: speed (cm/s)	37.4	8.4	15.1	25.7	12.4	8.8	9.6
Drifters at 1m or 2m*: Bearing (deg.)	16	160	93	130	76	154	154
Drifters at 4m**: speed (cm/s)			13.0	19.4	7.5	7.5	7.2
Drifters at 4m**: Bearing (deg.)			75	143	70	161	153
HF Radar: Speed (cm/s)	22.4	8.6	10.6	15.5	9.5	11.5	12.4
HF Radar: Bearing (deg.)	11	145	124	107	99	189	174
Angle of down-current measured by HF Radar relative to downwind	0	41	-14	31	30	44	27
Speed (cm/s) of down-current measured by HF Radar relative to drifter at 1 or 2 m	-15.0	0.2	-4.5	-10.2	-2.9	2.7	2.8
Angle of down-current measured by HF Radar relative to drifter at 1 or 2 m	-4	-15	32	-23	23	35	20

* at 1m for 8 November 2005 and 21-22 March 2006 experiments; at 2m for 21-22 June 2006 and 1-2 November 2006 experiments

** at 5m for 22 March 2006 experiment; at 4m for other experiments

The HF-Radar measurements of current did not in all cases agree with the drifter movements. As would be expected, better agreement in velocity bearing between HF-Radar and drifter measurements was observed when drifters were drogued at 1 m relative to 2 m. The best agreement in bearing between HF-Radar and drifter measured velocities was on 8 November 2005 and 21 March 2006 when drifters were drogued at 1 m. The relatively large discrepancy in

bearing on 22 March 2006 was likely related to high horizontal shear as indicated by the large spread of drifter trajectories (and variability of drifter velocities) with similar starting points (Figure 4-7).

Absolute differences in magnitude between HF-Radar velocities and drifter velocities were below 5 cm/s for all experiments with the exception of 8 November 2005, when the 1-m drifters advected ahead of the dye plume (as did 1-m drifters on 22 March 2006), and 21 June 2006. However, these differences are well within differences found between HF radar and other observation techniques (Paduan, 1996; Spaulding *et al.*, 2006; Ohlmann *et al.*, 2007), especially since horizontal shear over the spatial averaging area of the HF-Radar wasn't accounted for in the drifter velocities. Other discrepancies such as differences in sampling depth in later experiments would also be expected to play a role in observed differences.

Wind drift would be expected to affect HF-Radar velocities measured over 0-50 cm more than drifter velocities measured at depths of 1 or 2 m. An analysis was undertaken in order to test the wind drift algorithm and determine if the drifter and HF-Radar velocity differences were accounted for by differences in wind drift. For this exercise, wind drift vectors (based on the wind drift model that assumes a steady wind direction and speed to fully develop the waves – Section 5.2), were averaged both over the upper 50 cm (the depth range of the HF Radar) and at the depths of the drifters and then were subtracted from each measure of the current, leaving a residual current (Table 5-3). Assuming the wind drift model was applicable and valid (and that the HF Radar-measured current was accurate), the resulting residual current should presumably be the same for each instrument, unless other current shear exists in the surface 5 m at the scales of the measurements. This approach to testing the wind drift model assumes no other sources of shear, such as baroclinic motions from internal tides. Wind from station LJPC1 was used for this comparison because it was coherent with wind measured south of the dye release site at Imperial Beach, CA and with COAMPS nowcasts of winds at the dye release site over each experiment. The vectors indicated by the values in Tables 5-2 and 5-3 are plotted in Figures 5-3 to 5-9.

Table 5-3. Speed and bearing measured by drifters and HF-Radar with modeled wind drift subtracted (using winds at LJPC1).

Date	8 Nov 2005	21 Mar 2006	22 Mar 2006	21 Jun 2006	22 Jun 2006	1 Nov 2006	2 Nov 2006
Drifters at 1m* (less wind drift): speed (cm/s)	35.5	6.1	15.7	25.7	12.4	8.2	9.4
Drifters at 1m* (less wind drift): Bearing (deg.)	12	158	88	130	76	146	152
Drifters at 4m** (less wind drift): speed (cm/s)			13.0	19.4	7.5	7.5	7.2
Drifters at 4m** (less wind drift): Bearing (deg.)			75	143	70	161	153
HF Radar (less wind drift average over 0-50cm): speed (cm/s)	17.2	3.0	8.8	12.5	6.9	5.6	8.3
HF Radar (less wind drift average over 0-50cm): Bearing (deg.)	358	152	102	105	95	197	168

* at 2m for 21-22 June and 1-2 November 2006 experiments

** at 5m for 21 March 2006 experiment

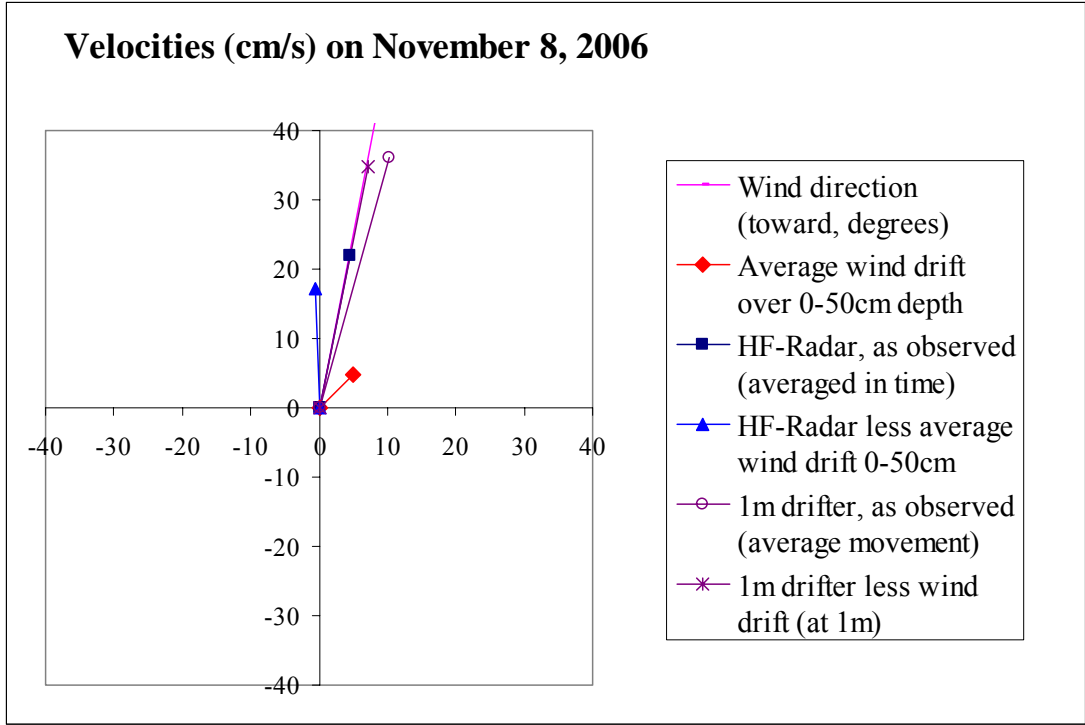


Figure 5-3. Vector plot of wind drift, HF-Radar (as measured and less wind drift) and drifter (as measured and less wind drift) velocities during the 8 November 2005 experiment.

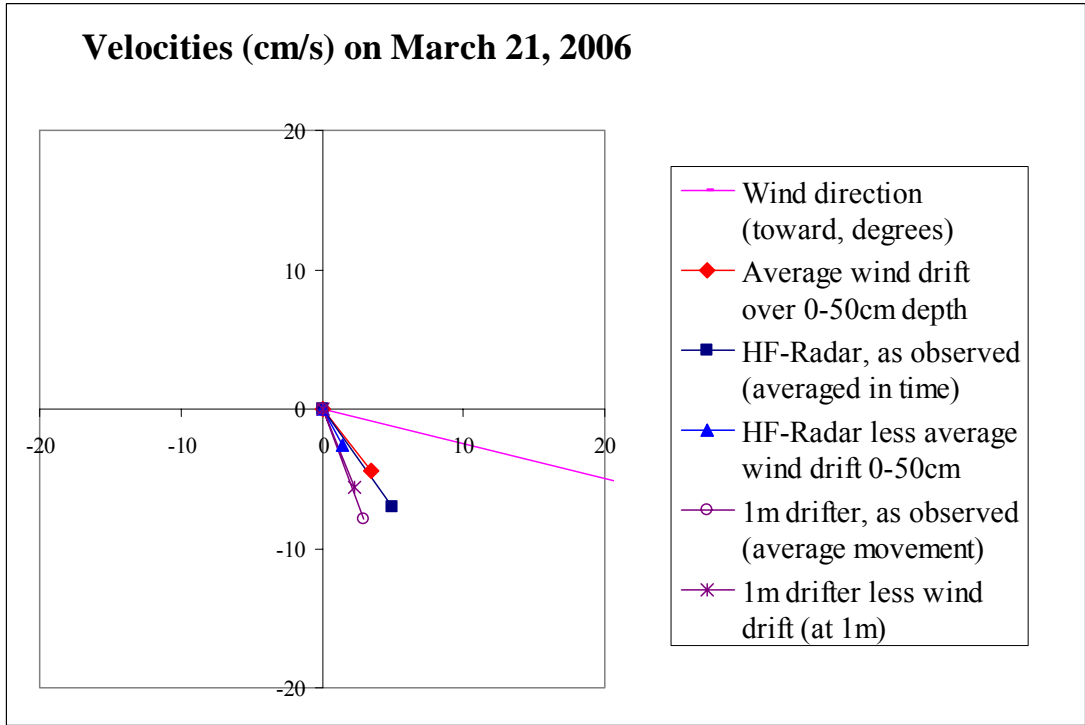


Figure 5-4. Vector plot of wind drift, HF-Radar (as measured and less wind drift) and drifter (as measured and less wind drift) velocities during the 21 March 2006 experiment.

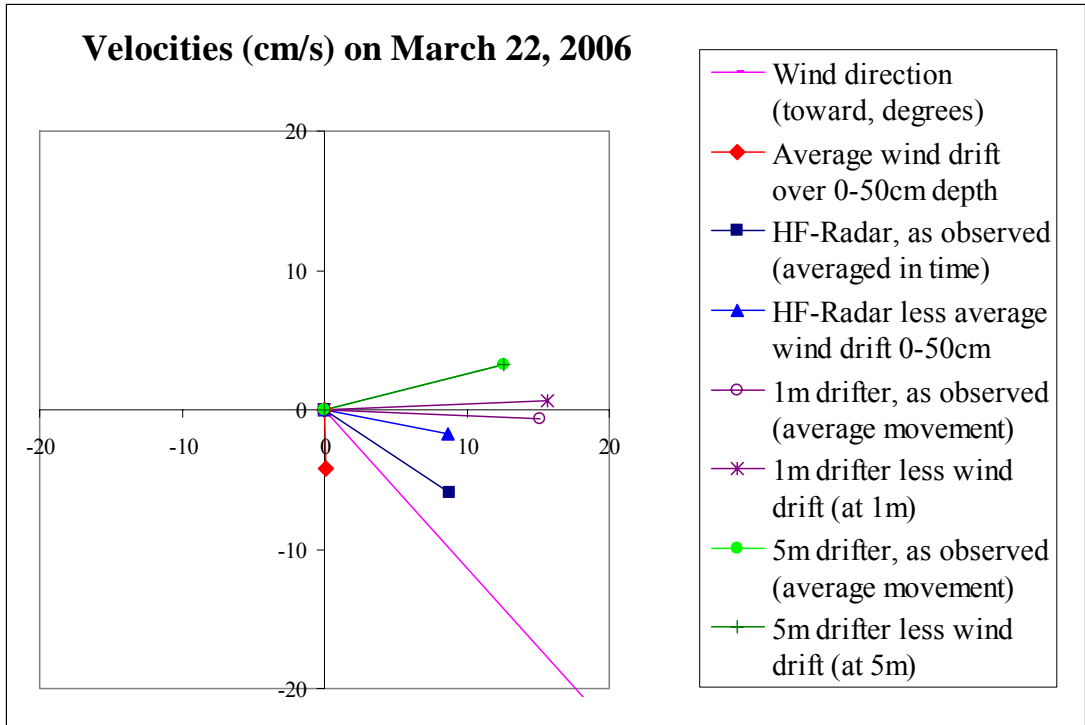


Figure 5-5. Vector plot of wind drift, HF-Radar (as measured and less wind drift) and drifter (as measured and less wind drift) velocities during the 22 March 2006 experiment.

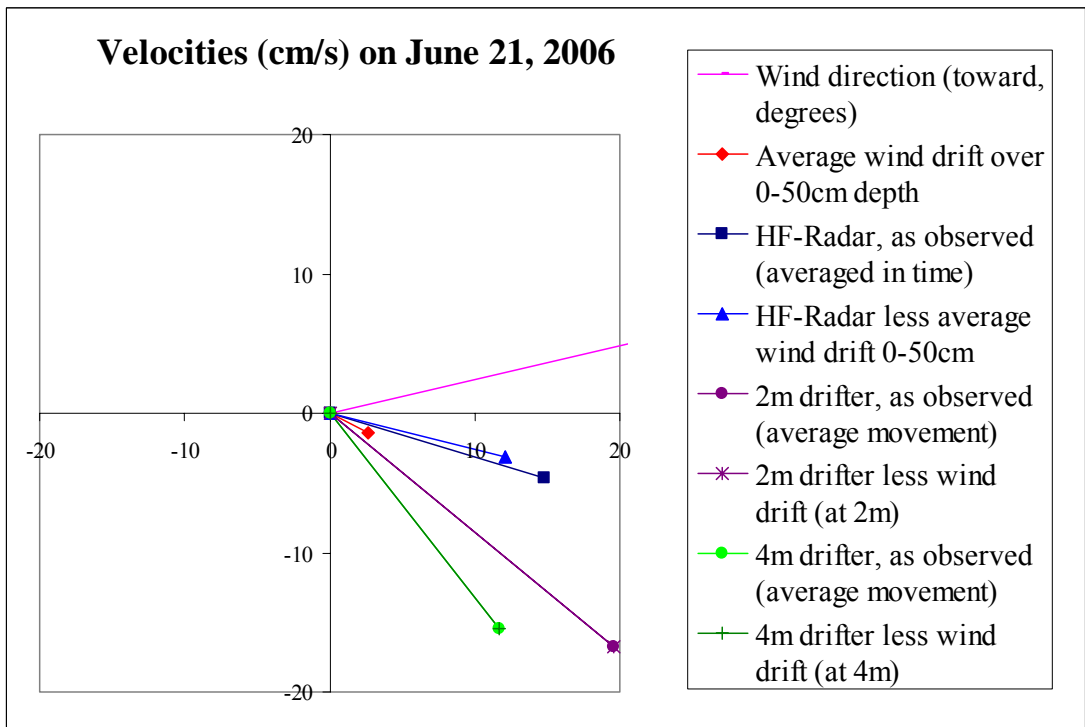


Figure 5-6. Vector plot of wind drift, HF-Radar (as measured and less wind drift) and drifter (as measured and less wind drift) velocities during the 21 June 2006 experiment.

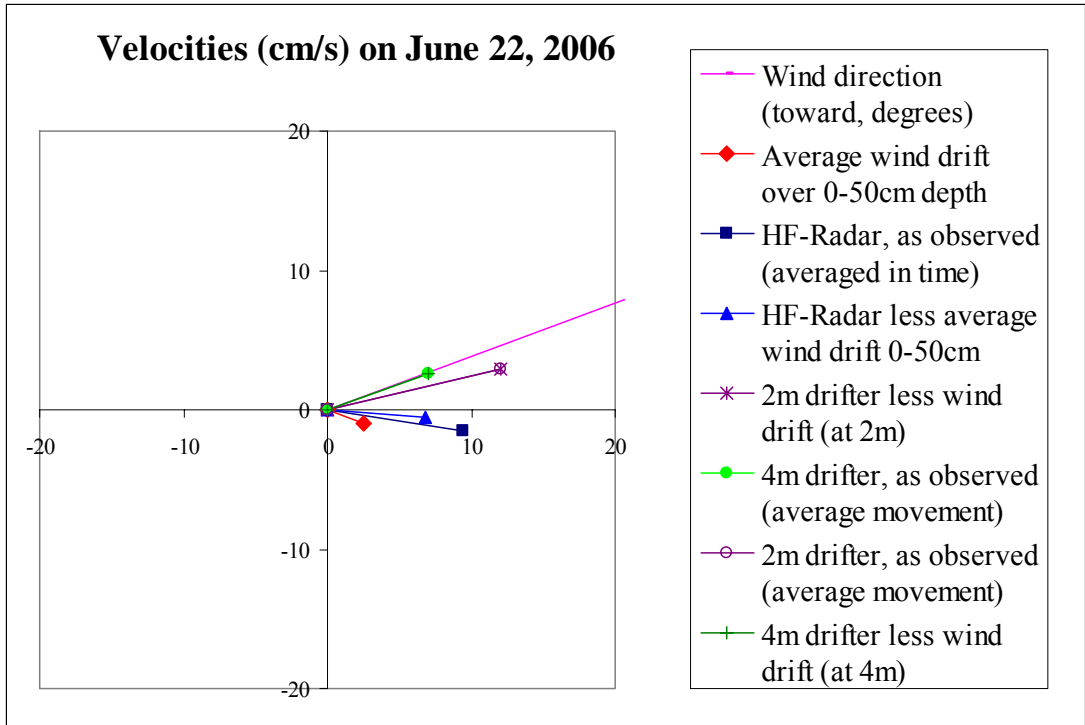


Figure 5-7. Vector plot of wind drift, HF-Radar (as measured and less wind drift) and drifter (as measured and less wind drift) velocities during the 22 June 2006 experiment.

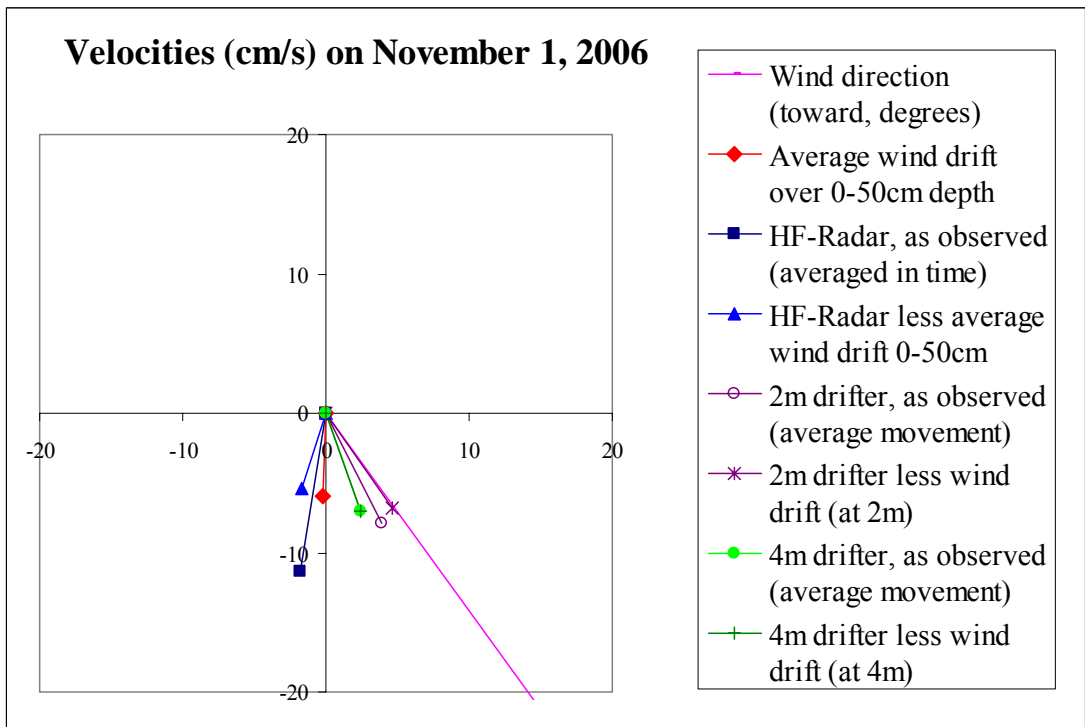


Figure 5-8. Vector plot of wind drift, HF-Radar (as measured and less wind drift) and drifter (as measured and less wind drift) velocities during the 1 November 2006 experiment.

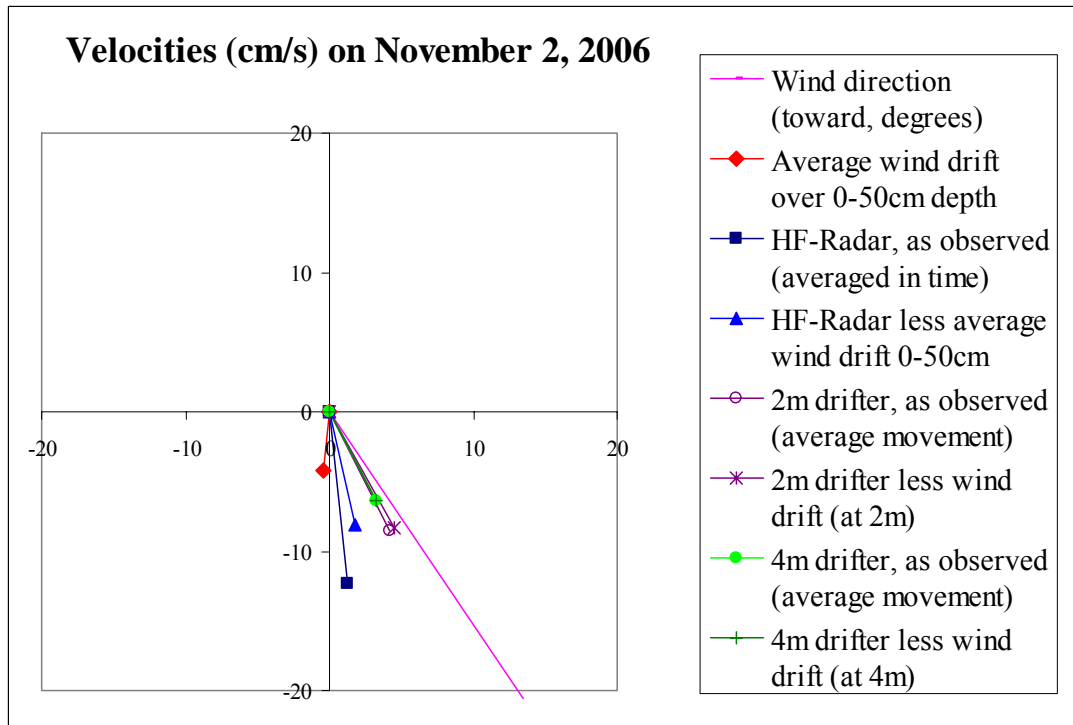


Figure 5-9. Vector plot of wind drift, HF-Radar (as measured and less wind drift) and drifter (as measured and less wind drift) velocities during the 2 November 2006 experiment.

The drifters in the 21 June 2006 experiment indicated more vertical shear than in the other experimental periods (Figure 5-6, as compared to Figures 5-3 to 5-9). In all experiments with drifters at two depths, removal of model-predicted wind drift (which was negligible for the 4-5m drifters) from the drifter velocities reduced, but did not entirely account for, the differences in speed among drifters at different depths. The drifter bearings were not significantly changed by the wind drift correction (Tables 5-2 and 5-3, Figures 5-3 to 5-9). Thus, wind drift alone, applied at the drogue depths for the drifters, was unable to account for differences observed between drifters when deployed at different depths. However, the modeled wind drift at these wind speeds and the drifter depths ranged from 0.6 to 2.6 cm/s, within the range of variability in net movement of the drifters over the experimental time period. Thus, the wind drift algorithm could not be statistically tested with this drifter data set.

The wind drift algorithm was not able to reconcile differences in velocities measured between the HF Radar and the drifters at 1 or 2 m in all cases. In the 21 and 22 June 2006 experiments, winds were light and wind drift was insignificant, leaving unresolved differences between the HF-Radar and the drifters (Figures 5-6 and 5-7). On 8 November 2005, the HF-Radar had about the same bearing as the drifters, but was slower than the measured drifter speed. Correction for wind drift assuming the fully-developed sea increased this error (Figure 5-3). However, on that date the wind was calm until just before the dye was released, and so the steady state wind drift algorithm would not apply. In the first hour after winds come up, the Youssef and Spaulding (1993, 1994) model (as do others) predicts wind drift directly down wind, as observed.

In the 21 March 2006 experiment, the wind drift model prediction was within 3 cm/s of the HF-Radar magnitude, and at the same angle of about 37° to the right of downwind. The HF-Radar and drifter (all drogued at 1m) velocities agreed well, either due to a background current aligned with (and augmented by) wind drift or because both HF-Radar and drifters were moved by similar magnitudes and angles of wind drift (Figure 5-4). The wind had been blowing consistently at the same speed and direction for 7 hours prior to the experiment, suggesting that the seas and wind drift had reached a quasi-steady state as predicted by the wind drift model.

On 22 March, the HF-Radar indicated current to the southeast, whereas the drifters and dye moved to the east. However, the wind was 90° to the right of the background current as indicated by the 5-m drifters, and removal of modeled wind drift from the HF-Radar resulted in a vector more similar in magnitude and bearing to the drifters (Figure 5-5). However, the wind had only been blowing consistently at the same speed and direction for 1 hour prior to the experiment, not sufficient time to fully develop the seas. Thus, the wind drift angle in reality was likely closer to downwind than the algorithm based on the steady-state wind condition. The HF-Radar velocity in this experiment was consistent with the sum of an underlying eastward current plus a developing (non-steady state) wind drift over the top 0.5 m. Since we did not have time series of the baroclinic motions, it is difficult to assess whether they contributed to this observed difference.

On 1 and 2 November 2006, the HF-Radar bearings were 35° and 20° to the right of the drifters (drogued at 2 m) and the dye movements (Table 5-3). The removal of wind drift lessened the differences in magnitude, but did not reconcile differences in bearings between the HF-Radar and the drifters (Figures 5-8 and 5-9). The winds had been blowing consistently at the same speed and direction for 4 and 2 hours on 1 and 2 November, respectively, prior to the experiment. Thus, as for the 22 March 2006 experiment, the wind drift angles in reality were likely closer to downwind than the algorithm based on the steady-state wind conditions, and the HF-Radar velocities in these experiments were consistent with the sum of an underlying southeastward current plus a developing (non-steady state) wind drift over the top 0.5 m

The wind drift model (Section 5.2) assumes a fully-developed sea and steady state condition. However, the winds varied on a diurnal cycle, and the wind velocities were typically steady for only a few hours before the dye was released, with the exception of the 21 March 2006 experiment (See Figures E-2 to E-8 in Appendix E). Thus, the steady state wind drift predictions were not able to resolve observed differences in velocities measured at different depths for other dates than 21 March. A non-steady state model is needed to resolve the wind drift dynamically and with better accuracy. The original Youssef and Spaulding (1993, 1994) model described the initial non-steady state development of the wind drift, which begins flowing in the downwind direction as the wind changes from zero to the modeled flow condition, and then progressively veers (in the northern hemisphere), approaching the steady-state condition in about 5-6 hours.

In addition, there were submesoscale (~ 1 km and smaller) physical processes at work over the area of the experiments and in the upper few meters of the water column that would not be accounted for by wind drift alone. Evidence for these submesoscale processes was observed as horizontal shear evident in HF-Radar measurements, as well as the divergence of drifter trajectories both at the same depth and between depths (Figures 4-3 to 4-11).

Differences between HF-Radar and drifters are likely also due to differences in measurement methods. HF-Radar velocities were averaged spatially over ~1km, temporally over 1 hour and vertically over the surface 0.5 m. Drifters measure velocities at a depth of 1 or 2 m, are Lagrangian, and represent an effective temporal average of 10 minutes. These sampling discrepancies would be expected to yield differing results in a time-dependent environment with horizontal and/or vertical shear.

Some of the differences between the HF-Radar and the 1-m or 2-m drifter vectors also were likely due to error in magnitude and bearing in the HF-Radar flow, which averaged on the order of 9 cm/s in magnitude (7.5 and 5.6 cm/s for the u and v components, respectively) for multiple observations in the San Diego system (Ohlmann *et al.*, 2007).

5.3.3 Langmuir Circulation

Langmuir circulation is believed to be produced by the interaction of surface wind-forced current and Stokes drift due to waves (Leibovich, 1983; Smith, 1992; Skillingstad, 2000). Langmuir cells appear if the wind is greater than a few knots (Smith, 1992; Thorpe, 2000). In the open ocean, Langmuir circulation exists in a continuum of scales from about 1-2 m to 100-200 m (Skillingstad, 2000; Thorpe, 2000). Over time the scale evolves from smaller to larger-scale circulation (Smith, 1992), with vertical scale limited by the pycnocline depth (Thorpe, 2000) or water depth. Circulation speeds have been found to range from 1-15 cm/sec (Thorpe, 2000). The cells are unstable and reform on time scales of minutes to an hour (Thorpe, 2000).

Floating oil tends to collect in the convergence bands of Langmuir cells. Oil droplets entrained in the water likely circulate within the cells and are dispersed over the water depth penetrated by the cells, typically to the mixed layer depth (D'Asaro, 2000; Simecek-Beatty and Lehr, 2000). Langmuir circulation enhances horizontal dispersion: the crosswind currents transport oil and the instability of the cells allows movement across previous cell boundaries. Downwind dispersion is enhanced by more rapid current transport in the convergence zones (D'Asaro, 2000), and this may possibly explain the rapid and nearly straight line movement of the 1-m drogued drifters during the 8 November 2005 experiment.

Because of the importance of Langmuir circulation to oil transport and mixing in the mixed layer, measurements of Langmuir cell dimensions were made for those dates where the images were clear enough to do so (in March and November 2006; 21 June images contained glare and the 22 June images had to be composited to develop the shapes of the entire plume), as summarized in Table 5-4. Both small (10-30m) and large (40-70m) scale cells were visible in dye images. Water depth at the experimental site is about 73 m. The Langmuir circulation appears to be the process responsible for rapidly mixing the dye through the surface mixed layer (at 1 cm/s it would take 17 min to reach 10 m depth). However, the dye did not penetrate below that mixed layer during the observational period of the experiments. It is not clear how deep the large scale cells penetrated the water column, but the density profiles did not indicate over-turn deeper than the surface mixed layer.

Table 5-5 lists the orientation of the Langmuir cells to the wind for each of three wind records (two observational stations and the COAMPS model). LJPC1 is the most representative observational record. The orientation of the cells is typical of the range described in the literature discussed above.

Table 5-4. Mean dimensions of Langmuir circulation cells.

Date	Total width of dye plume along minor axis (m)	Major cell spacing (m)	Major cell spacing as % of dye plume width	Minor cell spacing (m)	Minor cell spacing as % of dye plume width
21 Mar 2006	372	34	10	11	3
22 Mar 2006	268	71	25	10	3
1 Nov 2006	689	68	10	29	4
2 Nov 2006	846	40	5	15	2

Table 5-5. Orientations of Langmuir circulation cells to the wind direction at the times of the images examined.

Date	Cell orientation (degrees)	Wind Station	Wind direction (degrees)	Wind speed (knots)	Deviation from wind direction
21 Mar 2006	321	LJPC1	284	10	37
		46086	302	13	19
		COAMPS	286	14	35
22 Mar 2006	312	LJPC1	319	7	-6
		46086	347	10	-34
		COAMPS	302	9	10
1 Nov 2006	325	LJPC1	325	10	1
		46086	308	9	18
		COAMPS	301	11	25
2 Nov 2006	330	LJPC1	327	8	4
		46086	325	12	5
		COAMPS	318	11	12

The cell orientation of the Langmuir circulation (37° to the right of down wind Table 5-5) was aligned with the HF-Radar (Table 5-3) and the wind drift model for the surface 0.5 m (Figure 5-4) in the 21 March 2006 experiment, where the wind had been blowing consistently from the same direction for 7 hours prior to the experiment. In the 22 March 2006 experiments, the Langmuir cell orientation (6° to the left of downwind, Table 5-5) was not aligned with the HF-Radar (14° to the left of downwind, Table 5-3) or with the steady-state wind drift model for the surface 0.5 m (Figure 5-5). On 22 March 2006, the wind had only been blowing from the same direction for 1 hour prior to the dye release. Thus, the wind drift would be downwind at that time, and the cells were aligned accordingly. In the two November 2006 experiments, the Langmuir circulation was aligned with the wind direction (Table 5-5), while both the HF-Radar

(Table 5-3) and the wind drift model prediction for the surface 0.5 m (Figures 5-8 and 5-9) were oriented 27-44° to the right of downwind. Again, the winds had been blowing consistently at the same speed and direction for only 4 and 2 hours on 1 and 2 November, respectively, prior to the experiment. Thus, the Langmuir circulation was aligned with the theoretical wind drift direction.

The Langmuir circulation cell orientations were consistent with the drifters (which indicate the direction of currents at 1-5 m) in the 21 March 2006 and the two experiments in November 2006, but not aligned with the drifters in the 22 March 2006 experiment (Figures 5-4, 5-5, 5-8 and 5-9; Tables 5-3 and 5-5). The cell orientation was aligned with the wind in experiments where the wind had been blowing consistently from the same direction for 4 hours or less, and was aligned with the wind drift model (and HF-Radar) in the one experiment where the wind had been blowing consistently from the same direction for 7 hours. These orientations are consistent with the literature (e.g., Leibovich, 1983; Smith, 1992; Skillingstad, 2000), which describes a range of orientations to the wind and the fact that variability is not well understood.

5.3.4 Horizontal (D_x) and Vertical (D_z) Diffusion Coefficients

In all experiments but 22 March 2006 (Figure 4-7) and in most of the images, the major axis of the dye plume aligned with the downwind direction. Table 5-6 lists horizontal dispersion coefficients (D_x) calculated from the downwind and crosswind lengths of the dye plumes, as measured on the georectified images. The horizontal dispersion coefficients in the radial dimension were also calculated using the square root of the product of downwind and crosswind axis lengths. However, the horizontal dispersion coefficients vary in the downwind versus crosswind directions, indicating that horizontal dispersion is not actually isotropic (although it is often modeled that way). In the 8 November 2005 experiment (where dye images were only taken over the first hour), the dye did not spread in the crosswind axis (the slope being <0 but not significant) over the 3 images taken (after the entire dye volume was released).

When wind drift was subtracted from the axis dimensions (assuming the steady-state model algorithm and the LJPC1 wind), the downwind to crosswind difference was reduced but not eliminated, presumably because of Langmuir circulation, which induces a net down-wind motion. In some cases (where D_x is not significantly different from zero), the wind drift appeared to account for the observed spread of the dye, particularly in the crosswind axis. However, with the exception of 21 March 2006, the seas had not reached quasi-steady state by the time of the experiment, such that the wind drift model would be applicable. Thus, the wind drift was likely more in the downwind direction than these calculations reflect, accounting for some dispersion in that axis. While the purpose of this analysis was to evaluate if the wind drift could account for the non-isotropic dispersion; these data sets do not provide an appropriate test set.

The horizontal dispersion coefficients were inversely correlated with wind speed (correlation coefficients were -0.60 for downwind D_x and -0.61 for crosswind D_x), as well as with Richardson number, Ri , based on the wind-induced shear due to wind drift over the surface 3 m (correlation coefficients were 0.80-0.81 in all dimensional measures). The highest D_x was on 21 June where winds were very light and Ri was high, indicating a stable water column in the upper layer.

Table 5-6. Estimates of horizontal dispersion coefficients (D_x) derived from dimensions of the dye in images over time (based on linear regression; negative values are not significantly different from zero). [W = 0 is with no wind-drift correction; W = 1 is with wind-drift (wind station LJPC1) subtracted]

Date	W	8 Nov 2005	21 Mar 2006	22 Mar 2006	21 Jun 2006	22 Jun 2006	1 Nov 2006	2 Nov 2006
Downwind axis: D_x (m^2/s)	0	0.46	1.46	0.60	51.46	12.34	10.44	25.08
Downwind axis: Correlation (r^2)	0	0.965	0.876	0.970	0.936	0.932	0.973	0.926
Downwind axis: # observations	0	3	26	18	29	7	39	31
Crosswind axis: D_x (m^2/s)	0	-0.29	0.57	0.15	5.01	0.82	0.68	2.37
Crosswind axis: Correlation (r^2)	0	0.606	0.773	0.275	0.936	0.963	0.692	0.933
Crosswind axis: # observations	0	3	27	21	28	11	41	31
Radial spread: D_x (m^2/s)	0	0.01	1.01	0.45	17.32	4.19	3.17	8.27
Radial spread: Correlation (r^2)	0	0.002	0.966	0.930	0.959	0.954	0.960	0.946
Radial spread: # observations	0	3	23	17	28	7	39	31
Downwind axis: D_x (m^2/s)	1	-0.15	0.25	-0.01	46.19	9.32	4.20	14.06
Downwind axis: Correlation (r^2)	1	0.789	0.305	0.009	0.924	0.915	0.852	0.712
Downwind axis: # observations	1	3	26	18	29	7	39	31
Crosswind axis: D_x (m^2/s)	1	-0.35	-0.02	-0.27	3.53	0.28	-0.59	-0.13
Crosswind axis: Correlation (r^2)	1	0.767	0.012	0.556	0.869	0.756	0.698	0.017
Crosswind axis: # observations	1	3	27	22	28	11	41	31
Radial spread: D_x (m^2/s)	1	-0.26	0.08	-0.07	14.09	2.47	0.07	2.66
Radial spread: Correlation (r^2)	1	0.807	0.279	0.122	0.939	0.919	0.015	0.439
Radial spread: # observations	1	3	10	9	28	7	39	31

However, while such a relationship makes sense in that wind-drift shear is greatest in the lightest winds, this data set is not large enough to determine if this is a consistent trend. The presence of current shear related to other forcing factors, and its orientation relative to wind direction, would also influence horizontal dispersion.

Vertical (D_z) dispersion coefficients were estimated (using methods outlined in Section 3.2.4) for each experimental date using dye concentration in vertical casts or transects across the dye patch (see Appendices F and G for examples of dye concentration profiles). The vertical profiles were all taken after the initial downward mixing by Langmuir circulation in the first 20-30 min of the experiments. Thus, the coefficients appear to represent mixing rates and/or transport by Langmuir circulation after that initial phase.

The means of D_z on each date range from 6 to 30 cm^2/s (Table 5-7). However, there were only two vertical casts within the dye plume on 21 March 2006, making this estimate of 30 cm^2/s uncertain, in spite of the relatively low standard deviation (std dev). [We note that the winds were steady for many hours before the 21 March experiment, and the wind drift was apparently a fully-developed spiral as predicted by the wind drift algorithm, suggesting higher mixing rates resulting from the more developed vertical shear.]

There was no trend over time in the 8 November 2005 or the 21 March, 22 March, 21 June and 22 June 2006 experiments. However, in the 1 and 2 November 2006 experiments, a significant trend over time was seen and D_z was fit to a power curve (equations 13 and 14, with results as in Table 5-8. The value of D_z was on the order of 10 cm^2/s initially, but declined over the following 2 hours to 7 and 2 cm^2/s for 1 and 2 November, respectively. The change in D_z over time may reflect evolution in Langmuir circulation cell characteristics or, potentially, slowing of vertical mixing as the more stratified deeper water was penetrated by the dye.

Table 5-7. Estimates of vertical (D_z) dispersion coefficients based on vertical profiles of dye concentration. [Note the units here are cm^2/s , while the values of D_x in Table 5-6 are in m^2/s .]

Date	8 Nov 2005	21 Mar 2006	22 Mar 2006	21 Jun 2006	22 Jun 2006	1 Nov 2006	2 Nov 2006
Dz mean (cm^2/s)	16	30	6	6	8	10	11
Dz std dev (cm^2/s)	12	6	5	9	8	4	11
# observations	4	2	11	14	13	27	25

Table 5-8. Decline of vertical (D_z) dispersion coefficients over time (fit to equation 13, and predicted D_z using equation 14) in the 1 and 2 November experiments.

Parameter	1 Nov 2006	2 Nov 2006
slope (m in equation 13)	0.753	0.282
Intercept ($\log(a)$, equation 13)	-1.780	-0.158
Correlation (r^2)	0.837	0.437
a (equation 13)	0.017	0.696
D_z at 5min	12.9	10.0
D_z at 1 hrs	8.3	2.8
D_z at 2 hrs	7.0	1.7

5.4 SIMAP Model Application to Dye Experiments

Appendix H contains snapshots from SIMAP model simulations of the seven dye release experiments off Point Loma. These hindcasts were made with the following inputs:

- velocities as measured by the deepest drifter placed in the dye patch (which for 4-m and 5-m drifters, did not include significant wind drift);
- velocities as predicted by the wind drift model algorithm (Section 5.2.2) and added to the drifter velocities;
- the radial horizontal dispersion coefficient measured from the photo images (Table 5-6, no wind drift included);
- the vertical dispersion coefficients measured from fluorescence measurements (Tables 5-7 and 5-8); and
- a unit release of 100 MT (such that concentrations are relative to that release mass).

The model-predicted plume concentrations were plotted at times of photographic images, with the shape of the corresponding image overlaid on the modeled plume. Because the dye was simulated as if it was a 100MT release, and the concentrations were measured by color intensity in the aerial photo, the absolute concentrations were not compared. The figures allow comparison of modeled versus observed movements (horizontal advection) and spreading (horizontal dispersion) of the dye, as indicated by the dimensions of the plume in the bird's-eye view.

In all experiments, the modeled transport (advection) was primarily by the drifter-measured advection. The wind drift was a minor addition to the advective vectors used to transport the Lagrangian particles. Simulations without wind drift (not shown) were also made. The trajectories were very similar with or without wind drift included. Without the addition of the wind drift, the plumes were circular in shape (viewed from above), and of the same cross-wind dimension as for simulations including wind drift. The wind drift added vertical shear and spreading, primarily in the down-wind direction. A similar simulation result with down-wind stretching would also be produced using drifter velocities without wind drift added and different horizontal dispersion coefficients in the down-wind and cross-wind axes (as in Table 5-6).

In addition to tracking of the dye, on 21 and 22 March 2006, large patches of floating weed near the dye releases were followed and photographed from the air. The locations of the weed over time and SIMAP model simulations of floating material (simulating weed or oil), using velocities as predicted by the steady-state wind drift model algorithm (Section 5.2.2 in main report) added to the drifter velocities, are in Figures H.2-4 and H.3-6 of Appendix H. The model prediction (of wind drift added to observed drifter velocities) agrees well with the observed positions of the weed on 21 March (Figure H.2-4), confirming that the steady state wind drift algorithm fit the observations on this date. However, the model prediction does not agree with the observed positions of the weed patch on 22 March (Figure H.3-6), as the wind and resulting waves had not reached steady state. Thus, the steady state wind drift algorithm did not apply on 22 March 2006. Figure H.2-7 shows that the model using the drifter velocities plus 2.5% of wind speed with a zero angle best fit the observations on 22 March. This is consistent with wind drift theory and the spin-up described in Youssef and Spaulding (1993, 1994).

5.5 Discussion of Modeling Results

The drifters when drogued to a depth in the center of the vertical extent of the surface mixed layer, proved to follow the dye plumes for the temporal extent over which the studies were conducted. The results suggest they would be useful for tracking near-surface transport of oil and dissolved components. For experiments in 5-7 m/s winds where the surface mixed layer was unstable, the drifters drogued at 4-5m tracked the dye most accurately, whereas drifters drogued at 1-2m moved downwind just ahead of the dye plume. In experiments where the mixed layer was stratified, and wind drift was slow and shallow (due to light winds), drifters drogued at 2 m tracked the dye most accurately, with the 4-m drifters slower than the bulk dye movements. The dye concentration measurements also showed this shearing behavior, with the shallower dye moving faster downwind than the deeper part of the plume (see for example Figure 4.6-1 in Section 4.6). This behavior is as expected from Stokes drift theory.

Use of a HF Radar to provide current estimates for oil spill modeling can be a powerful tool as it is synoptic and operational in real time, and extends over large spatial areas. The analysis presented here suggest that if the goal of a model is to predict high fidelity 3-D motions of dispersed oil within the water column below the surface, that the model physics must accurately represent all physical processes at play in the surface wave layer. This includes Langmuir cells, surface wind drift, baroclinic and barotropic tides, wave breaking, and other vertical mixing and ocean boundary layer processes. HF radar data assimilation alone will not constrain these processes within the model. However, if the surface wind drift component of the HF Radar can be quantified; and dispersion coefficients can be used to parameterize the Langmuir circulation, wave breaking and other mixing processes; near-surface transport may be accurately simulated using HF-Radar data.

Since 25MHz HF radar derived currents are an average measurement in time (1hr) and space (0.50 m vertically, 1km² horizontally), the limitations of the system must be considered when developing metrics for comparison with other observational tools. These studies revealed that the radar, in general, tracked the direction and speed of the plume. However, since it is an average measurement, fine-scale properties of the plume (or Lagrangian tracks of the drifters)

were not observed. These measurement differences can be exacerbated when integrated in time. Likewise, measurement error in HF radar will also be additive when time integral trajectories are computed. Attempts to project the HF radar surface current measurement to depth were done using the steady-state wind drift model with varying results. For purposes of this analysis, only a wind drift model was assumed to control near-surface shear, whereas in the environment, other sources of shear can be present in the upper ocean from baroclinic tidal responses and Ekman layers.

The NRC (2005) identified estimation of turbulent dispersion coefficients (modeled as eddy diffusion) as a priority research area. Modeling results predicting hydrocarbon concentrations in the water column are highly sensitive to the assumed values for these mixing coefficients. Horizontal dispersion coefficients may be readily and accurately estimated from dye spreading as measured from aerial photographs. The photographic images are synoptic and may be made repeatedly at rapid intervals, something that cannot be done by sampling from a surface vessel. We are not aware of this approach being used in other dye studies. The results for the conditions studied indicated that the horizontal dispersion coefficient ranged from 0.1-50 m²/sec, in agreement with the literature examining these values for length scales on the order of a kilometer (e.g., Okubo, 1971; Okubo and Ozmidov, 1970). Elliott *et al.* (1997) performed similar dye study analyses for coastal and estuarine areas around Ireland, finding a range of 0.02-8 m²/s using estimated plume dimensions based on dye concentration measurements from transect sampling.

The density structure of the near-surface water is an important determinant of the dilution rate. Langmuir circulation would transport constituents into the mixed layer in a matter of minutes, as was observed in the field experiments. Vertical (D_z) dispersion coefficients were estimated for each experimental date using dye concentration in vertical casts or high-resolution transects across the dye patch, taken after the Langmuir circulation had moved dye down and into the mixed layer. The resulting coefficients were low and typical of estimates in the literature (Okubo; Okubo and Ozmidov, 1970), reflecting minimal transport at the pycnocline beneath the mixed layer. Thus, the majority of the dilution was in the horizontal dimensions, and particularly downwind, caused by wind drift and shear in the upper mixed layer, highlighting the importance of resolving wind drift and horizontal dispersion rates in order to estimate oil hydrocarbon exposure concentrations experienced by water column biota after oil is dispersed into the water column.

The SIMAP trajectory model, using the drifter velocities as current input, reproduced the trajectories of the dye (Appendix H), as expected, since that trajectory is controlled by the current data input and the drifters moved with the dye. The effect of wind drift transporting the surface material faster than subsurface materials has been identified as a spreading mechanism (Elliott *et al.*, 1986) and observed in many oil spills (e.g., as reviewed in Youssef and Spaulding 1993, 1994; Cox *et al.*, 2004), as well as in validation studies using intentional releases of Orimulsion (French *et al.*, 1997). Thus, subtraction of the wind drift from the shallower drifter velocities, and inclusion of wind drift in the transport model (e.g., SIMAP), would allow those velocities to be used for other depths than those tracked by drifters. The transport model would then be able to simulate the shearing of the plume, which disperses the constituents within that plume. The analysis herein indicates that this procedure produces accurate results using the wind

drift algorithm only if the seas are fully-developed (and only one test date fitting that criterion was available). A dynamic model would be needed for conditions where winds are not steady in order to reproduce the wind drift shearing in the water. Initially, as a new wind (direction) develops, the wind drift would be downwind at 3-4 percent of wind speed (a leeway often observed). The wind drift then veers (in the northern hemisphere) over time until reaching the steady-state condition.

Absent such a model that could be feasibly included in an oil transport model (i.e., a full hydrodynamic calculation of Stokes drift and surface wind-forced current would be too cumbersome to be practical, especially in real time), dispersion rates that include the wind-drift induced spreading could be applied, preferably using different parameters in the downwind and crosswind axes, as calculated in this study using the aerial photo image dye dimensions. The use of the radial spreading-based horizontal dispersion coefficients should be used in models where dispersion is assumed isotropic, but this would produce a less accurate result.

The SIMAP model hindcast of each dye experiment using the drifter velocities as current input and the measured dispersion coefficients from the dye studies, agreed with the observations of dye movement and spreading rate (again, as expected, as these are the important inputs to the model). The range of wind conditions examined was not large, and these experiments were all made in fairly low wind conditions. However, the approach of using drifters and dye to estimate advection and dispersion (based on dimensional analysis of aerial photo images) could be used in actual oil spill events to evaluate impacts of dispersed oil plumes. In addition, better georeferencing of the aerial images (i.e., with multiple horizontal and vertical position measurements per image) than the manual process dependant on a single position per image used here would reduce position error in the resulting dye shapes and more accurately measure transport.

6. Discussion and Importance to Oil Spill Response/Restoration

6.1 Summary of Project Results

Oil-spill fate and transport modeling may be used to evaluate water column hydrocarbon concentrations, potential exposure to organisms (zooplankton), and the impacts of oil spills with and without use of dispersants. Important inputs to transport modeling for such analyses are ocean currents and turbulent dispersion (eddy diffusion) coefficients. Fluorescein dye studies conducted off San Diego, California, were used to evaluate the ability of transport models to hindcast movement and dispersion of dye (and so water movements influencing transport of subsurface oil). Data included surface currents calculated from HF Radar, near-surface currents from drifter measurements drogued at several depths (1m, 2m, 4m or 5m), dye concentrations measured by fluorescence, spreading and dye intensity measurements based on aerial photography, and water density profiles from CTD casts.

Fluorescein dye plumes (initially about 500 m in diameter after all the dye was released) were tracked and sampled off the coast of San Diego, CA, on seven dates during the period from 8 November 2005 through 2 November 2006. In addition, photography and some oceanographic data were collected for a dye release during the Safe Seas exercise off San Francisco (9 August 2006). These non-toxic dye plumes served in lieu of dispersed oil to measure transport and spreading of neutrally buoyant and dissolved constituents as controlled by the hydrodynamics that would influence submerged oil droplet transport. The objectives of these studies were to develop and test the operational framework for repeated sampling of dispersed oil plumes; to measure small-scale transport processes (horizontal and vertical diffusivities); to evaluate CODAR (and HF-Radar, in general) for providing surface current input data to oil spill models; and to verify model-predicted movement of subsurface oil (dye) by comparison with drogued drifter movements and measured dye concentrations over three spatial dimensions and time.

In the San Diego experiments, drifters were deployed to track the plume and allow their observed trajectories to be compared with HF-Radar velocities and field observations of the dye movements. A Seabird CTD (conductivity, temperature, depth) profiling instrument was deployed to determine the mixed layer depth, where vertical dispersion would be more rapid than in deeper water. Vertical and horizontal profiles of dye concentrations, as measured by fluorescence, were made and used to determine the depth of penetration of the dye into the water column over time and horizontal dispersion rates. In the November 2005 and March 2006 cruises, an *in situ* fluorometer in the CTD package was used to measure vertical profiles of fluorescence. In June and November of 2006, a Wet Labs ECO FL-UR fluorometer was towed behind the sampling boat in an undulating mode between depths of 1 and 10 m. All these systems were deployed from the same sampling vessel during each cruise. Aerial photos taken from OSPR twin engine aircraft were used to track the movements and spreading of the dye over time.

Three HF-Radar systems are currently installed around the San Diego area at Pont Loma, the south end of the Tijuana Estuary, and South Coronado Island. Data from these systems were combined and processed by SIO, and maps of zonal (u) and meridional (v) current velocities were produced at 1 km resolution and 5-min intervals. Standard meteorological measurements were obtained from established weather stations maintained by NOAA and SIO in the vicinity of San Diego and San Francisco (reported on the NOAA National Data Buoy Center [NDBC] website), as well as for the San Diego experimental sites from the Coupled Ocean/Atmosphere Mesoscale Prediction System (COAMPS[®]) model (developed by the Marine Meteorology Division [MMD] of the Naval Research Laboratory [NRL]).

Analyses were performed to evaluate the ability of current data based on HF Radar and/or drifters to predict movements of a neutrally buoyant plume in the mixed layer. A surface wind drift algorithm was tested to evaluate its ability to predict vertical wind-forced shear. Horizontal and vertical dispersion rates were estimated from measurements of the horizontal expansion of georectified images from aerial photographs and from dye concentration data. While several different oceanographic weather states were encountered during the experiments, it is recognized that one cannot extrapolate from this limited set of measurements to all potential environmental scenarios. Thus, these measurements and algorithm developments were used to further the approach.

Typically, the dye penetrated to a depth of 7 to 15 m largely via Langmuir circulation within a half hour after release, but was not uniform in concentration over that (semi-) mixed layer. Modeling of wind-forced surface water drift as a function of wind speed and direction was based on published results of fluid dynamics studies. For experiments in 5-7 m/s winds where the surface mixed layer was deeper, the drifters drogued at 4-5m tracked the dye most accurately, whereas drifters drogued at 1-2m moved downwind just ahead of the dye plume, as predicted by the wind drift theory (Stokes drift). In experiments where the mixed layer was highly stable and wind drift was slow and shallow (due to light winds), drifters drogued at 2 m tracked the dye most accurately, with the 4-m drifters slower than the bulk dye movements.

The horizontal dye movements of dye and drifters had differences than trajectories computed with HF Radar derived surface currents, which are integrated measurements across the top 50 cm of the ocean's surface, are spatially averaged at a scale of 1 km², and are time averaged over 1 hour. These differences may be attributable to variable horizontal and vertical surface shear, other sources of vertical shear including baroclinic motions and Ekman layers, observation method response differences to Stokes drift, preferential sorting of the drifters by Langmuir cells, the measurement differences between the averaged velocity measured by the HF radar and Lagrangian measurements, and measurement error of the HF radar, especially the relative error at low velocity..

Simulation of dye (or subsurface oil) concentrations requires additional inputs to the advective transport rates: the turbulent dispersion (diffusion) coefficients. Modeling results are highly sensitive to the assumed values for these mixing coefficients over the range of likely values. In this study, dispersion rates were estimated based on dye spread as measured by aerial photography and vertical profiles of dye fluorescence over time. The use of photographic images is a novel approach that provides synoptic measures of the horizontal distribution

(vertically integrated) of dye made repeatedly at rapid intervals, something that cannot be done by sampling concentrations from a surface vessel. The results for the conditions studied indicated that the horizontal dispersion coefficient is typically 0.1-50 m²/sec, similar to the range identified in the literature for length scales on the order of a kilometer. Use of such data in an oil fate model can provide estimates of likely dispersed oil and dissolved hydrocarbon concentrations under similar conditions, which may be used to evaluate potential impacts on water column biota. However, other conditions should be examined before these results are generalized.

6.2 Implications for Oil Spill Model Development and Application

The specific objectives of this collaborative effort and multi-disciplinary program included collecting data sets to develop and verify transport models; evaluating and integrating regional observing systems data with circulation and transport forecasts; developing tools for quantifying injury to natural resources; and furthering studies to evaluate the efficacy and effects of dispersant use. In this context, the project also addressed several U.S. National Research Council identified priorities, including developing protocols and equipment for dispersed oil tracking and measuring near surface horizontal and vertical diffusivities (NRC 2005).

While we recognize that the scope of the program is unable to define the sea-state dependence of the diffusivity, the dye studies were intended to: (1) provide detailed data with which to develop and test algorithms for an empirical best fit to estimated horizontal and vertical diffusivities, (2) evaluate the usefulness and accuracy of high frequency radar in prediction of subsurface oil transport, and (3) be an unambiguous tracer to track the water flow independent of the drifters. The latter is important given the divergence, which can potentially occur between drifter tracks at different depths and spilled oil. Ultimately these data will have direct applicability to spill response decision making, net environmental benefit analysis, and education.

For all experiments, the fluorescein dye served in lieu of dispersed oil. As noted above, the salinity of the dye concentrate was adjusted to impart a near-neutral density compared to the receiving water, and thereby modeled the dissolved-phase components that would be generated from dispersed oil droplets and not the oil droplets themselves. The modeled transport and behavior of dispersed oil droplets (which have a finite rise velocity) is expected to be intermediate between the dissolved phase plume and the surface oil slick (as predicted by wind-drift theory). The diffusivities measured by the dye spreading and dispersion are appropriate inputs to subsurface transport models, where dissolved constituents are transported by advection and this turbulent dispersion while entrained droplets move both by these and buoyancy forces (e.g., Stokes Law).

Between the seven OSPR- and CRRC-sponsored cruises (Table 3-1) and the Safe Seas exercise, we had hoped that at least two (possibly seasonal) different oceanographic conditions might be encountered (winter storms with strong NW swells versus summer calm with occasional swells from W and SW), and while it is recognized that one cannot extrapolate from only a few sets of measurements to all potential environmental scenarios, these measurements and the algorithms correlating estimated diffusivities with measured underlying currents, sea-states, and wind

conditions were intended to further the approach. That is, the purpose of this project was to develop the methodology to measure (or estimate) small-scale diffusivities and use them in oil-spill models for other times and locations, and to the extent possible, correlate horizontal and vertical diffusivities to observed or measured sea-state (wind conditions, swell height, direction, and frequency) as well as advective transport by larger-scale currents. This information was intended to inform model development, and thereby be transferable to other locations and investigators.

To a large extent, these objectives were achieved, and nearly continuous and synoptic data have been obtained from seven cruises conducted over a 12-month period. The data have been verified (i.e., subjected to QA/QC checks for representativeness, completeness, accuracy, and precision), compiled for access by other investigators, and integrated to facilitate their use in model development and calibration.

With respect to modeling dispersed oil plumes, the results of this project suggest the following approach for estimating advection and dispersion. Accurate measurement of current velocities are needed as input. In areas where HF radar is available, it might be useful for this purpose if the wind drift component in the HF radar-measured near-surface currents can be estimated (with a steady state or dynamic model) and removed, allowing prediction of transport at all (near-surface) depths (assuming other sources of vertical shear are not significant such as baroclinic tidal responses and Ekman dynamics). Unless upper ocean processes are constrained well enough to project near-surface measurements to depth, direct measurements of velocity using drifters drogued to the depth of the center of the surface mixed layer are needed to produce accurate trajectories as mixing is rapid within the surface mixed layer. Advection, as well as horizontal dispersion coefficients, could be estimated from dye movements and spreading if an appropriate dye release can be made and monitored with aerial photography. This novel approach is synoptic and provides a high degree of accuracy. However, the data processing required makes this approach less feasible for a real time response (where modeling might be used to inform decisions, such as application of chemical dispersant), than for a hind cast used in impact and natural resource damage assessment. The estimation of the vertical dispersion coefficient is of lesser importance for near-surface transport, as vertical mixing to the mixed layer depth could be assumed to occur immediately. The mixed layer depth would need to be estimated from vertical profiles of water temperature and salinity.

Absent a model of wind drift that could be feasibly included in an oil transport model (i.e., a full hydrodynamic calculation of Stokes drift and surface wind-forced current would be too cumbersome to be practical, especially in real time), dispersion rates that include the wind-drift induced spreading could be applied, preferably using different parameters in the downwind and crosswind axes, as calculated in this study using the aerial photo image dye dimensions. The use of the radial spreading-based horizontal dispersion coefficients should be used in models where dispersion is assumed isotropic.

6.3 Planned Implementation of Sampling Protocols Developed and Evaluated Through this Study into the CA Dispersed Oil Monitoring Plan (DOMP)

6.3.1 Objective of the CA OSPR DOMP

The purpose of the California Dispersed Oil Monitoring Plan (DOMP), which is scheduled to be released in July/August 2007, is to identify the equipment and scientific approach required to determine the distribution of physically- and chemically-dispersed oil entrained into the water column, the concentrations of dissolved components and finite oil droplets in the water column, and the potential adverse impact on the aquatic resources of the affected water body. By virtue of the sampling design, the spill impacts with and without dispersant applications will be comparable and quantifiable.

6.3.2 Sampling Vessel and Observation Platform Requirements

Boats

A minimum of two boats should be available to implement the DOMP. They should be of sufficient size to support a combined scientific party and crew of 6-8 personnel, safely navigate in near-shore open-water conditions, and be equipped with USCG approved navigation and communication equipment. Ideally, they should have 120 V AC power available, although this can also be supplied by portable generator (as was done in this study). At least one of the vessels should be equipped with a conventional winch and hydrowire (or 3/8 inch synthetic line) for subsurface water-column sampling and towing plankton nets or other biological sampling systems. The programmable down rigger used for the high resolution *in situ* fluorescence profiling described in this study was mounted to the gunnel/rail of the vessels, and a similar approach can be used (with minor modifications) on any vessel of opportunity. Satellite communications would now allow for the system to be expanded providing real-time information to shore-based decision makers.

Aircraft

One observation aircraft (either fixed wing or helicopter) should be dedicated to supporting and photo-documenting the plume behavior and on-water sampling activities. The aircraft should have sufficient fuel capacity to sustain flight operations for 4-5 hours, if possible. A fixed-wing aircraft with a mounted digital camera with GPS recording capabilities (recording latitude, longitude, and altitude for multiple points in the image) for georeferencing images is the ideal platform.

Communications

At –sea, boat-to-boat and boat-to-aircraft communications are critical, and they are always problematic. In this project, we utilized handheld California Department of Fish and Game radios, marine band radios, air band radios, and cell phones. The ability to use multiple modes

of communication proved critical in all the field experiments, as at times one or more forms of communication failed or were unavailable. Satellite phones should be used if at all possible.

Sampling Equipment

At a minimum, CTD and *in situ* as well as continuous-flow fluorometers similar to those described in Section 3.1 should be available. GPS and radio-telemetry equipped drifters drogued at several depths will be required to track the subsurface plume over time after (or if) it is not readily visible from the surface vessels or observation aircraft. For the sake of simplicity in this discussion, we typically refer to drifters drogued at 2- and 4- meters; however, in practice we recommend completing a 30-meter CTD cast in the test area to determine the vertical extent of the near surface layer. Then, drogue depths of the drifters should be set at a range of depths across the surface mixed layer to account for any shear present within the near-surface layer. In addition, finite water-column sampling equipment, such as 4L Go-Flo[®] Bottles, should be provided for water column sampling at depth. Grab samples should include bulk (unfiltered) seawater for total petroleum hydrocarbon (TPH) measurements and samples processed through on-station filtration at the time of collection (such as that provided by the Portable Large Volume Water Sampling System (PLVWSS) developed by PECI (Payne *et al.*, 1999)). This will allow differentiation of dissolved-phase PAH components and whole-oil droplets to support modeling and toxicity estimates (Payne and Driskell, 2003). Biological samples (zooplankton) should be collected with “Bongo” net tows for organisms in the water column and “Manta” nets for organisms at the water surface. Care should be taken during biological sampling to avoid surface oil and the dispersant-treated plume to minimize equipment and sample contamination. Aircraft observations/support may be particularly useful in this regard to ensure that biological sampling nets are not towed through a surface slick or subsurface oil plume not immediately visible from the sampling vessel.

6.3.3 General Considerations and Approach

If dispersants are to be applied, such applications should not be delayed while assembling the sampling team, boats, and equipment necessary to implement the DOMP. However, individuals involved in the sampling effort should be notified as soon as the decision to use dispersants is made, and efforts should immediately be undertaken to begin staging equipment, boats, observation aircraft, and sampling personnel at locations convenient to the spill site with direct communication links to the Incident Command Center. Ideally, standby contracts for these individuals and the necessary equipment and sampling/observation platforms should be in place long before the spill event.

Background CTD casts and water column and biological sampling should be completed in at least 2-3 areas well away from the surface floating oil and the dispersed oil plume(s). If possible, this should be done both inshore and offshore of the slick to assess water-column structure as well as biological and chemical variability, and it should occur before the dispersant application and treated-slick sampling. If time doesn't allow for this, background sampling can be completed after those activities if proper precautions are taken to decontaminate sampling equipment. It is also important to obtain water samples beneath the non-dispersant-treated slick to evaluate background physical entrainment of oil into the water column before dispersant

applications are conducted. These water samples should be collected at the same depth intervals as the samples collected in the dispersed oil plume. Biological sampling gear (Otter trawls, plankton nets, etc.) should not be used in an area with surface oil or to sample within the dispersed oil plume because of extensive decontamination issues.

Sampling and analyses of water-column impacts should be done on an identified part of the oil slick as part of normal dispersant operations. That is, if dispersant operations are planned or on going, a spotter aircraft should be used to identify a portion of the surface oil that can be marked with smoke bombs and subsurface-drogued drifters, and then tracked/sampled over time as described below without interfering with other ongoing response operations.

During transit to the spill location, telephone and radio communications should be established and double checked. This includes communications with the Incident Command Center and between all surface vessels and the spotter/observation aircraft. In addition, telecommunications should be completed with personnel responsible for satellite-tracking of the drogued drifters to ensure that they are transmitting properly before being deployed. This communication link will also be critical later to provide correct latitude and longitude coordinates for GPS tracking and recovery of the drifters over time.

The following describes a stepwise protocol that may be used to implement the DOMP. It was developed through experience gained in this program and previous spill-of-opportunity studies where dispersants were applied (Payne *et al.*, 1991 and 1993). Additional details and rationale are presented in the complete California Dispersed Oil Monitoring Plan.

Identify the Target Slick for Detailed Study Through the DOMP

With very large oil spills it may be advantageous to identify a smaller or separate portion of the slick for detailed study using the DOMP. In any event, infrared (IR) video should be utilized by the dispersant applications contractor or spotter aircraft to identify the thicker portions of the slick to be treated. Once the target area or selected slick has been identified, the following steps should be implemented in this order to provide the most usable data.

- Deploy smoke bomb/markers from a boat or helicopter to mark the up-wind and down wind extent of the target area (try not to exceed 300-500 m length).
- Spray the dispersant within the target area (either by aircraft or boat).
- If possible, orthogonally position the two observation vessels up wind and to the side of the target area to monitor wind drift of the dispersant (if applied from an aircraft) away from the target area. Dispersants will not work if they don't hit the oil, so don't waste time trying to monitor the water-column impacts from an unsuccessful dispersant application.
- Redeploy additional smoke bombs to replace the original smoke markers before they are extinguished (or at least until the subsurface-drogued drifters can be deployed).
- Deploy the 2- and 4-meter (nominal, suggested depths – see Section 6.2.2 Sampling Equipment) drogued drifters in the center of the treated area using the smoke bombs and dispersed oil plume for visual reference. A minimum of four drifters with drogues at each depth is suggested. Additional support from the spotter aircraft may be extremely useful in properly placing the drifters near the center of the dispersed oil plume.

During previous spill of opportunity studies, Payne *et al.* (1991, 1993) noted that tracking drifters from the sea-surface becomes difficult with increasing sea states, and helicopter support was required to find the drifters and redirect the sampling vessels back into the center of the dispersed oil plumes. During the fluorescein dye studies described in this report, the subsurface-drogued drifters were tracked and recovered with the aid of GPS coordinates supplied by shore-based support personnel following the drifters through satellite tracking over time. Well-established cell phone communications were critical for this operation, and cell-phone coverage is not always guaranteed in offshore waters. In such instances, telecommunications through satellite phones or marine radio-placed calls to the shore-based facility may be required. If the drifters cannot be tracked by GPS, it may be appropriate to equip them with frequency-specific transmitters or flashing beacons, and possibly to equip the observation aircraft or one surface vessel with a receiver to assist in locating the drifters in less than optimal operational conditions.

Biological and Water-Column Sampling

As it will not be possible to synoptically sample both in and out of the plume in a design where statistical differences could be shown, the biological sampling should be designed to establish pre- or near-spill baseline data (by species number and weight, and life stage and/or size classes, as appropriate) to identify what types of organisms may be exposed. Considerations for biological sampling include:

- Do not sample in the oil slick or dispersed oil plume.
- Sample in uncontaminated adjacent waters for documentation of species and age-group composition.
- Complete separate tows for collection of live zooplankton and egg samples for later laboratory toxicity studies at field-observed PAH and free oil-droplet concentrations.
- These activities can be completed during or following the emergency phase of field operations.

Dispersed oil sampling location and depth

Use the 2- and 4-meter (nominal depths – see Section 6.2.2 Sampling Equipment) drogued drifters to track the center of the dispersed oil plume over time. Fluorescence transects through the dispersed oil plume should be repeated for a minimum of three-to-six hours (or as long as daylight permits), and the transects should extend into non-contaminated water to better define the structure of the subsurface plume. If conditions permit, the subsurface-drogued drifters should be left in the water overnight to facilitate location and additional dispersed-oil-plume sampling the following day. During the first day of operations when the dispersed oil plume may still be visible from the air, the direction of the sampling vessels into and out of the treated zones can also be improved by radio communications with the observation aircraft.

The dispersed oil plume structure should be delineated by *in situ* continuous UV/Fluorescence instrumentation towed through the plume with a programmable downrigger as described in this report to provide a three-dimensional picture over time. The *in situ* fluorometer should be equipped with GPS and pressure sensors that either store data internally or transfer information

to a computer on the sampling vessel for data storage and real-time analysis. Ideally, such data might be transmitted through radio-telemetry equipment back to the Incident Command Center. If such instrumentation is not available, conventional fluorometers (such as the Turner Designs A-10 systems currently used for the USCG SMART protocols) can be operated from the sampling vessel to continuously monitor the fluorescence signal at 2- and 5-meter depths. All data collected from such instrumentation should be stored on a computer-based data-logger with GPS and time continuously recorded.

Water-column sampling

Samples of effluent from the continuous-flowing UV/fluorometers should be collected periodically at fixed time intervals, and immediately after real-time UV/fluorescence signals indicating the presence of elevated dispersed oil droplets. Volumes of 1 L can be readily contained in commercially-available pre-cleaned narrow-mouth amber glass bottles with Teflon[®]-lined lids. The samples will contain both dissolved constituents and dispersed oil droplets; however, it will not be possible to differentiate the relative proportions of each. Nevertheless, the data will be useful for correlating UV/fluorescence measurements to whole-oil (TPH) concentrations in the water column.

Where the results from the towed *in situ* fluorometer or the continuous flowing UV/fluorescence measurements indicate elevated levels of dispersed oil droplets, grab samples at 2, 4, and 10 m should be collected with conventional water column sampling equipment (Go-Flo[®] Bottles or equivalent). With these samples, it is recommended that in addition to simply collecting 1 L grab samples, additional 3-4 L samples be filtered at the time of collection and the filtrate (containing the dissolved-phase) and the filter (which retains the dispersed oil droplets) be analyzed separately (Payne *et al.*, 1999). Collection of such samples with the Portable Large Volume Water Sampling System (PLVWSS) developed for NOAA by PECI (Payne *et al.*, 1999) will allow data on both dissolved-phase and particulate oil droplets to be generated (Payne and Driskell, 2003) so that measured concentration data can be used to validate computer-model predictions of the separate phases. These data can then be compared to values typically used in water accommodated fractions (WAF) generated for dispersed oil toxicity evaluations.

Sample preservation

Whole water column samples can be preserved by the addition of 6 Normal (N) HCl to lower the PAH to < 2. For 1 L samples addition of 3 mL of 6 N HCl from an auto pipette dispenser should be sufficient to drop the pH of seawater to < 2.0. For the filtered ~3.5 L samples collected with the PLVWSS, 12 mL of 6 N HCl will be required to overcome the buffering capacity of seawater. In addition to acid preservation, holding collected water samples on ice is recommended. Alternatively, water samples can be preserved by the addition of methylene chloride, although this will start the extraction process and introduces the finite possibility of sample contamination by handling organic solvents on a rolling boat where diesel or gasoline exhaust fumes may be present. Discrete glass fiber filters from the PLVWSS containing dispersed oil droplets can be preserved by addition of 3 mL of 6 N HCl to wide-mouth sample jars containing the filter and/or by freezing.

Preserved samples should be shipped in chain-of-custody-sealed coolers containing Blue Ice[®] to the analytical laboratory by overnight courier. Complete chain-of-custody forms should be included with each cooler indicating the cooler's contents and desired analytes. The samples should be analyzed using selected-ion-monitoring (SIM) gas chromatography/mass spectrometry (GC/MS) to include parent and C₁-C₄ alkylated homologues of polycyclic aromatic hydrocarbons (PAHs) spanning the molecular-weight range from naphthalene through benzo(g,h,i)perylene and gas chromatography/flame ionization detector (GC/FID) for saturated hydrocarbons (SHC) to include n-C₁₀ through n-C₃₄, plus pristane and phytane. These analytes are critical for differentiating the dissolved and particulate/oil-phase contributions (Payne and Driskell, 2003) to the water-column impact, and they will be important for relating the results of modeling and later toxicity studies to the conditions that actually existed at the time of the spill.

Additional Supporting Data and Measurements

In addition to the biological and chemistry samples, aerial photography from the spotter aircraft (with time and GPS data integrated into the digital image) should be collected throughout all operations. Additional oceanographic data should include:

- CTD casts before dispersant applications (to assist in selecting optimal drogue depths), and as the evolution of the dispersed oil plume occurs to document potentially changing water-column stratification over time.
- Wind and wave data from nearby oceanographic buoys.
- High frequency radar measured surface currents.
- Fluorometer calibrations.

Usually, UV-fluorescence instrumentation is calibrated with fluorescein dye, and these solutions should be used for reporting UV-fluorescence concentrations from the water column. If possible, these calibrations should be completed before moving equipment into the field. Calibration of UV fluorescence units with oil from the spill incident is important, but extremely difficult to complete because of separation of oil and water phases over time. It is recommended that after the field sampling activities are completed, mixtures of the dispersant and oil from the spill event (collected from the Responsible Party) be gravimetrically measured and diluted into known volumes of clean seawater. Calibration standards solutions should be thoroughly mixed/agitated in sealed volumetric containers and used immediately as oil and dispersant phases may separate from the water on standing. The use of dispersed oil droplets in addition to fluorescein dye for calibrating the fluorometers is recommended to provide a secondary standard.

Background Controls and Sample Contamination

Because most of the anticipated concentrations that will be measured from the field samples are expected to be very low [10-40 mg/liter (ppm) for whole-oil droplets and 1-20 µg/L (ppb) for dissolved PAH in the center of the dispersed oil plume, and possibly one to two orders-of-magnitude lower in control areas], it will be important to ensure that background contamination from the sampling vessels and other sources is kept to an absolute minimum. For this reason, it will be important to minimize or curtail any bilge water or on board wastewater discharges from the vessel at the time of all water sample collections. In addition, all sample manipulations (removal of filters from PLVWSS-collected samples, acid preservation, etc.) should be

completed upwind of sampling vessel exhaust discharges, if possible. To minimize sample cross-contamination, samples from clean/control areas should be collected before samples from the center of the dispersed oil plume whenever possible. It may also be prudent to maintain additional supplies of sampling hose, which should be replaced from subsurface sampling systems after particularly high concentrations of dispersed-oil droplets are encountered.

Finally distilled water should be obtained from the analytical laboratory supplying the sample bottles and used for collection of field/method and trip blanks. If possible, the analytical laboratory should analyze and certify the background SHC and PAH levels in their distilled water used for preparation of these blanks. If the laboratory cannot provide certified distilled water, commercially purchased distilled water may be used; however, it has been found that most commercial distilled water sources contain traces (low ppb levels) of parent and alkyl-substituted naphthalenes. Because of these limitations, it is sometimes appropriate to simply use seawater collected from stations remote from the spill and all dispersant applications for background controls and evaluation of sampler contamination.

6.4 Conclusions

The database developed through this program represents a technical resource that can be of value to physical and chemical oceanographers, modelers, oil-spill-response and contingency planners/decision makers, and stakeholders involved in the debate of whether or not to use dispersants to combat near-shore and open-ocean marine oil spills.

The results were obtained through a multidisciplinary effort involving numerous personnel and different state and federal agencies along with the private sector. The experience gained and described herein has direct relevance to implementing any sampling or monitoring program for Natural Resource Damage Assessment (NRDA) activities, and the California Dispersed Oil Monitoring Plan, in particular. The approach outlined in this report also may be useful in providing additional information to incident responders regarding dispersant effectiveness and potential impacts from dispersed oil plumes entering sensitive biological areas, if modifications to the data collection and storage systems can allow transmission of pertinent information to the Incident Command Center in a near real-time manner.

Obviously, these types of coordinated measurements are extremely difficult to execute (particularly during the emergency-response phase of a spill), so it is critically important to have a detailed plan in place before a spill event and to utilize a team with familiarity in the strengths and inherent weaknesses of the sampling and observation methods as well as past experience in working together as a coordinated unit to successfully execute such a plan.

7. Technology Transfer

Two papers from this project (Payne *et al.*, 2007 and French-McCay *et al.*, 2007) have been accepted for publication and will be presented at the Arctic Marine and Oilspill Program (AMOP) in June 2007. In addition, two abstracts have been submitted for consideration at the 2008 International Oil Spill Conference (IOSC), and the results of continued analyses and modeling will be the topic of several additional manuscripts. Project results have also been presented at three public meetings sponsored by CRRC: The 13-14 March 2006 Principal Investigator Workshop at the University of New Hampshire, the 1-2 February 2007 Dispersed Oil Research Forum in Red Bank, New Jersey, and the 19 April 2007 Project Investigator Symposium at the NOAA Sand Point facility in Seattle, Washington. The data will be available on-line through the CRRC website: <http://www.crrc.unh.edu/> and at an FTP site maintained by the Coastal Observing Research & Development Center at Scripps Institution of Oceanography (<ftp://ftp.mpl.ucsd.edu/pub/CORDC/outgoing/OSPR>).

References

- Allen, A. A. 1999. Leeway divergence, US Coast Guard Research and Development Center, Groton, CT, Report CG-D-XX-99.
- Allen, A. A. and J. V. Plourde. 1999. Review of Leeway: Field Experience and Implementation. US Coast Guard Research and Development Center, Groton, CT, Report CG-D-08-99.
- Boufadel, M.C., R. D. Bechtel, and J. Weaver. 2006a. The Movement of Oil Under Non-Breaking Waves. *Marine Pollution Bulletin* (52): 1056-1065.
- Boufadel M. C., K. Du, V. J. Kaku, and J. Weaver. 2006b. Lagrangian Simulation of Oil Droplets Transport due to Regular Waves. *Environmental Modelling and Software* (in press): 1-9.
- Cox, W. (ed.). 2004. The Prince William Sound 2004 Lagrangian Field Experiment. <http://www.pws-osri.org/publications/reports.shtml>
- Csanady, G.T., 1973. *Turbulent Diffusion in the Environment*. D. Reidel Publishing Company, Boston, 248p.
- D'Asaro. 2000. Simple Suggestions for Including Vertical Physics in Oil Spill Models. *Spill Science and Technology Bulletin* 6 (3): 209-211.
- Elliott, A.J., N. Hurford, and C.J. Penn. 1986. Shear diffusion and the spreading of oil slicks. *Marine Pollution Bulletin* 17(7): 308-313.
- Elliott, A.J.; A.G. Barr and D. Kennan. 1997. Diffusion in Irish Coastal Waters, *Estuarine, Coastal and Shelf Science* 44 (Supplement A): 15-23.
- French, D., M. Reed, K. Jayko, S. Feng, H. Rines, S. Pavignano, T. Isaji, S. Puckett, A. Keller, F.W. French III, D. Gifford, J. McCue, G. Brown, E. MacDonald, J. Quirk, S. Natzke, R. Bishop, M. Welsh, M. Phillips and B.S. Ingram. 1996. Final Report, The CERCLA Type A Natural Resource Damage Assessment Model for Coastal and Marine Environments (NRDAM/CME), Technical Documentation, Vol. I - V., Submitted to the Office of Environmental Policy and Compliance, U.S. Department of the Interior, Washington, DC, Contract No. 14-0001-91-C-11, April, 1996.
- French McCay, D.P. 2002. Development and Application of an Oil Toxicity and Exposure Model, OilToxEx. *Environmental Toxicology and Chemistry* 21(10): 2080-2094.
- French McCay, D.P. 2003. Development and Application of Damage Assessment Modeling: Example Assessment for the *North Cape* Oil Spill. *Marine Pollution Bulletin* 47(9-12): 341-359.

French McCay, D.P. 2004. Oil spill impact modeling: development and validation. *Environmental Toxicology and Chemistry* 23(10): 2441-2456.

French McCay, D.P. and J.R. Payne. 2001. Model of oil fate and water concentrations with and without application of dispersants. In: Proceedings of the Twenty-fourth Arctic and Marine Oil Spill Program (AMOP) Technical Seminar, Emergencies Science Division, Environment Canada, Ottawa, ON, pp. 611-645.

French, D.P., H. Rines and P. Masciangioli, Validation of an Orimulsion Spill Fates Model Using Observations from Field Test Spills. 1997. In: Proceedings of the Twentieth Arctic and Marine Oilspill Program (AMOP) Technical Seminar, Emergencies Science Division, Environment Canada, Ottawa, ON, pp. 933-961.

French-McCay, D.P., J.J. Rowe, W Nordhausen and J.R. Payne. 2006. Modeling Potential Impacts of Effective Dispersant Use on Aquatic Biota. In: Proceedings of the 29th Arctic and Marine Oil Spill Program (AMOP) Technical Seminar, Emergencies Science Division, Environment Canada, Ottawa, ON, Canada, pp. 855-878.

French McCay, D.P., C. Mueller, K. Jayko, B. Longval, M. Schroeder, E. Terrill, M. Carter, M. Otero, S.Y. Kim, J.R. Payne, W. Nordhausen, M. Lampinen, and C. Ohlmann. 2007. Evaluation of Field-Collected Data Measuring Fluorescein Dye Movements and Dispersion for Dispersed Oil Transport Modeling. In: Proceedings of the Thirtieth Arctic and Marine Oil Spill Program (AMOP) Technical Seminar, Environment Canada, Ottawa, ON,

Galt, J.A., 1998. Uncertainty Analysis Related to Oil Spill Modeling. *Spill Science and Technology Bulletin* 4(4): 231-238.

Graber, H.C., B.K. Haus, L.K. Shay, and R.D. Chapman. 1997. HF Radar Comparisons with Moored Estimates of Current Speed and Direction: Expected Differences and Implications, *Journal of Geophysical Research* 102: 18,749-18,766.

Kim, S.Y., E.J. Terrill, and B. Cornuelle. 2007. Objectively Mapping HF Radar-Derived Surface Current Data Using Measured and Idealized Data Covariance Matrices. *Journal of Geophysical Research*, (In Press).

Henry, C.B., P.O. Roberts, and E.B. Owens. 1999. A Primer on *In-Situ* Fluorimetry to Monitor Dispersed Oil. In: Proceedings of the 1999 International Oil Spill Conference, American Petroleum Institute, Washington, D.C., pp. 225-228.

Lange, P. and H. Hufnerfuss. 1978. Drift response of mono molecular slicks to wave and wind action. *Journal of Physical Oceanography* 8: 142-150.

Huang, N.E. 1979. On Surface Drift Currents in the Ocean. *Journal of Fluid Mechanics* 91: 191-208.

- Jenkins, A.D. 1986. A Theory for Steady and Variable Wind- and Wave-Induced Currents. *Journal of Physical Oceanography* 16: 1370-1377.
- Jenkins, A.D. 1987. Wind- and Wave-Induced Currents in a Rotating Sea with Depth-Varying Eddy Viscosity. *Journal of Physical Oceanography* 17: 938-951.
- Jenkins, A.D. 1989. The use of a wave prediction model for driving a near-surface current model. *Deutsches Hydrographisches Zeitschrift* 42: 3-6.
- Lange, P. and H. Hufnerfuss. 1978. Drift response of mono molecular slicks to wave and wind action. *Journal of Physical Oceanography* 8: 142-150.
- Langmuir, I. 1938. Surface motion of water induced by wind. *Science* 87: 119-123.
- Leibovich, S. 1977. On the evolution of the system of wind drift currents and Langmuir circulations in the ocean, Part 1, theory and averaged current. *Journal of Fluid Mechanics* 79: 715-743.
- Leibovich, S. 1983. The form and dynamics of Langmuir circulations, *Annual Reviews of Fluid Mechanics* 15: 391-427.
- Lehr, W.J., J.A. Galt, and R. Overstreet, 1995. Handling uncertainty in oil spill modeling. In: *Proceedings of the 18th Arctic and Marine Oil Spill Program (AMOP) Technical Seminar*, Environment Canada, pp.759-768.
- Lehr, W.J., D. Wesley, D. Simecek-Beatty, R. Jones, G. Kachook, and J. Lankford, 2000. Algorithm and interface modifications of the NOAA oil spill behavior model. In: *Proceedings of the 23rd Arctic and Marine Oil Spill Program (AMOP) Technical Seminar*, Vancouver, BC, Environmental Protection Service, Environment Canada, pp. 525-539.
- Mackay, D, W.Y. Shiu, K. Hossain, W. Stiver, D. McCurdy and S. Peterson. 1982. Development and calibration of an oil spill behavior model. Report No. CG-D-27-83, U.S. Coast Guard, Research and Development Center, Groton, Connecticut, 83p.
- McAuliffe, C.D., 1987. Organism exposure to volatile/soluble hydrocarbons from crude oil spills – a field and laboratory comparison. In: *Proceedings of the 1987 International Oil Spill Conference*, American Petroleum Institute, Washington, D.C., pp. 275-288.
- Moum, J.N., W.D. Smyth, 2001. Upper ocean mixing processes. *Encyclopedia of Ocean Sciences*. Academic Press, p.3093-3100.
- National Research Council (NRC), 2005. *Oil Spill Dispersants – Efficacy and Effects*. National Academy Press, Washington, D.C., 377 p.

Niiler, P.P., A.S. Sybrandy, K.N. Bi, P.M. Poulain, D. Bitterman. 1995. Measurements of the Water-Following Capability of Holey-Sock and TRISTAR Drifters. *Deep-Sea Research Part I – Oceanographic Research Papers* 42(11-12): 1951-1958.

Ohlmann, J.C., P.F. White, A.L. Sybrandy, and P.P. Niiler. 2005. GPS-cellular drifter technology for coastal ocean observing systems. *Journal of Atmospheric and Oceanic Technology* 22: 1381-1388.

Ohlmann, J.C., P. White, L. Washburn, E. Terrill, B. Emery, and M. Otero. 2007. Interpretation of Coastal HF Radar-Derived Surface Currents with High-Resolution Drifter Data. *Journal of Atmospheric and Oceanic Technology* 24: 666-680.

Okubo, A. 1971. Oceanic diffusion diagrams. *Deep-Sea Research* 8: 789-802.

Okubo, A. and R.V. Ozmidov. 1970. Empirical dependence of the coefficient of horizontal turbulent diffusion in the ocean on the scale of the phenomenon in question. *Atmospheric and Ocean Physics* 6(5): 534-536.

Ota, A., 2006. E-mail of January 6, 2006 from Allan Ota, EPA Region 9, to Dr. Walter Nordhausen. CA Fish and Game.

Paduan, J.D., and Rosenfeld, J.K. 1996. Remotely sensed surface currents in Monterey Bay from shore-based HF radar (Coastal Ocean Dynamics Application Radar). *Journal of Geophysical Research* 101(C9): 20669-20686.

Payne, J.R. and W.B. Driskell, 2003. The Importance of Distinguishing Dissolved- Versus Oil-Droplet Phases in Assessing the Fate, Transport, and Toxic Effects of Marine Oil Pollution. In: *Proceedings of the 2003 International Oil Spill Conference*, American Petroleum Institute, Washington, D.C., pp. 771-778.

Payne, J.R., J.R. Clayton, Jr., C.R. Phillips, J. Robinson, D. Kennedy, J. Talbot, G. Petrae, J. Michel, T. Ballou, and S. Onstad. 1991. Dispersant Trials Using the Pac Baroness, a Spill of Opportunity. In: *Proceedings of the 1991 Oil Spill Conference*, American Petroleum Institute, Washington, D.C., pp. 427-433.

Payne, J.R., T.J. Reilly, R.J. Martrano, G.P. Lindblom, M.C. Kennicutt II, and J.M. Brooks, 1993. Spill-of-Opportunity Testing of Dispersant Effectiveness at the Mega Borg Oil Spill. In: *Proceedings of the 1993 Oil Spill Conference*, American Petroleum Institute, Washington, D.C., pp. 791-793.

Payne, J.R., T.J. Reilly, and D.P. French. 1999. Fabrication of a Portable Large-Volume Water Sampling System to Support Oil Spill NRDA Efforts. In: *Proceedings of the 1999 International Oil Spill Conference*, American Petroleum Institute, Washington, D.C., pp. 1179-1184.

Payne, J.R., E. Terrill, M. Carter, M. Otero, W. Middleton, A. Chen, D. French-McCay, C. Mueller, K. Jayko, W. Nordhausen, R. Lewis, M. Lampinen, T. Evans, C. Ohlmann, G.L. Via, H. Ruiz-Santana, M. Maly, B. Willoughby, C. Varela, P. Lynch and P. Sanchez. 2007. Evaluation of Field-Collected Drifter and Subsurface Fluorescein Dye Concentration Data and Comparisons to High Frequency Radar Surface Current Mapping Data for Dispersed Oil Transport Modeling. In: Proceedings of the Thirtieth Arctic and Marine Oil Spill Program (AMOP) Technical Seminar, Emergencies Science Division, Environment Canada, Ottawa, ON.

Quality Assurance Plan (QAP). 2006. Field Verification of Oil Spill Fate & Transport Modeling and Linking HF-Radar Observation System Data with SIMAP Predictions. Quality Assurance Plan, Revision 2 – February 17, 2006, Payne Environmental Consultants, Inc., Encinitas, CA, U.S.A., 19 p..

Reed, M., O. Johansen, P.J. Brandvik, P. Daling, A. Lewis, R. Fiocco, D. Mackay, and R. Prentki. 1999. Oil spill modeling towards the close of the 20th century: Overview of the state-of-the-art. *Spill Science and Technology Bulletin* 5(1): 3-16.

Reed, M., P.S. Daling, O.G. Brakstd, I. Singsaas, L.-G. Faksness, B. Hetland, and N. Efröl. 2000. OSCAR 2000: A multi-component 3-dimensional oil spill contingency and response model. In: Proceedings of the 23rd Arctic Marine Oilspill Program (AMOP) Technical Seminar, Environment Canada, Ottawa, Ontario, pp.663-952.

Samuels, W. B., N. E. Huang, D. E. Amstutz. 1982. An oil spill trajectory analysis model with a variable wind deflection angle. *Ocean Engineering* 9: 347-360.

Simecek-Beatty, D. and W.J. Lehr. 2000. Langmuir Circulation and Oil Spill Trajectory Models Workshop – Comments and Recommendations. *Spill Science and Technology Bulletin* 6(3): 273-274.

Skyllingstad, E.D. 2000. Scales of Langmuir Circulation Generated using a Large-Eddy Simulation Model. *Spill Science and Technology Bulletin* 6(3): 239-246.

Smith, J.A. 1992. Observed growth of Langmuir circulation. *Journal of Geophysical Research* 97: 5651-5664.

Spaulding, M.L., S.B. Saila, E. Lorda, H.A. Walker, E.L. Anderson and J.C. Swanson. 1983. Oil spill fishery interaction modelling: Application to selected Georges Bank fish species. *Estuarine, Coastal and Shelf Science* 16: 511-541.

Spaulding, M.L. 1988. A state-of-the-art review of oil spill trajectory and fate modeling. *Oil and Chemical Pollution* 4: 39-55.

Thorpe, S.A. 1995. Dynamical processes at the sea surface. *Progress in Oceanography* 35:315-352.

- Thorpe, S.A. 2000. Langmuir Circulation and the Dispersion of Oil Spills in Shallow Seas. *Spill Science and Technology Bulletin* 6(3): 213-223.
- Thompson, R.E. and I.V. Fine. 2003. Estimating Mixed Layer Depth from Oceanic Profile Data, *Journal of Atmospheric and Oceanic Technology* 20(2): 319-329.
- U. S. Coast Guard (USCG). 1999. Response Plan Equipment Caps Review: Are Changes to Current Mechanical Recovery, Dispersant, and *in situ* Burn Equipment Requirements Practicable? Washington, D.C., United States Coast Guard, U. S. Department of Transportation, pp. 1-177, plus appendices.
- Weber, J.E. 1983. Steady wind- and wave-induced currents in the open ocean , *Journal of Physical Oceanography* 13: 524-530.
- Wu, J. 1980. Wind-stress coefficients over sea surface near neutral conditions - a revisit, *Journal of Physical Oceanography* 10: 727-740.
- Youssef, M. 1993. The Behavior of the Near Ocean Surface Under the Combined Action of Waves and Currents in Shallow Water, PhD Dissertation, Department of Ocean Engineering, University of Rhode Island, Narragansett, RI, 212 p.
- Youssef, M. and M. L. Spaulding. 1993. Drift Current Under the Action of Wind Waves. In: *Proceedings of the Sixteenth Arctic and Marine Oilspill Program Technical Seminar*, Ottawa, ON, Canada, pp. 587-615.
- Youssef, M. and M.L. Spaulding. 1994. Drift Current Under the Combined Action of Wind and Waves in Shallow Water. In: *Proceedings of the Seventeenth Arctic and Marine Oilspill Program (AMOP) Technical Seminar*, Ottawa, ON, Canada, pp. 767-784.